1991

The interaction of formic acid with Pt(111) and the effect of coadsorbed water, atomic oxygen, and carbon monoxide

Michael Ray Columbia
Iowa State University

Order Number 9212137

The interaction of formic acid with Pt(111) and the effect of coadsorbed water, atomic oxygen, and carbon monoxide

Columbia, Michael Ray, Ph.D.

Iowa State University, 1991

U·M·I
300 N. Zeeb Rd.
Ann Arbor, MI 48106

The interaction of formic acid with Pt(111) and the effect of coadsorbed water, atomic oxygen, and carbon monoxide

by

Michael Ray Columbia

A Dissertation Submitted to the
Graduate Faculty in Partial Fulfillment of the
Requirements for the Degree of
DOCTOR OF PHILOSOPHY

Department: Chemistry
Major: Analytical Chemistry

Approved:

Signature was redacted for privacy.

In Charge of Major Work

Signature was redacted for privacy.

For the Major Department

Signature was redacted for privacy.

For the Graduate College

Iowa State University
Ames, Iowa

1991

DEDICATION

To my high school chemistry teacher, Dr. Brent Garrison

TABLE OF CONTENTS

GENERAL INTRODUCTION

The reaction of formic acid with transition metals has been an active area of interest within the surface science community since the early 1970's. One genesis of this interest lies in the area of heterogeneous catalysis where the decomposition of formic acid has been studied as a model reaction for decades [1, 2]. These investigations have typically been performed in reactors which operate at higher pressures (10^{-5} to 100 Torr) than those utilized in modern surface science experiments [3]; general agreement exists that decomposition on metals occurs via two different pathways [1]: dehydration, which produces CO, and dehydrogenation, which produces CO_2. The advent of ultrahigh vacuum and its surface-sensitive analytical techniques has allowed exploration of the mechanisms and intermediates of these paths at the molecular level under well-defined conditions.

Another field piqued by the interaction of formic acid with metals exists within the electrochemical community. Here the development of fuel cells has proved an impetus for many researchers to explore the oxidation of formic acid owing to its potential use in such devices. Pt electrodes have been the focus of much of this research as far back as the 1920's [4-6] and remain so to the present

day. The oxidation of formic acid at Pt electrodes proceeds with nearly 100% efficiency; however, the reaction is observed to be self-poisoning [7]. Classical electrochemical methods have led most researchers to posit that oxidation involves an intermediate that can produce CO_2, which desorbs, or a species which remains adsorbed to the electrode surface; prime candidates for the intermediate and the poison are carboxylate (COOH), formyl (CHO) and hydroxymethylidyne (COH)[8-11]. More recently, the development and utilization of in situ infrared spectrometric techniques has identified the probable poison to be CO [12]. Vibrational studies of formic acid interactions with Pt in ultrahigh vacuum identify the decomposition intermediate to be formate, HCOO [13, 14].

The goal of the work presented in this thesis is to gain a fundamental knowledge of the interaction of formic acid with the Pt(111) surface utilizing ultrahigh vacuum techniques such as thermal desorption spectroscopy and high resolution electron energy loss spectroscopy. Such knowledge provides a starting point in determining the basic chemistry of this system by eliminating the perturbations of an aqueous environment and high potential field gradients found in fuel cells. It also provides a way to determine the influence of other coadsorbed species commonly found in the environment of fuel cells on the chemistry of this system at a molecular level.

The decomposition of HCOOH on metal surfaces studied in ultrahigh vacuum typically occurs in two steps: (1) The dehydration or dehydrogenation of the molecular acid, following adsorption, to produce a surface intermediate; (2) The decomposition of the intermediate to produce CO, CO_2, and H_2, as well as atomic carbon and oxygen. In the following section the surface science literature pertaining to the adsorption and decomposition of formic acid on metal surfaces studied in ultrahigh vacuum is reviewed. Madix reviewed this literature in 1980 for Cu, Fe, W, Ni, Ru, and Ag [15]. These metals as well as Pt, Au, Rh, and Pd are included.

Review

1. Molecular adsorption

Thermal desorption of molecular HCOOH has been observed from several metals: Ag(110) [16], Au(110) [17], Cu(110) [18-20], Ni(111) [21], Ni(110) [22], Ni(100)-p(2 x 2)C [23], Pt(100) [24], Pt(111) [13, 25, 26], Rh(111) [27], Ru(001) [28], and Ru(100) [29]. The majority of these studies [16, 17, 19, 23, 24, 26-29] identified two states: one assigned to desorption from multilayers and the

other to desorption from a chemisorbed layer; the peak desorption temperatures (T_p) reported for these two states vary, depending on the surface, between 145-190 K and 160-210 K, respectively. Desorption of molecular HCOOH has been detected from Pt(111) [25] and Ni(110) [22] (T_p = 230-250 K) following adsorption of HCOOH at 200 K, a temperature too high to populate the two states mentioned previously.

Joyner and Roberts studied the adsorption and decomposition of HCOOH on polycrystalline surfaces of Cu, Ni, and Au with photoelectron spectroscopy [30]. They proposed that molecular formic acid adopts the same structure on all three metals following adsorption at 80 K; this structure consisted of hydrogen-bonded chains of HCOOH with the molecular plane parallel to the surface. Such a structure is very similar to solid-phase HCOOH [31-34]. Heating the overlayer caused changes in the photoelectron spectra which are assigned to 1) breakdown of the hydrogen-bonded chains (120-150 K) producing HCOOH monomers, 2) reorientation of the monomers relative to the surface plane (150-170 K), and 3) loss of the hydroxyl proton (170-190 K). This agreed well with Bowker and Madix's interpretation of photoelectron spectra of HCOOH adsorbed on Cu(110) at 140 K [18]; they identified HCOOH monomers bonded end-on through the hydroxyl oxygen atom.

Vibrational spectroscopy has also provided information pertaining to the configuration of molecular HCOOH. An infrared reflection-absorption spectroscopic (IRAS) study by Hayden et al. [19] of HCOOH on Cu(110) revealed that HCOOH in direct contact with the surface is not oriented with its molecular plane parallel to the surface, possibly forming dimer pairs; HCOOH multilayers adsorbed on Cu(100) [35] and Ag(110) [16] exhibited the same nonparallel orientation in high resolution electron energy loss spectroscopy (HREEL) spectra. On Pt(111) Avery used HREEL to definitively identify that multilayer adsorption adopted a hydrogen-bonded chain structure with the HCOOH molecular plane nearly parallel to the surface [13]; this configuration exhibited vibrational features associated with the HCOOH solid-state alpha polymorph [33]. Columbia et al., also using HREELS, have observed evidence for both the alpha and beta polymorphs, as well as dimer pairs for submonolayer HCOOH coverages on the same surface with a temperature- and coverage-dependent interconversion among these [36]. Chtaib et al. reported a dependence on substrate geometry with dimer pairs present on Au(111) and hydrogen-bonded chains on Au(110) [37].

2. Decomposition

2.1 Nickel

Madix and coworkers studied the interaction of formic acid on clean Ni(110) and on that same surface covered with atomic carbon or oxygen utilizing thermal desorption spectroscopy (TDS), Auger electron spectroscopy (AES), and low energy electron diffraction (LEED) [3, 22, 38-44]. They reported that formic acid, adsorbed on the clean surface at room temperature, decomposes resulting in the desorption of water (T_p = 320 K), followed by desorption of CO_2 and H_2 (T_p = 390 K) and CO at (T_p = 390 K, 440 K) [3]. TD experiments utilizing deuterated formic acid identified the source of water desorption as the hydroxyl groups [22]; this suggested bimolecular dehydration, resulting in a formic anhydride. This intermediate decomposed at 390 K producing simultaneous desorption of CO_2, H_2, and CO. This desorption occurred over a very narrow temperature range [3], as well as accelerating during constant temperature experiments [39]. Madix and coworkers concluded this decomposition to be autocatalytic. They proposed that attractive interactions between the anhydride adspecies produce densely packed islands on the surface; decomposition of one adspecies immediately destabilized neighboring adspecies, producing a chain reaction [40]. The decomposition also left CO on the surface, affording additional CO desorption (T_p = 440 K).

Adsorption at lower temperatures (ca. 200 K) decreased the ability to form islands and diminishes the autocatalytic behavior, broadening and decreasing the temperature range of decomposition [22]. The presence of a surface carbide produced formate as the principle surface intermediate, resulting in less CO desorption and decomposition over a higher, broader temperature range [38, 41, 42]. The coadsorption of oxygen stabilized the formic anhydride at low coverages, while also producing formate as the dominant surface intermediate as oxygen coverage increased [44].

The (100) face of Ni decomposes adsorbed HCOOH in a manner similar to Ni(110) [23, 45]. On the (100) surface H_2O desorbed at temperatures ca. 100 K lower than on the (110), while the desorption temperatures of the other decomposition products did not shift significantly; however, desorption features produced by decomposition of formic anhydride were not as sharp as those from the (110) [45]. Benziger and Madix attributed this to diminished attractive interaction between the anhydride adspecies induced by different substrate geometry [45]. The decomposition also oxidized the surface; this resulted in formate as the dominant intermediate. The presence of surface carbide also produced formate as the dominant intermediate with a marked decrease in the amounts of CO_2 and H_2 desorbed [23].

Benziger and Schoofs investigated the effect of the monomer\dimer composition of the HCOOH vapor exposed to the Ni(111) surface on decomposition [46]. For vapor dominated by HCOOH dimers decomposition closely followed the autocatalytic behavior attributed to formic anhydride; however, for vapor consisting primarily of monomers, decomposition which resembled that where formate is the intermediate occurred. Erley and Sander have also reported autocatalytic behavior for the adsorption of formic acid dimers on the same surface [21].

Vibrational studies of HCOOH decomposition have also produced evidence for both formic anhydride and formate as intermediates. Madix et al. probed the intermediate on Ni(110) using HREELS; they observed the presence of coadsorbed CO and symmetrically-bonded formate [47]. This contradicted the idea of formic anhydride as the intermediate responsible for autocatalytic decomposition and suggested that bimolecular dehydration produces formate and formyl (CHO) instead, followed almost immediately by decomposition of the formyl to CO and atomic hydrogen [47]. However, Jones, Richardson and coworkers, using HREELS and LEED, observed *only* formate on Ni(110) in an ordered c(2 x 2) overlayer; they also determined the formate to be bonded in a "bridging" configuration (bonding via both formate oxygen atoms to two equivalent surface sites). [48, 49]. Erley and Sander, utilizing infrared

reflection-absorption spectroscopy (IRAS), reported the presence of formic anhydride on a Ni(111) surface which also exhibited autocatalytic behavior [21].

2.2 Copper

CO_2 and H_2 were the only desorption products resulting from HCOOH exposure to clean Cu(110) at temperatures above 200 K [18, 19, 50]. H_2 desorbed in a broad state, T_p = 270-280 K, and a narrower state, T_p = 450-475 K; CO_2 desorption was peaked also at 450-475 K and the peak shape was identical to the higher temperature H_2 desorption feature. The simultaneous desorption of CO_2 and H_2 was attributed to decomposition of a formate intermediate. The use of deuterated formic acid revealed that low temperature H_2 desorption was due to hydrogen atoms produced when the molecular acid lost its hydroxyl proton; the desorption temperature was, however, 50 K lower than H_2 desorption from hydrogen adatoms on clean Cu(110) [18, 50]. A possible reason for this was site-blocking by the coadsorbed formate which forces hydrogen adatoms out of preferred adsorption sites [18]. Similar desorption occurred from Cu(100) with the exception of the low temperature H_2 feature, which appeared much closer to the peak temperature for H_2 desorption from the clean surface [51].

The coadsorption of atomic oxygen with formic acid on the (110) face increased the amount of formate intermediate produced and suppresses the low

temperature H_2 desorption. This was attributed to extraction of the acidic proton by the oxygen adatoms resulting in surface hydroxyl groups and subsequent water desorption [18, 20]. Coadsorbed Cs accelerated the decomposition of formate, as well as forming a surface carbonate with the formate fragments at higher Cs coverages [20].

Sexton identified formate as the decomposition intermediate on Cu(100) using HREELS [35, 52]. The adspecies produced following adsorption of several layers of formic acid at 100 K and subsequent heating to 400 K possessed the bridging configuration (this agreed with photoelectron spectroscopic results showing the formate oxygen atoms to be equivalent [18]); however, cooling to 100 K lowered the symmetry of the formate, possibly resulting from the adoption of nonequivalent binding sites for the formate oxygen atoms [35]. Hayden et al., utilizing IRAS, observed bridging formate on Cu(110) following HCOOH adsorption at 100 K and heating to 290 K, but no temperature-dependent symmetry degradation occurred as on the (100) surface, however, the phenomenon was observed following exposure of the annealed overlayer to additional formic acid [19, 53]. Dubois et al. also failed to reproduce Sexton's results on Cu(100), and, as on Cu(110), observed symmetry degradation only after exposing a formate overlayer to additional formic acid [51]. They concluded the

symmetry degradation results from tilting of the formate caused by hydrogen-bonding to molecular HCOOH.

Surface-extended (SEXAFS) and near-edge X-ray fine structure (SEXAFS and NEXAFS, respectively) have been used to determine the adsorption site of formate on Cu. Stœhr et al. proposed that formate on the (100) surface was situated with its oxygen atoms located near the four-fold hollow sites; the resulting Cu-O bond distance was 2.3 to 2.4 Å, at least 0.3 Å longer than expected from bulk copper formate [54, 55]. On Cu(110) Puschmann, Crapper and coworkers determined that formate is adsorbed along the [1 $\bar{1}$ 0] direction with the oxygen atoms sitting nearly on top of adjacent row atoms; this positioning permitted a Cu-O bond distance identical to the bulk Cu formate value [56, 57]. Results probing formate on the (100) with photoelectron diffraction coupled with reanalysis of the SEXAFS and NEXAFS data suggested that the Cu-O bond distance was ca. 2 Å with the formate oxygen atoms located in atop sites [58-60].

2.3 Platinum

Thermal desorption results reported for the low index faces of Pt vary greatly. Kizhakevariam and Stuve observed no decomposition products from clean Pt(100), but did observe desorption of CO_2 (T_p = 310 K) and H_2O (T_p = 180 K, 310 K) from a Pt(100) surface predosed with atomic oxygen [24]. Madix

reported desorption of D_2O, H_2O, D_2, H_2, CO, and CO_2 from Pt(110) exposed to DCOOH at 200 K with only the peak desorption temperature of CO_2 listed (T_p = 260 K) [15]. On Pt(111) Abbas and Madix observed desorption of CO_2 (T_p = 265 K, 361 K, 426 K), H_2O, D_2O and HDO (T_p = 265 K, 295 K), H_2, D_2 and HD (T_p = 310-320 K), and CO (T_p = 473 K, 531 K) from exposure to DCOOH at 195 K; at saturation, the majority products were CO_2 and the hydrogenic species leading to the assignment of CO and the aqueous species to reaction at surface defect sites [25]. Avery [13], and Columbia and Thiel [26] reported only CO_2 (T_p = 260 K) and H_2 (T_p = 360-370 K) as desorption products following adsorption of HCOOH at 130 K or below; any CO desorption is ascribed to ambient adsorption. These reports contrasted with the observations of Seebauer et al.; who observed CO and H_2O as the majority products with a CO/CO_2 ratio of 2 [61].

As mentioned above, atomic oxygen induced HCOOH decomposition on Pt(100) [24]; it increased the extent of decomposition on Pt(111) by a factor of 4 to 7, as well as producing H_2O, in addition to CO_2 and H_2 [13, 62]. The presence of coadsorbed sulfur suppressed the amount of CO and H_2O produced by decomposition, presumably by preferentially adsorbing at defect sites [25]. The coadsorption of CO (a suggested poison in electrochemical oxidation) suppressed decomposition by preventing deprotonation [63].

HREEL spectra reveal bridging formate to be the intermediate formed on Pt(110) and Pt(111) [13, 14, 36, 64]. Additionally, Avery reported the existence of monodentate formate on oxygen-predosed Pt(111) for submonolayer doses of HCOOH at 130 K [64]; he observed conversion from this to the bridging configuration over a period of 20 minutes. Columbia et al. also observed monodentate formate on the same surface but only for exposures made at 100 K; heating to 120 K is sufficient to cause conversion [36].

2.4 Ruthenium

Larson and Dickinson studied formic acid decomposition on Ru(100) utilizing thermal desorption [29]; desorption of H_2O (T_p = 183-220 K), H_2 (T_p = 390 K), CO_2 (T_p = 390 K), and CO (T_p = 488 K) are observed. The H_2O peak desorption temperature decreased with increasing HCOOH exposure suggesting a second order dehydration similar to that proposed for Ni via an anhydride intermediate; unlike Ni, its decomposition did not exhibit autocatalysis.

Avery, Toby and coworkers identified the bridging formate as the decomposition intermediate on Ru(001) using HREELS [65, 66]. They also identified losses caused by the presence of CO, similar to the HREEL spectra for Ni(110) [47]; the intensity of these losses increased with surface temperature as the intensities of the formate losses decreased.

Sun and Weinberg reported the same desorption products from the (001) surface as from the (100) surface [28]; however, the (001) surface displayed autocatalytic behavior with CO_2 desorption features exhibiting narrower FWHM and higher peak desorption temperatures (from 330 K at onset to 395 K at saturation). Desorption of H_2 (due to the acyl proton) and H_2O also followed this trend. Desorption of H_2 (due to the hydroxyl proton) occurred at lower temperatures (T_p = 320 K) and was clearly discernible at saturation. CO desorbed in two states: one followed the CO_2 desorption (attributed to cracking of CO_2), the other appeared at temperatures above 400 K. Sun and Weinberg proposed a decomposition mechanism based on the formate intermediate. In this model decomposition of one formate adspecies via C-H bond cleavage produced a "hot" hydrogen atom which inserted itself between the carbon atom and oxygen atom of a neighboring formate adspecies. This ruptures that C-O bond producing CO as well as hydroxyl adspecies and hydrogen and oxygen adatoms. This produced desorption of CO_2, H_2, and H_2O between 330 K and 395 K, desorption-limited CO above 400 K and a small amount of atomic oxygen which did not desorb. The increasing temperature of the autocatalytic desorption was explained by attractive interactions between the formate adspecies.

2.5 Palladium

The decomposition of formic acid has been studied on the Pd(100) surface by Jorgensen and Madix [67], and Sander and Erley [68]. Jorgensen and Madix reported the only desorption products to be molecular acid (T_p = 180 K) and CO (T_p = 515 K) following HCOOH adsorption at 80 K. They verified this with HREELS which identified vibrations associated with molecular HCOOH prior to its desorption; a CO loss appeared and remained the only loss after molecular desorption was complete [67]. Sander and Erley report desorption of CO_2 and H_2O (T_p = 180 K), H_2 (T_p = 330-350 K) and CO (T_p = 470 K) prior to the onset of molecular desorption; their FT-IRA spectra, however, revealed only molecular HCOOH vibrations prior to heating to 170 K and only a CO vibration after heating to 190 K. No vibrations were ever observed for formate or formic anhydride [68]. Jorgensen and Madix did observe the presence of formate on an oxygen-predosed Pd(100) surface which produced CO_2 desorption (T_p = 265 K) upon decomposition [67]. Formate was also identified with photoelectron spectroscopy on Pd(100) covered with Na adatoms [69].

2.6 Rhodium

Solymosi et al. have studied the decomposition of HCOOH on Rh(111) using TDS, AES, photoelectron spectroscopy, and electron energy loss (EEL) [27, 70, 71]. Adsorption of HCOOH at 100 K produced desorption of CO_2 (two states,

T_p = 230-255 K and 262-290 K), H_2 (T_p = 323-358 K), H_2O (T_p = 251-263 K), and CO (T_p = 530-537 K). Saturation levels for CO and H_2O were attained at exposures 20-25% of those needed to saturate CO_2 and H_2 desorption. Photoelectron and EEL spectroscopies identified the presence of formate above 150 K; above 240 K formate disappeared and CO emerged. Two formate decomposition reactions were proposed to explain these observations: the majority reaction involved breaking of the formate C-H bond resulting in CO_2 desorption and hydrogen adatoms, while the minority reaction relied on the rupture of a formate C-O bond; this produces CO admolecules and hydrogen and oxygen adatoms, which could combine to produce water desorption. The scheme was similar to that proposed for formate decomposition on Ni(110) and Ru(001). The presence of both atomic oxygen and atomic potassium enhanced the initial dehydrogenation of molecular formic acid and increased the amount of formate produced.

2.7 Silver and gold

Formic acid has not been observed to decompose on clean Ag ; coadsorbed oxygen was needed to initiate deprotonation and produce formate [16, 72]. Barteau et al. report the desorption of H_2 and CO_2 (T_p = 410 K) following adsorption of HCOOH by an oxygen-dosed Ag(110) surface at 300 K; a small amount of molecular HCOOH desorption accompanied this with H_2O

desorption occurring immediately upon adsorption at this temperature [72] (HCOOH adsorption at 100 K allowed observation of this desorption (T_p = 200-210 K) [16]). Similar results were reported for HCOOH adsorption on an oxygen-dosed Au(110) surface. Outka and Madix reported desorption of H_2O (T_p = 200 K, 340 K) and CO_2 (T_p = 340 K); molecular desorption accompanied the desorption features at 340 K, but no H_2 desorption was observed [17]. On both surfaces H_2O desorption with peak temperatures around ca. 200 K was attributed to H_2O resulting from deprotonation of HCOOH with CO_2 desorption produced by decomposition of a surface formate.

Sexton and Madix used HREELS to identify formate as the intermediate formed following reaction between atomic oxygen and molecular HCOOH on Ag(110) [16]. The formate produced following adsorption of HCOOH at 100 K and heating to 175 K exhibited a monodentate configuration. An irreversible conversion to a bridging configuration results from heating the overlayer above 300 K; this was similar to the behavior observed on Cu(100), where the conversion was reported to be reversible [35]. This conversion also possessed a coverage dependence with the bridging configuration observed exclusively at low HCOOH exposures. Increasing exposure resulted in the predominance of the monodentate configuration; this was explained by surface crowding caused by coadsorbed H_2O. Heating to 300 K desorbs H_2O and provided enough energy to

reorient the formate. NEXAFS studies showed the orientation of formate on Ag(110) differed from that on Cu(110) with indications of a molecular plane tilt away from the surface normal and of a lack of azimuthal alignment [73].

Chtaib et al. studied the interaction of HCOOH with the clean (111) and (110) faces of Au utilizing HREELS [74]. They observed no evidence for the presence of formate on the (110) surface after heating the overlayer to temperatures as high as 500 K, but did see loss features indicative of oxygen adatoms at this temperature. On the (110) face the existence of formic anhydride was posited based on the loss spectrum produced after the HCOOH overlayer was heated to 245 K.

2.8 Tungsten and iron

Benziger and Madix have studied the reaction of formic acid with Fe(100) using thermal desorption and X-ray photoelectron spectroscopy (XPS) [75, 76]. They observed simultaneous desorption of CO, CO_2, and H_2 (T_p = 490 K) following adsorption of HCOOH at 160 K; additional desorption states for H_2 (T_p = 350 K) and CO (T_p = 800 K) were reported. XPS identified a symmetrically-bonded formate as the reaction intermediate following loss of the molecular acid's hydroxyl proton. This produced hydrogen adatoms which desorb as H_2 (T_p = 350 K). Formate decomposed above 400 K resulting in the simultaneous

desorption of CO, CO_2, and H_2. This decomposition also yielded oxygen and carbon adatoms which combined and desorbed as CO above 700 K.

Benziger, Ko, and Madix found tungsten to be extremely vigorous in its decomposition of HCOOH [77]. The only desorption product they observed following low HCOOH exposures (< 0.7 L) on W(100) at 300 K and subsequent heating to 800 K was H_2; AES identified the surface to be covered by oxygen and carbon adatoms following this desorption. For higher exposures simultaneous desorption of CO_2, H_2, and H_2O occurs (T_p = 580 K); this desorption was attributed to decomposition of a formate adspecies. The buildup of adatoms on the surface diminished its ability to completely dissociate the molecular acid resulting in the production of formate. This was confirmed by the production of formate at lower HCOOH exposures on a W(100) - (5 x 1)C surface. Bhattacharya suggested molecular formaldehyde and formyl, in addition to formate, as possible reaction intermediates on clean W(100) based on an ultraviolet photoelectron spectroscopic (UPS) study [78].

3. Summary

Formic acid generally reacts with transition metal in three steps: molecular adsorption, reaction of the molecular acid to form a surface intermediate, and decomposition of this intermediate. Molecular HCOOH adsorbs in configurations which resemble its solid phase (hydrogen-bonded chains) and gas phase (dimer pairs) forms. The molecular acid then is dehydrated or dehydrogenated by the metal; on more inert metals, like Ag and Au, this step occurs only in the presence of coadsorbed atomic oxygen. Dehydrogenation leads to the a formate intermediate, HCOO, while dehydration can lead to either formate or anhydride, OCHOHCO. Decomposition of the anhydride leads to desorption of CO_2, H_2, and CO, while formate has two proposed pathways: C-H bond cleavage, producing CO_2 and hydrogen adatoms, or C-O bond cleavage, producing CO and oxygen and hydrogen adatoms

Formate is the more commonly observed intermediate, being the only species identified on Cu, Pt, Ru, Pd, Rh, Ag, and Fe by vibrational and photoelectron spectroscopies. On Ni formate and anhydride have been reported and anhydride has also been observed on Au. On W formate, formaldehyde and formyl have all been suggested.

No CO desorption occurs from Au, Ag or Cu surfaces indicating that C-H bond cleavage is the only path available to formate decomposition; it is the predominant path on Pt and Rh. C-O bond cleavage reaches the probability level of C-H bond cleavage on Ru, Ni and Fe; this produces CO/CO_2 ratios of about one. Decomposition of anhydride produces a similar ratio. Intermediate decomposition on clean Pd is less easily explained owing to the lack of an obvious transition between molecular HCOOH and CO monitored by HREELS. W proves to be most vigourous toward decomposition leading to a large production of atomic species.

Explanation of Dissertation Format

This dissertation is arranged according to the alternate style format. Five papers are included. Section I, "The Reaction of Formic Acid with Clean and Water-Covered Pt(111)" appears in Volume 235 of Surface Science on pages 53-59, 1990. Section II, "The Coverage and Temperature Dependences of Adsorbed Formic Acid and Its Conversion to Formate on Pt(111)", is accepted for publication in the Journal of the American Chemical Society. Section III, "The Overlayer Structure of Coadsorbed Formic Acid and Water on Pt(111)", has been submitted to Surface Science. Section IV, "The Effect of Coadsorbed Atomic Oxygen on the Interaction of Formic Acid and Pt(111)", will be submitted to the Journal of Chemical Physics. Section V, "The Influence of Coadsorbed Carbon Monoxide on the Decomposition of Formic Acid on Pt(111)", will be submitted to the Journal of Electroanalytical Chemistry and Interfacial Phenomena. Appendix I appears in Volume 58 of Review of Scientific Instrumentation on pages 309-310, 1987. On all the listed sections I was the principal investigator and, with the exception of Section I and Appendix I, I was the principal author. The references compiled on pages 213-218 are only those cited in the Introduction and Conclusions of this dissertation.

SECTION I:

THE REACTION OF FORMIC ACID WITH CLEAN AND WATER-COVERED PT(111)

The Reaction of Formic Acid with Clean and Water-Covered Pt(111)

by

M. R. Columbia and P. A. Thiel*

Department of Chemistry and Ames Laboratory
Iowa State University
Ames, Iowa 50011 USA

Published in *Surface Science,* 235 (1990) 35

Abstract.

We have studied the interaction of formic acid with clean and water-covered Pt(111) in vacuum, using the technique of thermal desorption. We find that formic acid dissociates on clean Pt(111), forming gaseous CO_2 and H_2 exclusively at low exposure. At higher exposure, molecular formic acid begins to desorb at 200 K; simultaneously, the yields of CO_2 and H_2 saturate. At twice this exposure, the 200 K state saturates and multilayer desorption begins in a state centered at 165 K. Coadsorbed water does not measurably influence formic acid adsorption and dissociation. Finally, water is displaced from its own normal, high-temperature state but this displacement is never complete, suggesting that formic acid or its dissociation products may not completely exclude water from metal sites.

1. Introduction

Within the field of surface science, there have been many studies of formic acid and its reactions at metal surfaces (e.g. refs. [1-22]). These studies have been designed to clarify heterogeneous catalytic reactions which involve oxygenated hydrocarbons. However, the electrochemical community is also very active in this area. It is driven by the desire to develop fuel cells which utilize methanol and oxygen, and to identify the self-poisoning reaction which prevents such cells from attaining commercial viability (e.g. refs. [23-25]) Platinum is the best known electrocatalyst for this reaction,and oxidation of formic acid at platinum is believed to produce the same poison as oxidation of methanol [25, 26]. This has motivated many electrochemical studies of formic acid oxidation at platinum, and platinum-group, metals.

We hope to shed light on the fundamental processes which occur in this class of fuel cells, using the techniques of surface science. In this paper we report preliminary results on the reaction of formic acid at clean Pt(111), using thermal desorption spectroscopy. We have also investigated the effect of co-adsorbed water, as a first step toward understanding the role which solvent may play at a real electrode surface.

2. Experimental Details

Details of the experimental apparatus and procedures have appeared, or will appear, elsewhere [27-30]. In brief, the experiments are conducted in a stainless steel ultrahigh vacuum chamber, base pressure typically 1 to 2 x 10^{-10} Torr. The chamber is equipped with a cylindrical mirror analyzer and coaxial electron gun for Auger electron spectroscopy, an ion bombardment gun, and an electron energy loss spectrometer. During thermal desorption of gases, the partial pressures of up to eight different ions are monitored (effectively simultaneously) using a computer-interfaced, apertured quadrupole mass spectrometer. The sample is exposed to formic acid through a gas doser consisting of a conductance-limiting aperture, and a spatially-collimating aperture, in series. This doser is designed to be used with gas pressures of 100 mTorr or below in the backing line, thus avoiding dimerization of formic acid in the gas phase [18]. Water exposure is achieved with a different gas doser, used with pressures of about 18 Torr behind the conductance-limiting aperture. Exposures are reported in units of Torr-s, the product of the average pressure behind the conductance-limiting aperture during the dose and the length of the exposure. An exposure of 25 Torr-s of CO, obtained with the doser, is equivalent

to 1 Langmuir obtained by backfilling the chamber, based upon desorption peak areas. In other words, the effective pressure at the sample is 4×10^{-8} Torr using the doser, while the pressure in the chamber never rises above 7×10^{-10}. The sample is held at temperatures of 80 to 100 K during all exposures.

The Pt crystal is cut and polished using established metallurgical techniques and aligned to within 0.5^{o} of the (111) face as verified by Laue diffraction. Initial cleaning in vacuum involves several cycles of heating to 1200 K and ion bombardment (400 eV in 5×10^{-5} Torr Ar). This procedure significantly reduces all contaminant levels except carbon. Carbon is removed by prolonged heating; up to 1000 K, in 1×10^{-6} Torr O_2 followed by flashes in vacuum to 1600 K. Auger electron spectroscopy and reproduction of published thermal desorption results for H_2, CO, O_2 and H_2 [31-34] serve to verify surface cleanliness. Carbon which accumulates overnight is removed by heating in 1×10^{-7} Torr O_2 at 1100 K followed by flashing to 1600 K to remove oxygen. Cleaning between thermal desorption experiments consists of exposing the crystal to 1 L O_2 at 1100 K followed by heating in vacuum to 1600 K.

3. Results

Exposure of formic acid to clean Pt(111) at low temperature and heating leads to desorption of H_2 (m/e =2), CO_2 (m/e = 44), and HCOOH (m/e = 29 and 44). Figure 1 illustrates thermal desorption traces for these three products, obtained after various exposures of formic acid. We do not observe generation of H_2O (m/e = 18) or CO (m/e = 28), other than that which can be attributed to fragmentation of formic acid within the mass spectrometer ionizer.

Figures 1A and 1B illustrate that CO_2 and H_2 evolve from the surface even after the very shortest exposures. (The small features in the range 170-200 K, visible after 10 Torr-sec exposure in Fig. 1B, are probably due to fragmentation of molecular formic acid within the mass spectrometer ionizer. Compare these small features with the data of Fig. 1C.) The desorption peak temperature of CO_2 is invariant, within experimental error, at 260 $\pm$ 3 K, and that of hydrogen decreases from 390 to 365($\pm$ 2) K. Based upon previous work by Avery, gaseous CO_2 is probably released immediately upon dissociation of adsorbed formate species, i.e. desorption of CO_2 is reaction-rate limited [1, 2]. By contrast, hydrogen evolution appears to be desorption-rate-limited, rather than reaction-rate-limited, based on the fact that the positions and shapes of the hydrogen

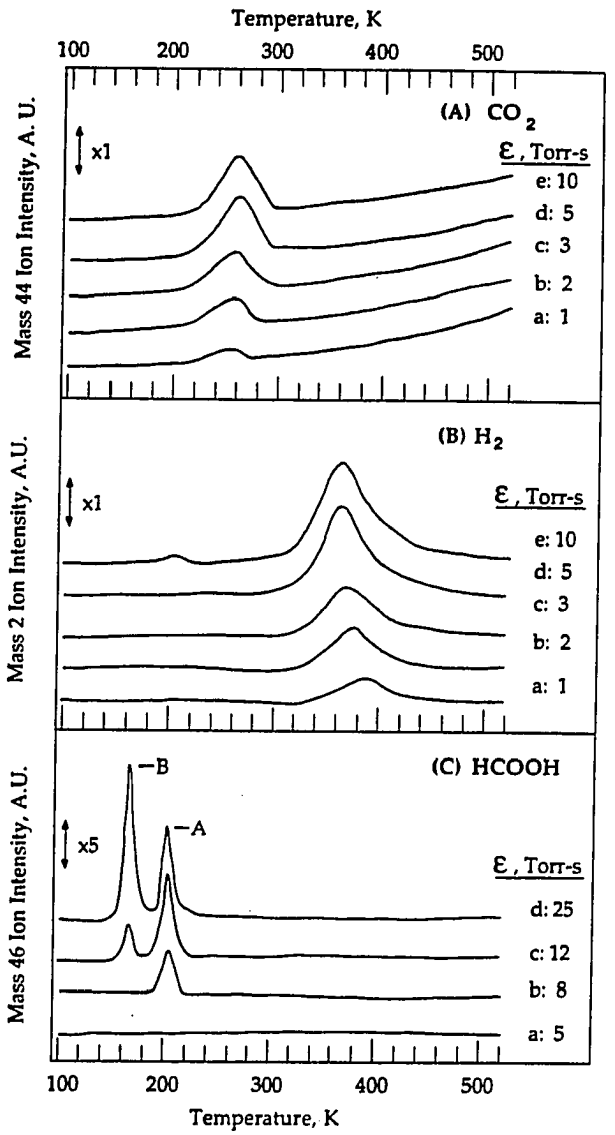

Figure 1. Thermal desorption traces of various gases following adsorption of formic acid at 80 to 100 K. The heating rate is constant at 11 K/s between 100 and 200 K, and drops continuously to 5.5 K/s at 350 K. (A) M/e = 44, CO_2 desorption traces. (B) M/e = 2, H_2 desorption traces. (C) M/e = 46, HCOOH desorption traces.

desorption traces compare favorably with those obtained by other authors following hydrogen adsorption on clean Pt(111) [31, 32]. We estimate that the saturation coverage of hydrogen produced by formic acid decomposition is about 10 to 20% of a saturation hydrogen coverage on Pt(111). Assuming absolute coverage of hydrogen at saturation is unity [32, 35], this corresponds to 0.1 to 0.2 monolayers of hydrogen and 0.05 to 0.1 monolayers of parent formic acid.

Inspection of Figs. 1A and 1B reveals that, at exposures below 4 Torr-s, the yields of H_2 and CO_2 increase with increasing exposure. Figure 1C shows that in this same exposure range, there is no desorption of molecular formic acid. Between about 4 and 6 Torr-s (~0.2 Langmuir equivalents), the yields of H_2 and CO_2 saturate. At exactly the same exposure, desorption of molecular formic acid begins, in a state centered at 200 $\pm$ 2 K. The peak position is invariant with increasing exposure. This state (which we label A) continues to intensify until about 10 Torr-s (about 0.4 Langmuir equivalents), where a lower-temperature state appears. The latter state, which we label B, is centered at about 165 K, and we assign it to sublimation from a bulk-like multilayer (condensed phase). Note that the exposure at which the B-state appears, and the A-state saturates, is just *twice* the exposure at which the A-state appears, and the CO_2 and H_2 yields saturate. If we assume constant sticking coefficient, then these data indicate that

the number of formic acid molecules which dissociate to CO_2 and H_2 is the same as that required to saturate the molecular A-state.

The exposure-dependence of the desorption yields is shown more clearly in Fig. 2, where the integrated areas of various thermal desorption features are illustrated as a function of exposure for clean Pt(111).

We have also investigated the role which coadsorbed water plays in adsorption and decomposition of formic acid on Pt(111). Fisher and Gland (FG) have previously reported that thermal desorption of water from Pt(111) occurs in two main states, centered at 170-180 K and at 160 K [33]. We have reproduced their work, and agree with the major aspects of their results. For the clean Pt surface, we also observe two main states, one centered at 175 K (this shifts upward as exposure increases, by about 5 K) and the other first appears at 150 K (again, this shifts upward with increasing exposure). The state at 180 K has also been described by Wagner and Moylan [34]. FG's interpretation, and ours, is that the 175-180 K state represents a water layer (or layers) stabilized by interaction with the metal surface, whereas the 150 K state is due to multilayer sublimation [33, 36]. We have repeated the experiments illustrated in Figs. 1 and 2, substituting a water-covered surface for the clean metal. The coverage of water which we use is sufficient to populate the 175-180 K state of H_2O, and just below

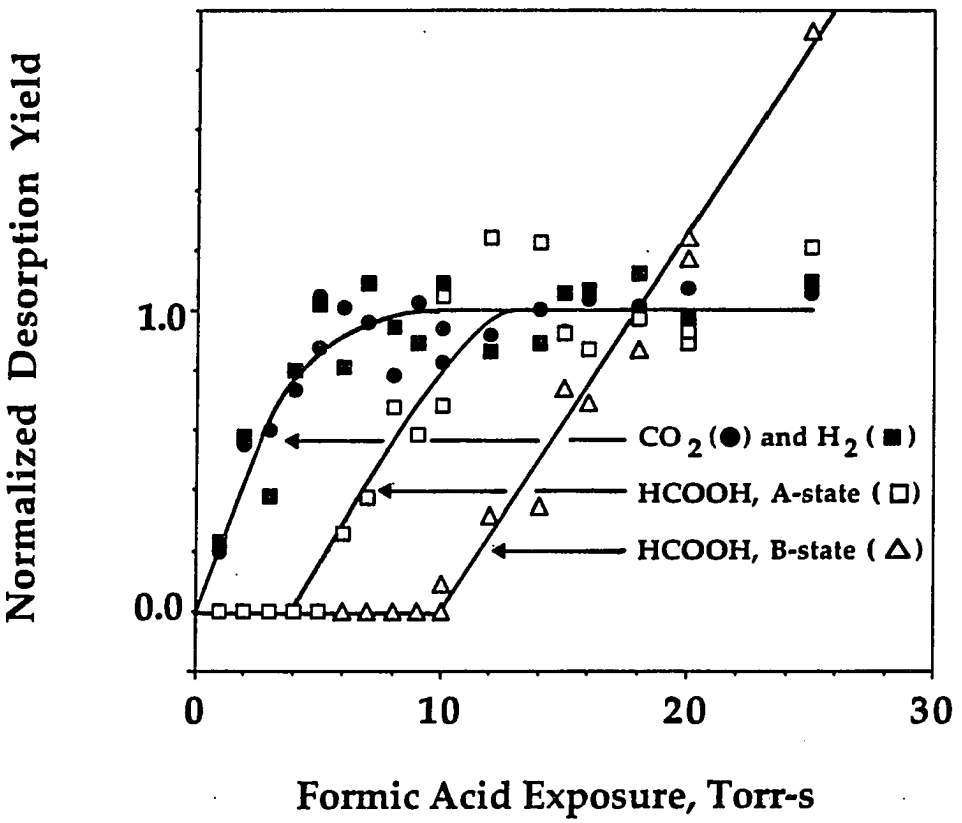

Figure 2. Desorption yields (integrated desorption peak areas) of CO_2, H_2, and the A- and B-states of formic acid as a function of formic acid exposure on clean Pt(111), derived from data such as shown in Fig. 1, following adsorption of HCOOH on clean Pt(111). The yields of CO_2, H_2, and A-state HCOOH are independently normalized to unity at saturation. The yield of the B-state of HCOOH is multiplied by the same factor as the A-state of HCOOH, even though the B-state does not saturate.

that necessary for the H_2O multilayer state to emerge. We find that adsorption and desorption of formic acid are not affected in any major way by the presence of coadsorbed water. Specifically, both H_2 and CO_2 are again observed as decomposition products, and are the only gas-phase products (except for H_2O) below about 4 Torr-s exposure. The temperatures of the desorption peak maxima at saturation are within $\pm$ 2 K of their corresponding values on clean Pt(111). The saturation yields of H_2 and CO_2 are independent of water, within experimental error. This is shown by Fig. 3, where the CO_2 yield as a function of exposure is compared for the clean surface and the water-covered surface. No CO is released, indicating that water does not change the decomposition pathway. At exposures past saturation of the H_2 and CO_2 desorption yields, both the A and B states are observed, at the same temperatures (to within $\pm$ 2 K) as on the clean surface. Their relative intensity is changed by the presence of the water, indicating that water may interfere with these more weakly-bound states of formic acid. The main point, however, is that pre-adsorbed water does not hinder adsorption and decomposition of formic acid in any measurable way.

Water itself is affected by formic acid quite markedly. As formic acid exposure increases, water is progressively displaced from its high-temperature

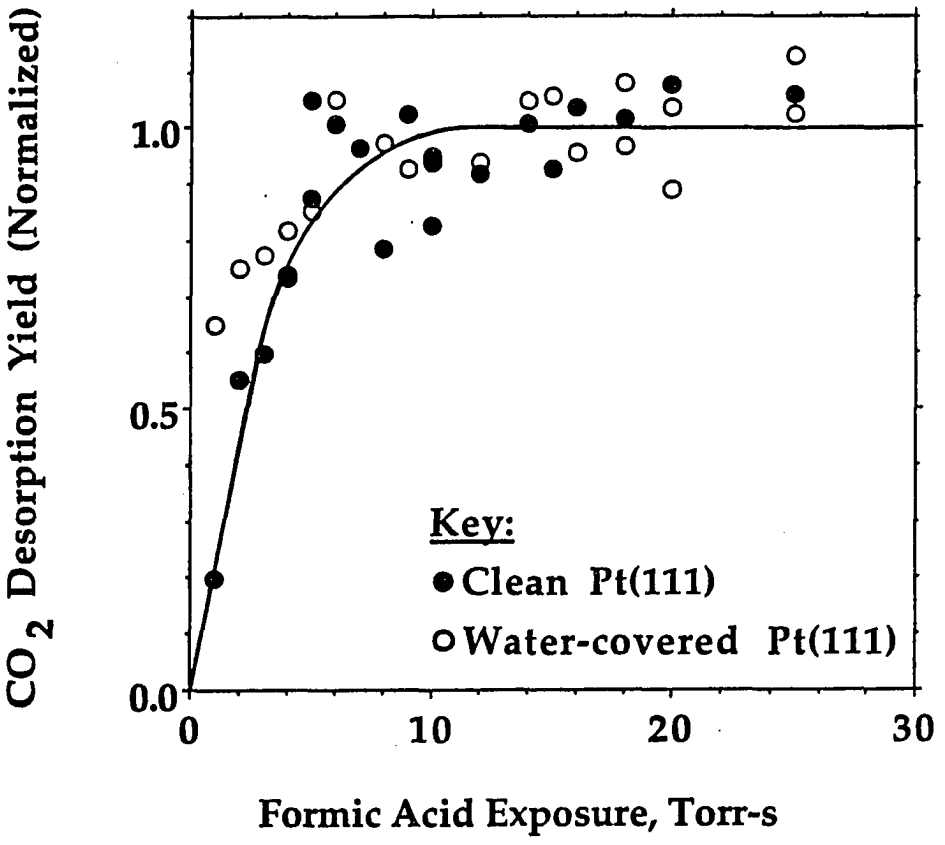

Figure 3. Desorption yields (integrated desorption peak areas) of CO_2 as a function of exposure, following adsorption of formic acid on clean and water-covered Pt(111). The yields are normalized to unity at saturation. The same normalization factor is used for both sets of data, i.e. the saturation yield of CO_2 is virtually independent of water.

desorption state to its low-temperature, multilayer state. (The latter is not populated at all in the absence of formic acid, at this selected coverage.) This displacement is illustrated in Fig. 4. The peak temperatures of both water states may be shifted upward by as much as 5 K in the presence of formic acid, but this effect is in any case very small. In other experiments, we have confirmed that the displacement occurs also when water is isotopically labelled, i.e. the data of Fig. 4 are reproduced very closely when D_2O is substituted for H_2O.

Displacement proceeds until the ratio of peak heights (multilayer : first layer) reaches a constant value, in these experiments, of 2; in other experiments, the value falls between 2 and 3.

4. Discussion

4.1 Formic acid adsorption on clean Pt(111)

There have been three other studies of formic acid adsorption on Pt(111) surfaces [1-3, 33, 36]. In two, Avery used electron energy loss spectroscopy to identify adsorbed formate at temperatures of 130-260 K, both on clean and oxygen-dosed Pt(111) [1, 2]. Formate has been observed spectroscopically on

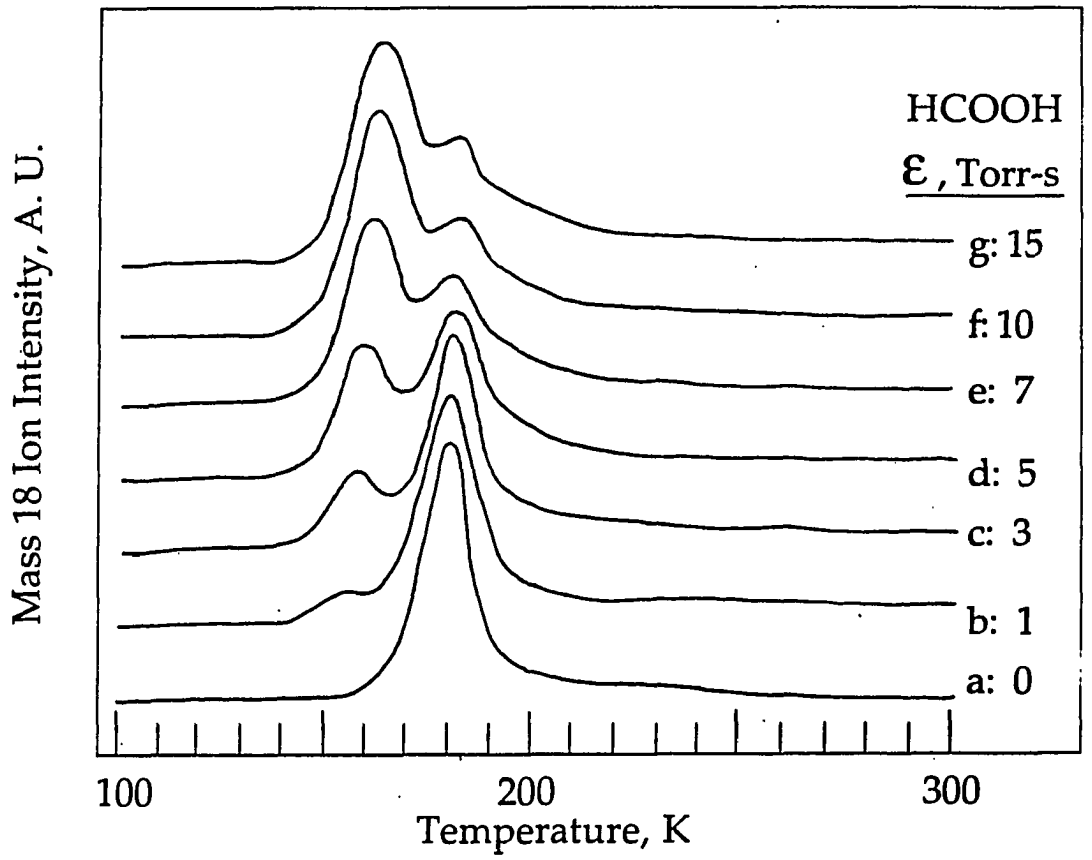

Figure 4. Desorption traces of H_2O (m/e = 18) following adsorption of formic acid on water-covered Pt(111). The exposure of water is constant, while the exposure of formic acid varies as indicated by the labels.

Pt(110) at 155 K [4], and on other surfaces of other metals, including Ag, Cu, Ni, Rh, and Ru (e.g. refs. [5-15, 19, 20]). Several reaction schemes have been proposed for the formation, and/or decomposition, of this formate intermediate. These mechanisms can be broadly divided into dehydrogenation to gaseous H_2 and CO_2, and dehydration to gaseous H_2O and CO [13, 16, 17]. Thus, the identification of the gaseous dissociation products is important to determine which of these broad classes of mechanisms is operative.

The identity of the gas-phase products of formic acid adsorption on clean Pt(111) is controversial. On clean Pt(111), Avery has described CO_2 (with T_p, desorption peak temperature, = 260 K) and H_2 (T_p = 370 K) as desorption products, following adsorption at 130 K. (Although Avery also observes gaseous CO, he attributes this to desorption from the edges and back of the crystal, since electron energy loss spectroscopy fails to detect chemisorbed CO on the front face.) This result would indicate that formic acid only dehydrogenates on Pt(111). Abbas and Madix (AM), however, report CO and H_2O as additional desorption products from clean Pt(111), following exposure at 200 K [3]. They propose that one out of every four formic acid molecules dissociates via dehydration at saturation coverage.

Our work is a more complete description of the desorption products of formic acid on clean Pt(111), and the conditions of exposure necessary to produce them, than has been previously published [1-3]. Using an apertured mass spectrometer to reduce or eliminate spurious desorption features, we observe no evolution of CO on clean Pt(111) at any exposure. On this point we are in agreement with Avery [1, 2]. This suggests that formic acid dehydrogenates, but does not dehydrate, on Pt(111).

Furthermore, our peak temperatures for H_2 and CO_2 agree well with those of Avery, while the hydrogen peak temperatures reported by AM at saturation are 44-56 K lower than ours [3]. The lower peak temperatures reported by AM are consistent with the fact that AM report excess hydrogen adsorption from the background, which would lead to a higher hydrogen coverage than in our work. This could also be related to the observation of CO and H_2O as dissociation products in AM's experiments, since excess adsorbed hydrogen (a dehydrogenation product) might shift the reaction equilibrium significantly in favor of dehydration.

Our work, showing no CO as a vacuum decomposition product of formic acid, contrasts with electrochemical research, where CO has been identified in-situ as an adsorbed by-product of formic acid oxidation on polycrystalline Pt

surfaces (e.g. refs. [37, 38]). Our work also contrasts with recent results by Kizhakevariam and Stuve [39], who find *no* decomposition on Pt(100). These comparisons suggest that the decomposition pathway of formic acid may be quite structure-sensitive on Pt surfaces, and/or dependent upon differences in the chemical environment such as those provided in the electrochemical cell.

Another discrepancy in the published literature regards the molecular desorption of formic acid. Avery observes molecular desorption of HCOOH only at T_p = 170 K, following exposure at 130 K [1, 2]. Abbas and Madix report desorption of molecular formic acid, T_p = 235 K, following exposure at 200 K. We do not observe the 235 K state reported by AM at any exposure, although in our experiments adsorption takes place at considerably lower temperature, 80-100 K. We do observe the 170 (165) K state of Avery, and an additional state at 200 K. There have been similar reports of two desorption states, at ~170 K and 190-210 K, on other surfaces. These include Ag(110) [5], Au(110) [22], and Rh(111) [19]. The low temperature state is unanimously attributed to multilayer sublimation, while the high temperature state (which always saturates with increasing exposure) is usually attributed to a first (non-dissociative) layer.

We propose two possible explanations for our molecular state at 200 K. One is that formic acid layers grow sequentially on the surface. The first layer, in

direct contact with the metal, dissociates to formate and hydrogen, perhaps upon adsorption at 80 K, but at least by 130 K [1, 2]. The formate decomposes further at about 260 K, yielding CO_2 as a direct gas-phase product at this temperature. The acyl hydrogen must be released simultaneously to form additional adsorbed hydrogen but the atomic hydrogen does not combine and desorb until higher temperatures (365-390 K) because the adsorption bond strength of hydrogen is much higher than that of CO_2. When the first dissociative layer is saturated, at exposures between 4 and 6 Torr-s, a second layer begins to fill. Upon heating, this layer desorbs, without dissociation, in the A-state. After the second layer is filled, at about 10 Torr-s, the multilayer appears and grows. This hypothesis of sequential layer filling is supported by the data of Fig. 2, if one assumes a constant sticking coefficient, and that the space occupied by a second-layer formic acid molecule is about the same as that occupied by an adsorbed formate particle of formate-precursor. Under these assumptions, it is reasonable that the formic acid exposure necessary to saturate the first layer (as measured by the yields of CO_2 and H_2) should be just half that necessary to saturate the second layer (as measured by the yield of the molecular A-state). The coverage within each layer then equals 0.05 to 0.1 monolayers. Larson and Dickinson also proposed this hypothesis to explain similar behavior, which they observed on Ru(100) [21].

The second possibility is that the A-state represents formic acid molecules which are in direct contact with the metal, but which intermingle with adsorbed formate, or formate-precursor. This model resembles those which have been proposed for the other metallic surfaces with states analogous to the A-state (e.g. refs. [5, 19, 22]). Making the same assumptions as those described above, the data of Fig. 2 then suggest that there is a 1 : 1 stoichiometry between the molecules which eventually dissociate, and those which do not, within the first layer.

4.2 Adsorption on water-covered Pt(111)

Ours is the first study of the interaction between formic acid and water on a metal surface. We find that water does not measurably hinder adsorption and dissociation of the acid. Further, the absence of CO evolution both with and without water indicates that water does not change the dissociation pathway of the acid, i.e. dehydrogenation still occurs but not dehydration. These results suggest that water probably exerts little influence on formic acid chemistry at a Pt surface in aqueous solution.

We also find that water is displaced from its metal-stabilized, high-temperature state to its multilayer, low-temperature state by the acid. The water

coverage used is sufficient to saturate the high-temperature state but not sufficient to initiate the low-temperature state in the absence of formic acid. Subsequent adsorption of formic acid displaces water from the high-temperature state to the low-temperature state until the ratio of peak heights between these two states reaches a value of two. This intriguing result suggests that there may be empty "pockets" in a well-ordered first layer formed by the adsorption products of formic acid, into which water molecules can fit without interference. Alternatively, there may be a specific, stoichiometric hydrogen-bonded complex which forms between the first layer formic acid products and the water molecules. This will be the subject of continuing investigation in our laboratory.

5. Summary

We find that formic acid dissociates on clean Pt(111), forming gaseous CO_2 and H_2 exclusively at low exposure. At higher exposure, molecular formic acid begins to desorb at 200 K; simultaneously, the yields of CO_2 and H_2 saturate. At twice this exposure, the 200 K state (the A-state) saturates and multilayer desorption begins. Assuming constant sticking coefficient, this means that the

number of molecules necessary to saturate the dissociative state equals that necessary to saturate the molecular A-state. The A-state may represent a second layer, or formic acid molecules intermixed with dissociation products (formate plus hydrogen) or their precursors, in the first layer.

Coadsorbed water does not measurably inhibit formate adsorption and dissociation. It also does not change the decomposition pathway, judging by the constant distribution of decomposition products. (CO_2 and H_2, but not CO, are evolved.) Finally, water itself is displaced from its high-temperature state but this displacement is never complete, suggesting that formic acid or its dissociation products may not completely exclude water from metal sites.

Acknowledgments

We thank P. K. Leavitt for generous assistance and cooperation in using the experimental equipment. We thank E. M. Stuve for providing ref. [39] prior to its publication. Acknowledgement is made to the Donors of the Petroleum Research Fund, administered by the American Chemical Society. Some equipment and all facilities are provided by the Ames Laboratory, which is operated for the U. S. Department of Energy by Iowa State University under Contract No. W-7405-ENG-82.

References

1. N. R. Avery, App. Surf. Sci., 11/12 (1982) 774

2. N. R. Avery, App. Surf. Sci, 14 (1982-83) 149

3. N. Abbas and R. J. Madix, App. Surf. Sci., 16 (1983) 424

4. P. Hofmann, S. R. Bare, N. V. Richardson and D. A. King, Surf. Sci., 133 (1983) L459

5. B. A. Sexton and R. J. Madix, Surf. Sci., 105 (1981) 177

6. B. A. Sexton, Surf. Sci., 88 (1979) 319

7. M. Bowker and R. J. Madix, Surf. Sci., 102 (1981) 542

8. B. E. Hayden, K. Prince, D. P. Woodruff and A. M. Bradshaw, Surf. Sci., 133 (1983) 589

9. J. Stœhr, D. A. Outka, R. J. Madix and U. Dœbler, Phys. Rev. Lett., 54 (1985) 1256

10. L. H. Dubois, T. H. Ellis, B. R. Zegarski and S. D. Kevan, Surf. Sci., 172 (1986) 385

11. M. D. Crapper, C. E. Riley, D. P. Woodruff, A. Puschmann and J. Haase, Surf. Sci., 171 (1986) 1

12. P. Hofmann and D. Menzel, Surf. Sci., 191 (1987) 353

13. R. J. Madix, J. L. Gland, G. E. Mitchell and B. A. Sexton, Surf. Sci., 125 (1983) 481

14. T. S. Jones and N. V. Richardson, Phys. Rev. Lett., 61 (1988) 1752

15. T. S. Jones, M. R. Ashton and N. V. Richardson, J. Chem. Phys., 90 (1989) 7564

16. J. McCarty, J. Falconer and R. J. Madix, J. Cat., 30 (1973) 235

17. J. B. Benziger and R. J. Madix, Surf. Sci., 79 (1979) 394

18. J. B. Benziger and G. B. Schoofs, J. Phys. Chem., 88 (1984) 4439

19. F. Solymosi, J. Kiss and I. Kovacs, Surf. Sci., 192 (1987) 47

20. N. R. Avery, B. H. Toby, A. B. Anton and W. H. Weinberg, Surf. Sci., 122 (1982) L574

21. L. A. Larson and J. T. Dickinson, Surf. Sci., 84 (1979) 17

22. D. A. Outka and R. J. Madix, Surf. Sci., 179 (1987) 361

23. J. O. Bockris and S. Srinivasan, Fuel Cells: Their Electrochemistry (McGraw-Hill, New York, 1969)

24. M. W. Breiter, Electrochemical Processes in Fuel Cells (Springer, Berlin 1969)

25. B. D. McNicol, in: The Electrocatalysis of Fuel Cells Reactions, Eds. W. E. O'Grady, S. Srinivasan and R. F. Dudley (The Electrochemical Society, Princeton, NJ, 1978) pp. 93-113

26. R. R. Adzic, in: Advances in Electrochemistry and Electrochemical Engineering, Vol. 13, Ed. H. Gerischer (Wiley, New York, 1984) pp. 159-260

27. M. R. Columbia and P. A. Thiel, Rev. Sci. Instrum., 58 (1987) 309

28. M. R. Columbia and P. A. Thiel, Proc. DOE Workshop -Direct Methanol/Air Fuel Cells, to be published

29. P. K. Leavitt, J. L. Davis, J. S. Dyer and P. A. Thiel, Surf. Sci., 218 (1989) 346

30. P. A. Thiel and J. W. Anderegg, Rev. Sci. Instrum., 55 (1984) 1669

31. D. M. Collins and W. E. Spicer, Surf. Sci., 69 (1977) 85

32. K. Christmann, G. Ertl and T. Pignet, Surf. Sci., 54 (1976) 365

33. G. B. Fisher and J. L.Gland, Surf. Sci., 94 (1980) 446

34. F. T. Wagner and T. E. Moylan, Surf. Sci., 206 (1988) 187

35. P. R. Norton, J. A. Davies and T. E. Jackman, Surf. Sci., 121 (1982) 103

36. B. A. Sexton, Surf. Sci., 94 (1980) 435

37. K. Kunimatsu and H. Kita, J. Electroanal. Chem., 218 (1987) 155

38. D. S. Corrigan and M. J. Weaver, J. Electroanal. Chem., 241 (1988) 143

39. N. Kizhakevariam and E. M. Stuve, J. Vac. Sci. Technol. A, 8 (1990) 235

SECTION II:

THE TEMPERATURE AND COVERAGE DEPENDENCES OF ADSORBED FORMIC ACID AND ITS CONVERSION TO FORMATE ON PT(111)

The Temperature and Coverage Dependences of Adsorbed Formic Acid and Its Conversion to Formate on Pt(111)

by

M. R. Columbia, A. M. Crabtree, and P. A. Thiel

Department of Chemistry and Ames Laboratory
Iowa State University
Ames, IA 50011 USA

Accepted for publication in the *Journal of the American Chemical Society*

Abstract

We have studied the adsorption of HCOOH on Pt(111) at 100 K and its conversion to formate with increasing surface temperature. The techniques employed are thermal desorption spectroscopy and high resolution electron energy loss spectroscopy. At very low exposures (<< 0.2 L) we conjecture that HCOOH adsorbs molecularly as monomers. As exposure increases these monomers form hydrogen-bonded chains with the molecular plane of HCOOH nearly parallel to the surface. At an exposure of 0.2 L these chains resemble the solid phase β-polymorph as indicated by the vibrational frequencies of the OH out-of-plane bending vibration. Heating this surface causes the chains to break apart into discrete dimer pairs, followed by deprotonation to a bridging formate adspecies. The formate decomposes between 210 K and 280 K, causing CO_2 desorption and leaving hydrogen adatoms. Increasing the exposure above 0.6 L causes the chains to adopt a structure similar to the denser α-polymorph. Heating this surface causes molecular desorption in two states. One is centered at 160 K and is dominated by gaseous HCOOH dimers. Desorption in this state leaves bridging formate and β-polymorphic HCOOH coexistent on the surface. The other is centered at 200 K and is primarily gaseous monomers. Desorption in this state leaves only the formate

adspecies Its decomposition then proceeds as on the surface exposed to 0.2 L HCOOH.

1. Introduction

The adsorption of formic acid (HCOOH) on transition metal surfaces and its subsequent reactions are ongoing interests within the surface scientific community. The majority of studies focus on the decomposition intermediates of the acid and their ultimate products [1-18]. Decomposition can occur via dehydrogenation, as on Pt[1-4] and Cu[5-7] or by a combination of dehydrogenation and dehydration, as on Ni[8-15] and Ru[16-18]. The most commonly observed intermediate is formate in a bridging configuration (bonding through the oxygen atoms to two surface atomic sites), although formic anhydride has recently been identified on Ni(111) using IR spectroscopy[15].

Far fewer studies deal with the topic of this paper, molecular adsorption of HCOOH and its conversion to formate[19-23]. These studies involve more inert metals such as Ag[19, 20] and Au[21, 22]. Thermal desorption from these surfaces shows only molecular desorption, which appears in 2 states at 160-180 K and 190-210 K, attributed to multilayer and first layer desorption, respectively. High resolution electron energy loss (HREEL) spectra show that conversion to formate occurs in the presence of coadsorbed atomic oxygen, but no HREEL spectra have been reported for formate on the clean surfaces of these

metals. Vibrational spectra of the molecular acid indicate that, upon adsorption, the molecules form hydrogen-bonded structures similar to gas-phase dimers on Cu(100) [6] and Au(111) [21] and solid-phase catameric chains on Pt(111) [2] and Au(110) [21]. Vibrational spectra of acetic acid adsorbed on Pd(111) [24] and Pt(111) [25, 26] show evidence of similar hydrogen-bonded structures.

Joyner and Roberts [23] have used photoelectron spectroscopy to compare acid-to-formate conversion on polycrystalline surfaces of Cu, Ni, and Au. They demonstrate similar temperature-dependent changes in the photoelectron spectra for HCOOH on all 3 metals. Their subsequent interpretation presents a common scheme of molecular acid-to-formate conversion involving (1) the formation of hydrogen-bonded chains following adsorption at 80 K; (2) the breaking of hydrogen bonds between 120 K and 150 K; and (3) the loss of the hydroxyl proton to the surface accompanied by reorientation to give a formate adspecies with its molecular plane perpendicular to the surface between 150 K and 170 K. This adspecies is stable on Cu and Ni eventually decomposing to give CO_2 and H_2; however, owing to its lower stability on Au, recombinative desorption occurs instead above 170 K.

We have studied the interaction of HCOOH with clean Pt(111) using thermal desorption spectroscopy (TDS) and high resolution electron energy loss

spectroscopy (HREELS) in order to better characterize the coverage and temperature dependence of the molecular acid-to-formate conversion on this surface. We have previously reported desorption of molecular HCOOH and decomposition products (CO_2 and H_2) from a saturated first layer, as well as additional molecular desorption states for higher exposures[1, 27]. We now present detailed models to explain this desorption behavior and the observed temperature and coverage dependent changes in our HREEL spectra based on comparison to vibrational spectra of HCOOH in the gas phase[28, 29] and solid phase[29-31], as well as adsorbed formate on Pt(111)[2, 3].

2. Experimental Details

The ultrahigh vacuum system, the method of performing thermal desorption experiments, and the Pt(111) crystal used for these experiments have been previously outlined [1, 32, 33]. The exposure units reported in this paper are Langmuir, although the surface is exposed to HCOOH through a directional doser containing a conductance-limiting aperture. We determine the Langmuir equivalence of these exposures based on comparison of CO thermal desorption

areas for exposure via the doser with areas for exposure via backfilling. The conductance of the limiting aperture allows pressures of 100 mTorr to be used in the dosing line; this ensures that HCOOH exposed to the Pt(111) surface is primarily monomeric [34]. We desire this condition to avoid the complications which arise from adsorption of dimeric HCOOH reported by Benziger and Schoofs on Ni(111) [14].

The high resolution electron energy loss spectrometer has also been described previously [33]. The elastic peaks for the experiments we report here have intensities between 50 kHz and 350 kHz and full-widths at half-maxima between 8 and 11 meV (65 cm^{-1} to 89 cm^{-1}). For those experiments which probe the effect of temperature on the vibrational spectrum, exposure temperatures are between 80 and 100 K; the surface is then heated to the indicated temperature at ~5 K/s, followed by determination of the loss spectrum while the surface cools. This method of heating differs from the continuous heating performed in TDS experiments. This difference results in desorption states occurring at higher temperatures than the corresponding changes in the vibrational spectrum.

3. Results

3.1 Thermal desorption

In previous work[1, 27] we have shown that the sequence of appearance of desorption products with increasing HCOOH exposure is: (1) H_2 and CO_2; (2) HCOOH at 200 K; (3) HCOOH at 160-170 K; and (4) HCOOH at 160 K. The first three sets of desorption products each saturate at about the point where the next appears. We observe only H_2 and CO_2 at exposures below 0.3 L; the molecular acid state at 200 K develops between 0.3 and 0.6 L; that at 160-170 K develops between 0.6 and 1.2 L; and a final molecular state at 160 K appears at 1.2 L, then grows without limit. The behavior of the latter suggests that it is a multilayer state. The two exposures which are emphasized in this paper, 0.2 and 0.8 L, fall in the first and third adsorption regimes; they are 0.7 and 2.7 times the exposure necessary to saturate the dissociation products, H_2 and CO_2. Direct measurements of coverage vs. exposure have not been made for this system, and so we present our data in terms of exposures only; all evidence supports the assumption, however, that coverage is an increasing function of exposure at 100 K.

Figs. 1 and 2 display thermal desorption spectra for masses 2, 44, 29, and 47 for Pt(111) at 100 K exposed to 0.2 L and 0.8 L HCOOH, respectively. For an exposure of 0.2 L all adsorbed HCOOH converts to formate. In Fig. 1 we observe primarily the decomposition products CO_2 and H_2. The CO_2 desorption peaked at 260 K is attributed to the decomposition of a surface formate species at 210-280 K with the remaining H adatoms desorbing at 300-400 K, a temperature similar to that observed for a Pt(111) surface exposed to only H_2 [35]. A small amount of molecular desorption occurs between 200 K and 250 K (mass 29 spectrum); this is most probably recombination of surface formate with H adatoms. The mass 47 spectrum has no features at this exposure.

For 0.8 L exposure the surface produces molecular desorption, as well as CO_2 and H_2 desorption. At this exposure, features at 160 K and 200 K in the spectra for masses 29 and 47 (Fig. 2), indicate molecular desorption. There is a marked difference in these spectra regarding the intensities of these features. In the mass 29 spectrum the 200 K feature is the more intense with 3 times the desorption area of the 160 K feature. Just the opposite occurs in the mass 47 spectrum with the 160 K spectrum having a desorption area 6 times that of the 200 K feature. There is little change in the desorption features for masses 44 and 2.

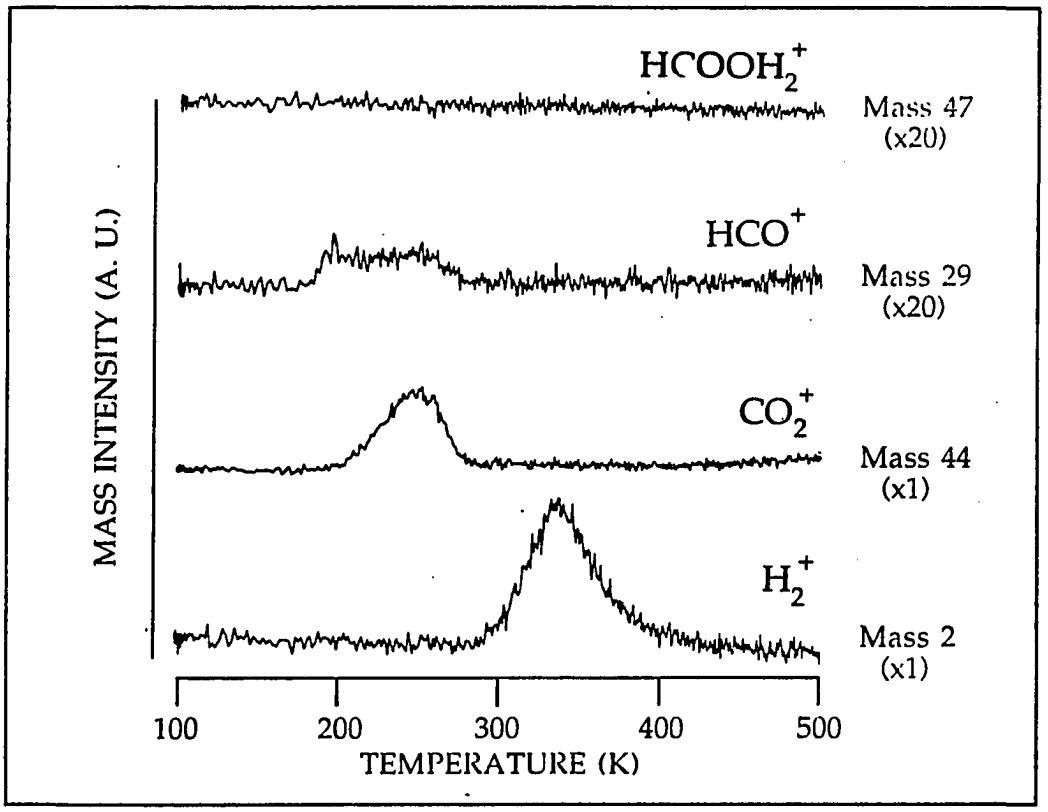

Figure 1. Thermal desorption traces of H_2^+, CO_2^+, HCO^+, and $HCOOH_2^+$ following exposure of 0.2 L HCOOH at 100 K. The heating rate is 6.2 K/s at 100 K and drops continuously to 1.9 K/s at 500 K. (HCO^+ monitors monomeric HCOOH desorption and $HCOOH_2^+$ monitors dimeric HCOOH desorption.)

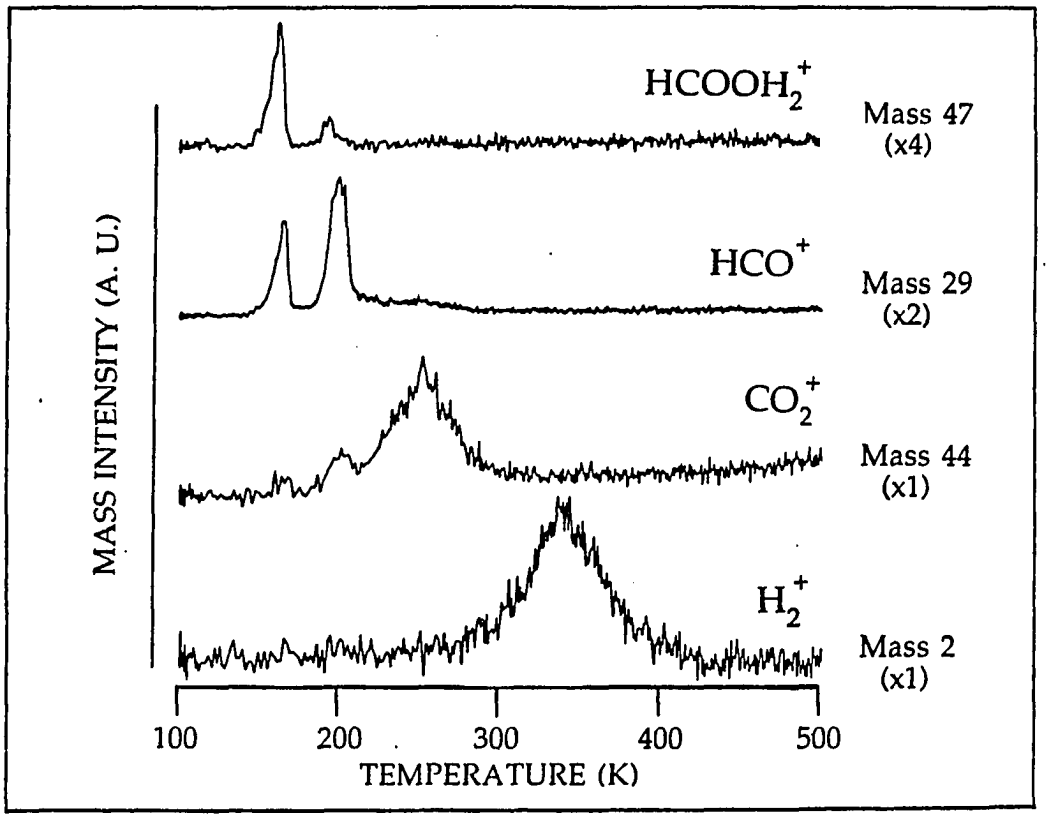

Figure 2. Thermal desorption traces of H_2^+, CO_2^+, HCO^+, and $HCOOH_2^+$ following exposure of 0.8 L HCOOH at 100 K. The heating rate is 6.2 K/s at 100 K and drops continuously to 1.9 K/s at 500 K. (HCO^+ monitors monomeric HCOOH desorption and $HCOOH_2^+$ monitors dimeric HCOOH desorption.) The small offset between the mass 47 and 29 peaks at 160 K may be an experimental artifact; the larger offset at 200 K probably indicates that dimer desorption precedes monomer desorption in this state.

3.2 High resolution electron energy loss spectroscopy

Figures 3 and 4 show HREEL spectra which contain all loss features observed in this system, thus serving as a basis for the mode assignments. Fig. 3 is obtained after exposing Pt(111) at 100 K to 0.8 L HCOOH followed by heating to 130 K. Under these conditions, we assign all loss features to molecularly-adsorbed acid. At 130 K there is better surface ordering than at 100 K (ascertained from the quality of the elastic conditions for the two temperatures) but the heating produces no desorption from the surface. Fig. 4 shows the HREEL spectrum for the same exposure followed by heating to 190 K. By this temperature molecular desorption is complete; all remaining loss features can be assigned to adsorbed formate.

Assignments of the prominent losses are based upon comparison to Avery [2] and are summarized in Fig. 5 for molecular HCOOH (Fig. 3) and bridging formate (Fig. 4). Avery argues convincingly for the assignment of the formate losses to a bridging, rather than mono- or bi-dentate species; the molecular acid adsorbs in a layer structure with the molecular plane nearly parallel to the surface. The similarity between our data and his suggests that the same interpretations are valid here.

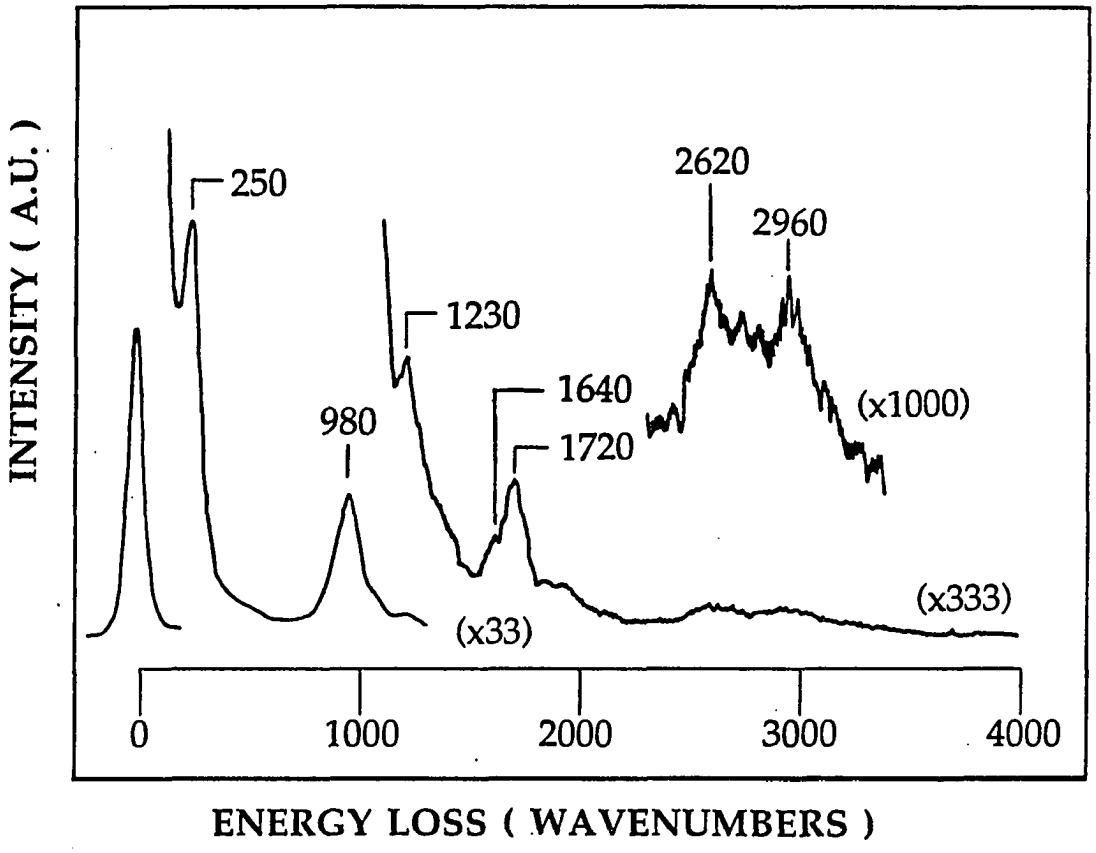

Figure 3. High resolution electron energy loss spectrum following exposure of 0.8 L HCOOH at 100 K and heating to 130 K. The elastic peak has an intensity of 350 kHz and a FWHM of 9 mV.

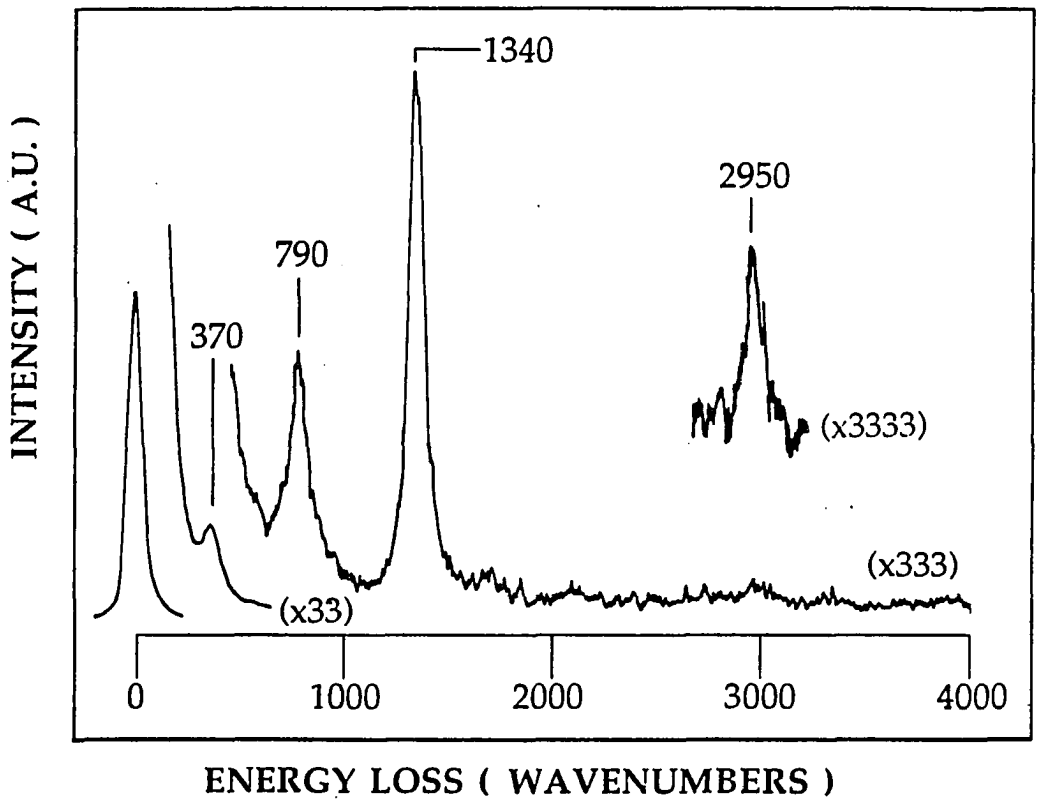

Figure 4. High resolution electron energy loss spectrum following exposure of 0.8 L HCOOH at 100 K and heating to 190 K. The elastic peak has an intensity of 110 kHz and a FWHM of 10 mV.

Formic acid		Formate	
Loss	Mode	Loss	Mode
250	lattice	370	ν (PtO)
980	π (OH)	790	δ (OCO)
1230	ν (C–O)	1340	ν_s (OCO)
1640	ν (C=O)	2950	ν (CH)
1720	ν (C=O)		
2620	ν (OH)		
2960	ν (CH)		

Figure 5. Loss assignments for high resolution electron energy loss spectra of molecular HCOOH (Fig. 3) and bridging formate (Fig. 4) on Pt(111). Mode determination made from comparison to Avery [2].

For the molecular acid, we do not observe losses at 715 cm^{-1} (δ(OCO), 1070 cm^{-1})(π(CH)) and 1385 cm^{-1} (δ(CH) reported by Avery; this can be explained by a higher HCOOH coverage and better resolution in Avery's work. The in-plane bending modes (δ) produce relatively small dipole changes perpendicular to the surface resulting in small dipolar scattering cross sections; higher coverages are required to observe them. The low intensity of the π(CH) vibration, the out-of-plane deformation, is unexpected based on the adsorption geometry but is consistent with a strong impact scattering contribution observed for ν(CH) for formate adsorbed on Pt(110) [36] and Ni(110) [12]

The splitting of the ν(C=O) mode and the frequency of the π(OH) mode give information about the structure of the molecular acid. The π(OH) frequency is higher than those of monomeric or dimeric HCOOH (see Fig. 6). It is much closer to those measured for solid HCOOH, which exists in two polymorphic structures[30, 31]. The α-polymorph exhibits tautomerism giving rise to two ν(C=O) modes; the β-polymorph exhibits no tautomerism and only one ν(C=O) mode. The splitting in our spectrum indicates that we, like Avery, observe an overlayer structure similar to the HCOOH α-polymorph. (This is also supported by the π(OH) frequency.) The consequences of polymorphism on surface adstructure are discussed later.

HCOOH π (OH) frequency (wavenumbers)

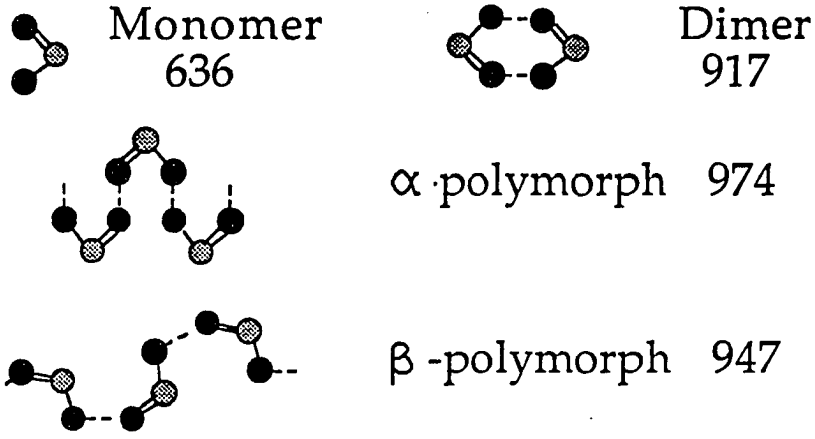

Adspecies π (OH) loss (wavenumbers)	
0.8 L HCOOH @ 130 K	978 ± 11
0.8 L HCOOH @ 150 K	945 ± 4
0.2 L HCOOH @ 130 K	938 ± 4
0.2 L HCOOH @ 150 K	898 ± 4

Figure 6. Frequencies (in wavenumbers) for the OH out-of-plane bend of molecular HCOOH. The values for the monomer and the dimer are reported for the gas phase [28, 29] and those for the two polymorphs are reported for solid HCOOH [29-31]. The adspecies' values are averages of 5-7 measurements for each surface condition described. The uncertainties reported reflect one standard deviation.

The most intense losses for this overlayer are assigned to out-of-plane vibrations: a lattice vibration at 250 cm^{-1} and the out-of-plane OH deformation at 980 cm^{-1}. The dipolar scattering requirement of dipole moment change perpendicular to the surface indicates that the HCOOH molecular plane is oriented nearly parallel to the surface. We illustrate these vibrations in Fig. 7. The other losses are much lower in intensity due to dipole moment changes in the molecular plane.

The molecular HCOOH loss at 250 cm^{-1} assigned to a lattice vibration has been used previously as an indication of multilayer population [20]. However, we observe this loss clearly for exposures as low as 0.3 L, which is insufficient to populate any multilayer-like desorption state on Pt(111) (data not shown). Instead, we believe the adsorbed HCOOH layer to consist of quasi-one-dimensional chains with practically no interaction between chains. This loss, as assigned by Mikawa et al [31], then results from simultaneous displacement of the hydroxyl oxygen atom and its proton above the molecular plane, and the carbon atom and its proton below it, as shown in Fig. 7.

Sequential heating-measurement cycles between 130 and 190 K allow correlation of surface changes with desorption states. Fig. 8 displays a series of HREEL spectra obtained after exposing Pt(111) at 100 K to 0.2 L HCOOH followed

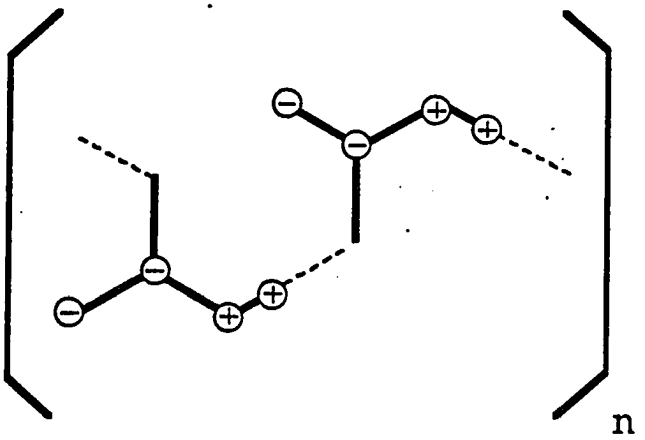

Lattice vibration

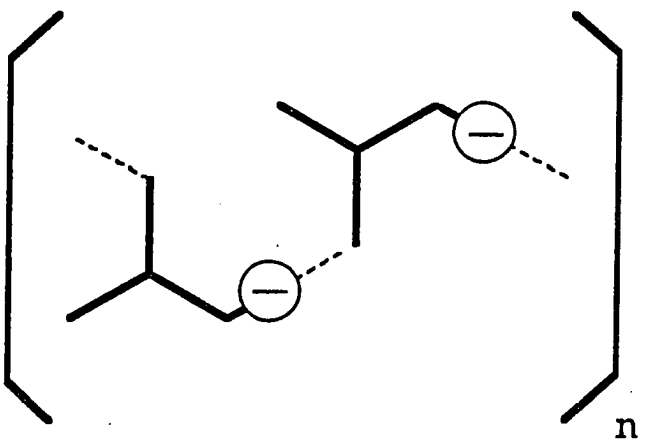

OH out-of-plane bend

Figure 7. Geometric representations of solid HCOOH lattice vibration and OH out-of-plane bend. (+) and (-) signify displacement of atoms above and below the molecular plane, respectively. Taken from Mikawa et al [31].

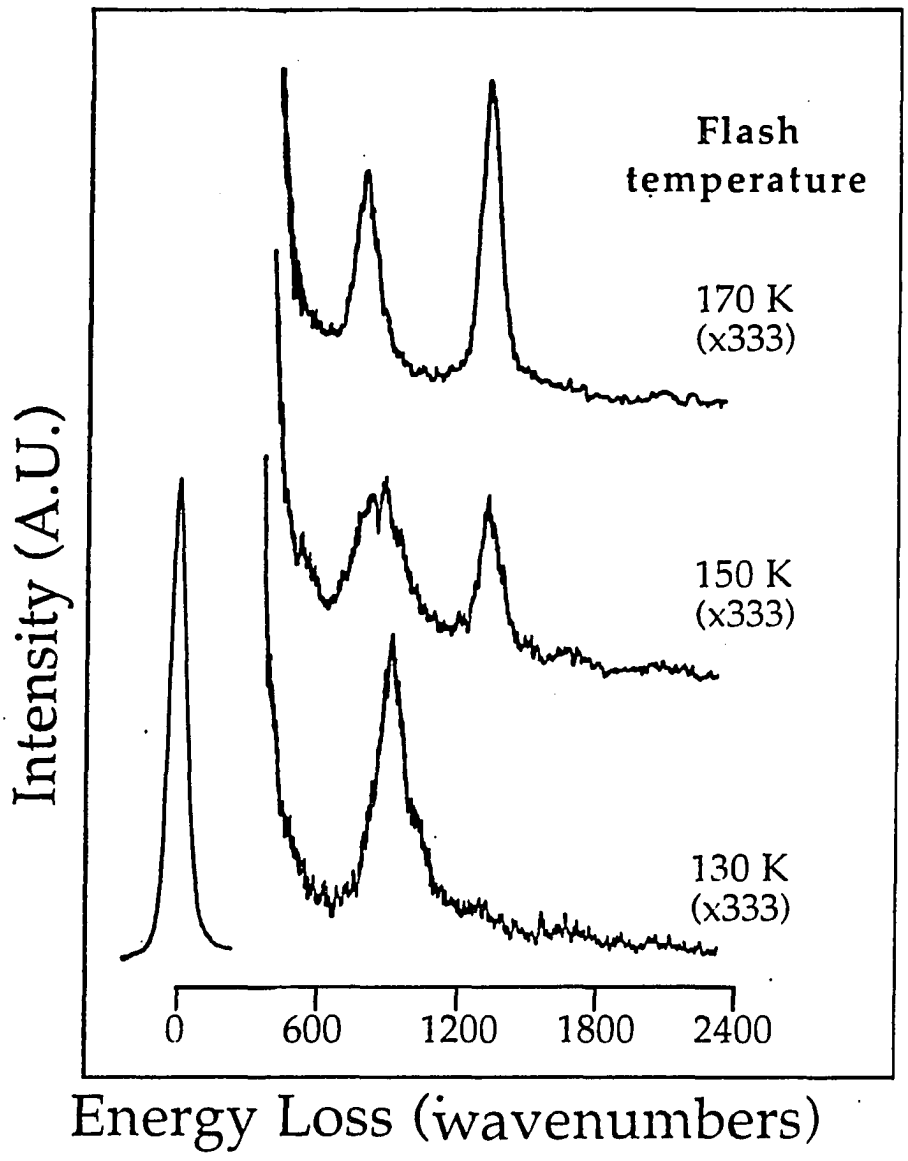

Figure 8. Series of high resolution electron energy loss spectra following exposure of 0.2 L HCOOH at 100 K and heating to 130 K, 150 K, and 170 K, respectively. The elastic peak has an intensity of 50 kHz and a FWHM of 11 mV.

by heating to 130 K, 150 K, and 170 K. The only prominent loss in the 130 K spectrum occurs at 940 cm^{-1}. We assign this to the OH out-of-plane bend for the molecular HCOOH and note that it shifts down by 40 cm^{-1} relative to the spectrum in Fig. 3. In the 150 K spectrum this loss shifts further down to ca. 900 cm^{-1} and decreases in intensity; new losses appear at 790 cm^{-1} and 1340 cm^{-1} indicating the presence of bridging formate. By 170 K the spectrum exhibits only the losses from the formate adspecies.

Fig. 9 shows an HREEL spectral series obtained after exposing Pt(111) at 100 K to 0.8 L HCOOH followed by heating to 130 K, 150 K, 170 K, and 190 K. The only prominent loss observed in the spectrum at 130 K occurs at 980 cm^{-1} agreeing with the OH out-of-plane bend for molecular HCOOH in Fig. 3. The 150 K spectrum shows that this loss shifts down to 945 cm^{-1} and decreases in intensity, while a new loss at 1330 cm^{-1} appears indicating the presence of bridging formate. The 170 K spectrum shows an increase for the formate loss intensity but little change in the molecular HCOOH loss. By 190 K the spectrum exhibits no losses for molecular HCOOH and a new loss at 790 cm^{-1}; this spectrum is in good agreement with the one in Fig. 4 where only bridging formate is present on the surface.

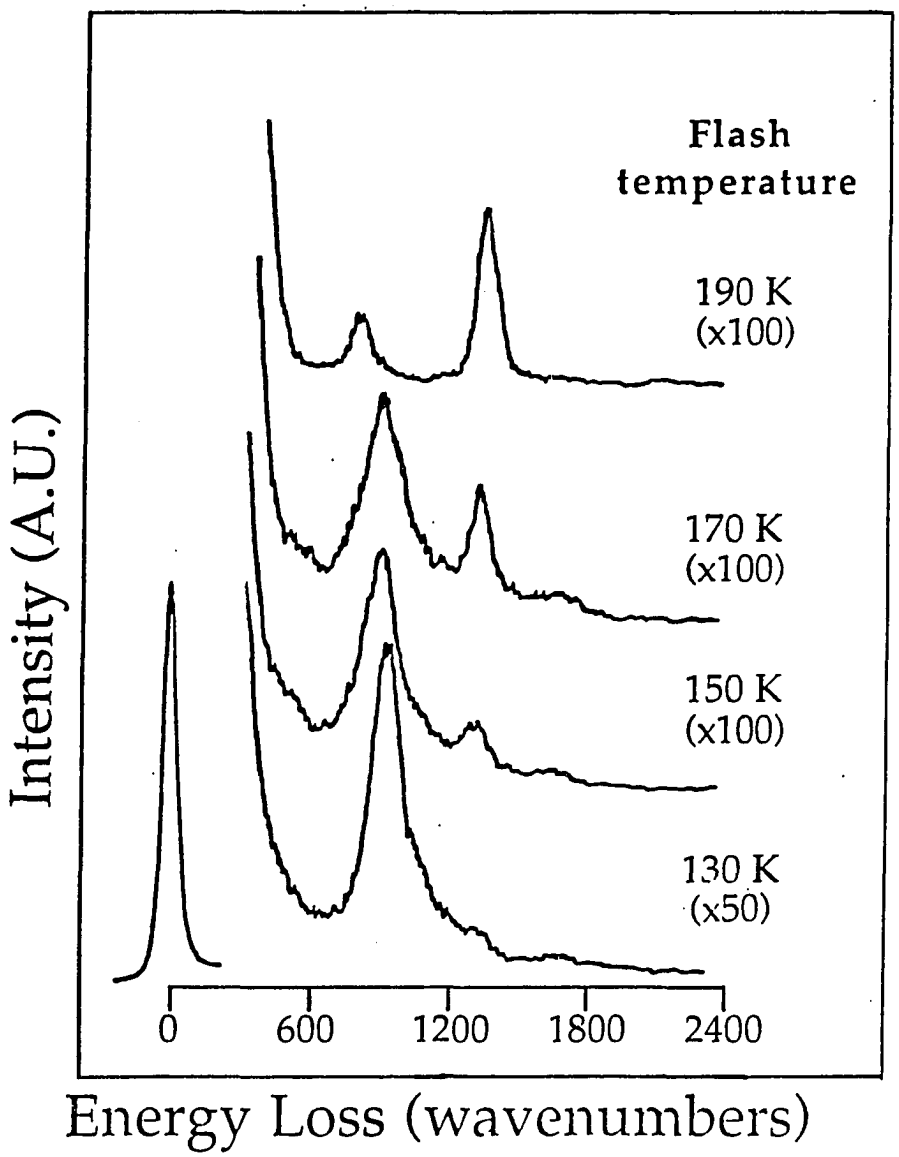

Figure 9. Series of high resolution electron energy loss spectra following exposure of 0.8 L HCOOH at 100 K and heating to 130 K, 150 K, 170 K, and 190 K, respectively. The elastic peak has an intensity of 100 kHz and a FWHM of 8 mV.

Figs. 10a and 10b depict the conversion of molecular HCOOH to formate in a graphical manner. In Fig. 10a the loss intensity of the OH out-of-plane bend for molecular HCOOH normalized to the elastic intensity is plotted versus surface temperature for 0.2 L and 0.8 L HCOOH exposures. For the lower exposure there is a constant intensity decrease to extinction between 170 K and 180 K.; however, the intensity decrease for the higher exposure produces a plateau between 160 K and 180 K before extinction at 190 K. In Fig. 10b the normalized loss intensity for the OCO symmetric stretch for the bridging formate is plotted versus temperature for the same exposures. For the lower exposure, the intensity increases rapidly between 130 K and 150 K and reaches a maximum around 180 K. This increase occurs more slowly at the higher exposure up to 170 K; beyond this temperature the intensity increases rapidly to its maximum at 190 K.

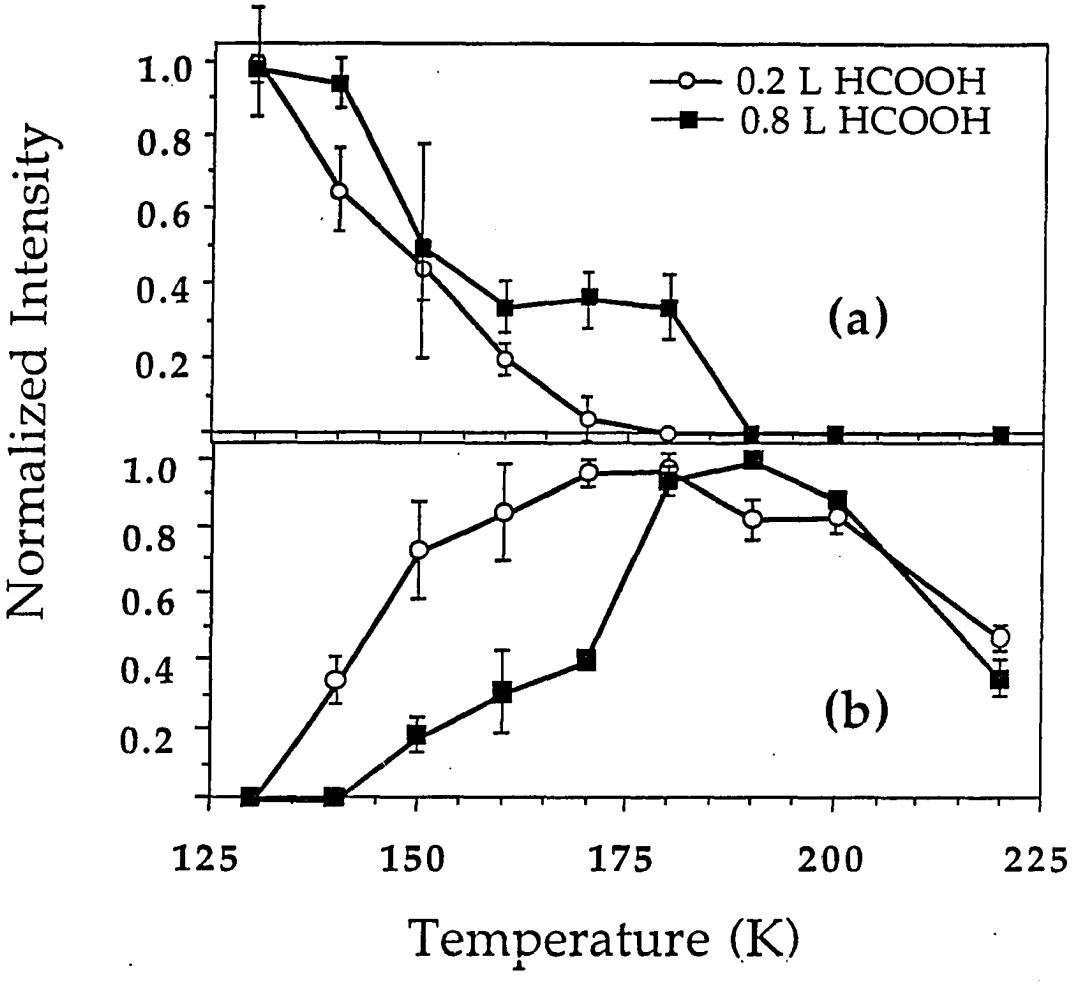

Figure 10. Loss intensities of the HCOOH out-of-plane OH bend (a) and the formate OCO symmetric stretch (b) normalized to the elastic intensity as a function of temperature for exposures of 0.2 L and 0.8 L at 100 K. Each normalized value is the average of 3-5 measurements made at the stated temperature and the error bars reflect ± one standard deviation.

4. Discussion

4.1 Temperature and coverage dependence of the OH out-of-plane bend frequency.

In the HREEL spectra for conditions where molecular HCOOH exists on the surface, the most intense loss belongs to the OH out-of-plane bend. The frequency of this loss occurs in 3 distinct ranges depending on the exposure and surface temperature. These frequencies and the conditions where we observe them are listed in Fig. 6 along with frequencies for various forms of molecular HCOOH. The monomer and dimer frequencies are available for those species in the gas phase [28, 29]; the alpha (α) and beta (β) polymorph frequencies are available for solid HCOOH [29-31]. The vibrational frequencies for the different forms of formic acid increase with increasing strength of hydrogen bonding; this is in accord with Novak's review of several molecules which exhibit hydrogen-bonding in the solid phase [37]. Rough molecular models are also shown for each of these forms accompanying the appropriate π(OH) frequency.

For the 0.8 L exposure at 130 K the OH bend has an average frequency of 978 cm^{-1}, the same frequency as the α-polymorph; heating this surface to 150 K causes the average frequency to shift to 945 cm^{-1}, close to the frequency of the β-

polymorph. In Fig. 11 we display possible structures for these polymorphs as they might exist on the Pt(111) surface. We construct these by attempting to maximize symmetry and registry with the surface. This requires lengthening the (OH-O) bond distances from 0.258 nm to 0.277 nm No bond angles have been distorted beyond reported uncertainty [38].

It is easily observed, qualitatively and quantitatively, that the α-phase is the denser of the two polymorphs. The absolute coverages of the α- and β-polymorphs, as shown in Fig. 11, are 0.3 and 0.2 monolayers, respectively. These values are based on the shortest interchain distance which maintains registry with the surface and provides good agreement with the same distances in solid HCOOH [38]. These distances between chains in the bulk solid are 0.375 nm for C-C separation, 0.328 nm for O-O separation, and 0.318 nm for C-O separation; in Fig. 11, the shortest interchain distance is the C-C separation for the α-polymorph at 0.368 nm and the O-O separation for the β-polymorph at 0.368 nm. We interpret the frequency shift as function of temperature to indicate a transition of the molecular HCOOH from the α-polymorph at 130 K to the β-polymorph at 150 K. Such a transition results in displacement of HCOOH molecules from direct contact with the surface and could explain the 160 K molecular desorption state at this exposure.

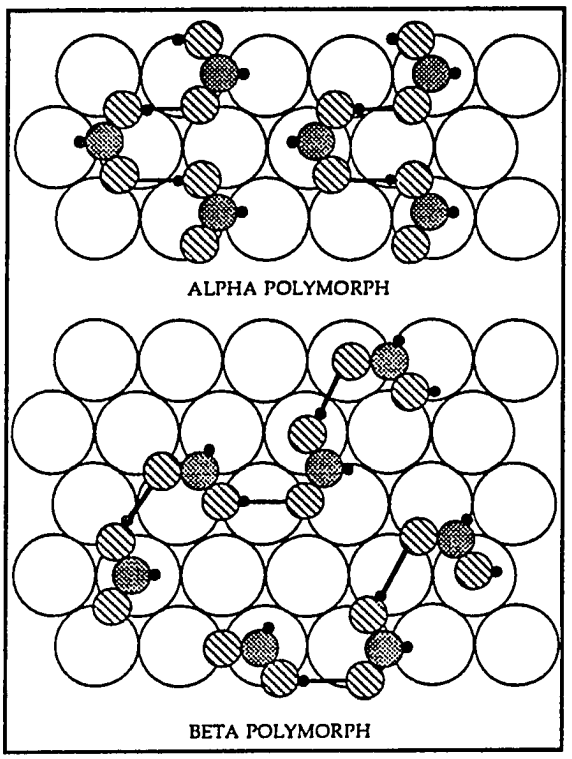

Figure 11. Models of HCOOH overlayer structures on Pt(111) are based on the solid phase α and β polymorphs. These models are constructed by elongating each O-H-O hydrogen bond distance from 0.258 nm to match the Pt-Pt distance on the (111) surface, 0.277 nm, and positioning the oxygen atoms in two-fold hollow or on-top sites. Interchain distances do not allow atoms in different chains to approach closer than 0.368 nm center to center. No bond angles are distorted beyond reported uncertainty [38].

For the 0.2 L exposure at 130 K the average OH bend frequency appears at 938 cm^{-1} and shifts to 898 cm^{-1} at 150 K. From Fig. 6, these frequencies suggest a transition from the β-polymorph to discrete HCOOH dimer pairs over this temperature range. The difference between these frequencies and those for their gas and solid phase counterparts can be attributed to perturbation from the surface. At this lower exposure (coverage) the perturbation per molecule is greater than on a surface exposed to more HCOOH due to a lower level of lateral interaction between HCOOH adspecies.

4.2 Temperature and coverage dependence of conversion of molecular HCOOH to bridging formate.

The vibrational information obtained from HREELS indicates both temperature and coverage dependences for the conversion of molecular HCOOH to bridging formate. For an exposure of 0.2 L the decrease in the loss intensity for the molecular HCOOH out-of-plane OH bend and the concurrent increase in the loss intensity for the formate symmetric OCO stretch are both continuous between 130 K and 170 K. Beyond 170 K the OH bend loss is not observed and the OCO stretch loss reaches a maximum. At this exposure also, a very small amount of molecular desorption occurs between 200 K and 250 K.

We deduce a simple sequence of events which occurs at this exposure: At 100 K HCOOH adsorbs molecularly, perhaps through the hydroxyl oxygen atom. Mobility of surface monomers allows the formation of hydrogen-bonded chains similar to the β-polymorph of solid HCOOH. Above 130 K the chains convert to discrete dimer pairs. In this form the HCOOH molecules begin to lose their hydroxyl protons to the surface forming hydrogen adatoms; this is accompanied by formation of a bond between the surface and the carbonyl oxygen, yielding bridging formate. This conversion is complete by 170 K with almost all of the HCOOH reacting by this route.

For the surface exposed to 0.8 L HCOOH the temperature dependence of the intensities of these losses is significantly changed. The loss intensity for the OH bend shows only a slight decrease before 140 K, followed by a sharp drop to a plateau between 160 K and 180 K. and finally extinction at 190 K. The loss for the OCO stretch appears above 140 K (10 K higher than at the lower exposure) and its intensity increases slowly up to 170 K. Above this, its intensity increases rapidly to a maximum at 190 K.

These data can be explained by considering the molecular desorption states and shift in OH bend frequency occurring at 0.8 L exposure. As noted previously, the OH bend frequency shifts by 40 cm^{-1} between 130 K and 150 K indicating a

transition from the α-polymorph to the β-polymorph. The resultant desorption must contribute to the dramatic drop in the molecular HCOOH loss intensity between 140 K and 160 K, although the data of Fig. 10b suggest that there is simultaneous loss of the acid due to formate conversion. The increase of 10 K for the appearance of formate relative to the 0.2 L exposure could be explained by the α-to-β transition. The conversion from molecular HCOOH to formate could require a certain ensemble of surface atoms which is only available after transition to the less densely packed β-phase or the orientation of the HCOOH molecules in the β-phase might allow conversion more readily than in the α-phase.

The coexistence of the plateau in the molecular HCOOH loss intensity with the continual increase in the formate loss intensity, shown in Fig. 10, is more problematic. Consideration of possible coverage-dependent changes in the scattering cross sections for these vibrations makes any discussion somewhat speculative; however, a possible explanation might proceed as follows: The plateau between 160 and 180 K in Fig. 10a suggests that deprotonation is complete by 160 K. Yet in this same temperature range the intensity of the formate-related loss rises, especially between 170 and 180 K, as shown by Fig. 10b.

10b. Perhaps the increase in intensity of the formate feature in this temperature regime is due to reorientation from an almost-parallel configuration, to a perpendicular one where the OCO stretch is completely dipole-allowed. Reorientation may be inhibited at this high coverage by the coexistent molecular acid, owing to hydrogen bonding between the two adspecies. Above 170 K, the reorientation rate accelerates, implying a breakdown in the hydrogen bonding. Perhaps this acceleration is linked to desorption of molecular HCOOH at 200 K, although the constancy of the data in Fig. 10a between 160 and 180 K suggest that desorption of the acid does not actually begin until 180-190 K in these experiments.

4.3 Coverage dependence of thermal desorption states

Decomposition of bridging formate causes almost all the desorption observed from the surface exposed to 0.2 L HCOOH. This formate results from the reaction of discrete pairs of HCOOH dimers with the Pt(111) surface outlined above. This formate decomposes above 200 K giving CO_2 desorption peaked at 260 K, followed by desorption-limited H_2 centered at 350 K. There is also a small amount of molecular desorption which roughly follows the CO_2 desorption. Considering that bridging formate is the only adspecies observed in the

vibrational spectra above 170 K, this molecular desorption must arise from recombination of formate and H adatoms.

Increasing the exposure to 0.8 L HCOOH populates 2 molecular desorption states. The desorption spectra for masses 29 and 47 exhibit these states centered at 160 K and 200 K, but the relative intensities of these states are different in the two spectra. This suggests that there are two different forms of molecular HCOOH desorbing, namely, monomers and dimers. The 160 K state in the mass 47 spectrum is 6 times as intense as the 200 K state (mass 47 is the molecular weight of one HCOOH molecule plus one proton). The 200 K state in the mass 29 spectrum is 3 times larger than the 160 K state. We suggest that desorption from the 160 K state is dominated by HCOOH dimers and that from the 200 K state by HCOOH monomers. Additionally, at high HCOOH exposures (> 2.3 L), we observe broad desorption features in mass 91 spectra (not shown) centered between 160 K and 170 K; we believe this further supports the predominance of dimers in the lower temperature desorption state, although we cannot rule out desorption of higher oligomers. (Mass 91 is the molecular weight of a formic acid dimer missing a proton.)

We offer two scenarios to explain the differences in the two molecular desorption states: (1) Desorption from the 160 K state is from a second layer with

no HCOOH in direct contact with the surface. The presence of this second layer constrains the HCOOH in contact with the surface to the α-polymorph configuration. Heating the surface beyond 140 K desorbs the second layer in the form of HCOOH dimers and allows the first layer HCOOH to convert to the β-polymorph, with subsequent reaction to form bridging formate; or (2) Desorption from the 160 K state is from HCOOH in direct contact with the surface. Such an overlayer would be in the denser α-polymorph. Heating this surface beyond 140 K would cause rupture of the hydrogen-bonded chains, squeezing out HCOOH dimers and allowing conversion to the β-polymorph.

We can extract from the second model an explanation to support immediate deprotonation of HCOOH resulting from the α-to-β conversion. Rupture of the hydrogen-bonded chains via dimer displacement would result in a higher number of terminal HCOOH molecules. Chain rupture could be followed or accompanied by deprotonation of these terminal molecules; reorientation would be slowed by their continued interaction with linking HCOOH molecules in the shortened chains.

More supporting evidence for the second model comes from the exposures required to populate the molecular desorption states. Above 1.2 L a third molecular desorption state appears at 160 K, which we attribute to a true

multilayer; by this exposure the second molecular desorption state has moved up to a peak temperature of 170 K. If the sticking coefficient at 100 K is unity, the HCOOH coverage at 1.2 L is 0.24 monolayer. This is 80% of the estimated ideal coverage of the α-polymorph overlayer. Considering the disorder of the overlayer and the low coherence of the chains, such a deviation from ideality is not unreasonable. Similarly, one must conclude that the exposure of 0.6 L HCOOH produces a coverage of 0.12 monolayer, or 60% of the ideal β-polymorph coverage. This is the exposure at which the second molecular desorption state at 160-170 K first appears. At this point, we postulate that the increasing surface density forces the β-polymorph chains to adopt the more compact α-polymorph arrangement; again, it is reasonable that this transition would occur at 60% of the ideal β–polymer coverage.

5. Summary

The scheme for the reaction of HCOOH with Pt(111) is summarized in Fig. 12. For extremely low exposures at 100 K, we posit that HCOOH adsorbs molecularly as monomers or discrete dimer pairs. As surface temperature

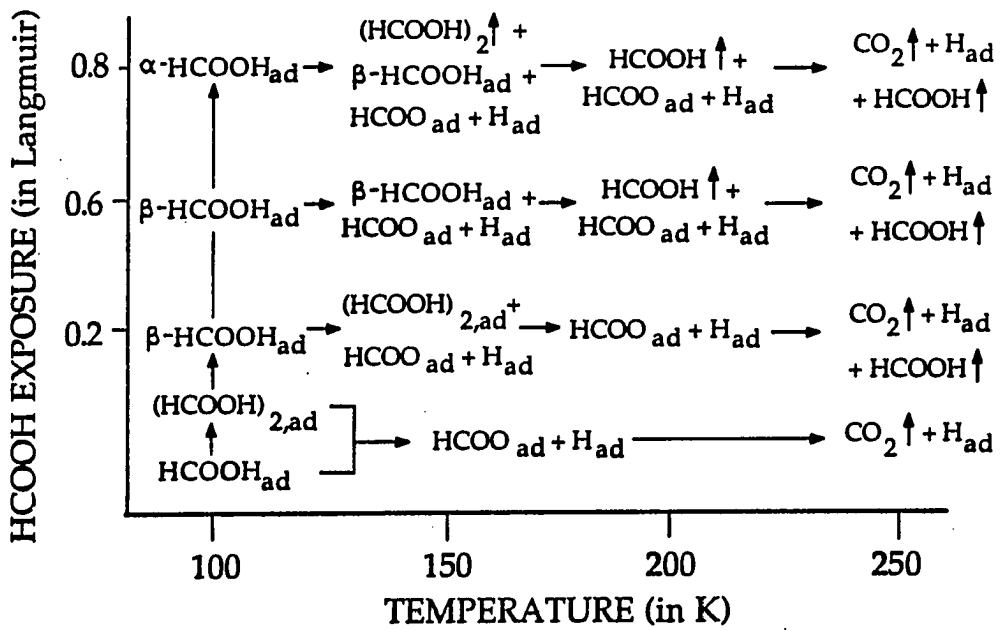

Figure 12. Summary of the coverage dependence of the HCOOH overlayer for adsorption at 100 K and its temperature dependence for conversion to formate for different coverages.

increases, the acid deprotonates to produce bridging formate and hydrogen adatoms. As exposure increases at 100 K, the population of HCOOH reaches a level sufficient to form hydrogen bonded chains in a configuration similar to the solid phase β-polymorph. This is the surface condition we observe for an exposure of 0.2 L. Heating this overlayer to 150 K causes reversion to discrete dimer pairs, followed by conversion to bridging formate. By 170 K, conversion is complete. Between 200 K and 250 K a small amount of formate recombines with atomic hydrogen to desorb molecularly; however, the majority of formate decomposes resulting in CO_2 desorption peaking at ~260 K.

We believe the β-polymorph remains the preferred configuration for HCOOH adsorbed at 100 K up to an exposure which populates the second molecular desorption state (0.6 L); however, at higher exposures the hydrogen bonded chains resemble the denser α-polymorph. Heating the surface above 130 K transforms the α-phase to the β-phase; this is tied to the second molecular HCOOH desorption state. Desorption results from depopulation of a second layer or rupture of first-layer chains; the desorption products are gaseous dimers. A fraction of the HCOOH which remains in the overlayer immediately deprotonates and reorients to a perpendicular, bridging configuration with

increasing surface temperature. The HCOOH which does not deprotonate desorbs from the surface (peaked at 200 K) as monomers.

Increasing exposure between 0.2 L and 0.6 L changes the pathway of formate formation. As described above for 0.2 L HCOOH exposure at 100 K, production of formate is preceded by the reversion of HCOOH chains to discrete dimer pairs. Increasing coverage eventually prevents this reversion, leading to formate production directly from HCOOH chains and desorption of molecular HCOOH peaked at 200 K. Subsequent formate decomposition proceeds as for the 0.2 L exposure.

Acknowledgements

Acknowledgement is made to the Donors of The Petroleum Research Fund, administered by the American Chemical Society, for the support of this research. Some equipment and all facilities are provided by the Ames Laboratory, which is operated for the U. S. Department of Energy by Iowa State University under Contract No. W-7405-ENG-82.

References

1. M. R. Columbia and P. A. Thiel, Surf. Sci., 235 (1990) 53

2. N. R. Avery, App. Surf. Sci., 11/12 (1982) 774

3. N. R. Avery, App. Surf. Sci, 14 (1982-83) 149

4. N. Abbas and R. J. Madix, App. Surf. Sci., 16 (1983) 424

5. D. H. S. Ying and R. J. Madix, J. Cat., 61 (1980) 48

6. B. E. Hayden, K. Prince, D. P. Woodruff and A. M. Bradshaw, Surf. Sci., 133 (1983) 589

7. L. H. Dubois, T. H. Ellis, B. R. Zegarski and S. D. Kevan, Surf. Sci., 172 (1986) 385

8. J. McCarty, J. Falconer and R. J. Madix, J. Cat., 30 (1973) 235

9. J. L. Falconer and R. J. Madix, Surf. Sci., 46 (1974) 473

10. R. J. Madix, J. L. Gland, G. E. Mitchell and B. A. Sexton, Surf. Sci., 125 (1983) 481

11. T. S. Jones, N. V. Richardson and A. W. Joshi, Surf. Sci., 207 (1988) L948

12. T. S. Jones, M. R. Ashton and N. V. Richardson, J. Chem. Phys., 90 (1989) 7564

13. J. B. Benziger and R. J. Madix, Surf. Sci., 79 (1979) 394

14. J. B. Benziger and G. B. Schoofs, J. Phys. Chem., 88 (1984) 4439

15. W. Erley and D. Sander, J. Vac. Sci Technol. A, 7 (1989) 2238

16. L. A. Larson and J. T. Dickinson, Surf. Sci., 84 (1979) 17

17. N. R. Avery, B. H. Toby, A. B. Anton and W. H. Weinberg, Surf. Sci., 122 (1982) L574

18. Y.-K. Sun and W. H. Weinberg, J. Chem. Phys., 94 (1991) 4587

19. M. A. Barteau, M. Bowker and R. J. Madix, Surf. Sci., 94 (1980) 303

20. B. A. Sexton and R. J. Madix, Surf. Sci., 105 (1981) 177

21. M. Chtaib, P. A. Thiry, J. J. Pireaux, J. P. Delrue and R. Caudano, Surf. Sci., 162 (1985) 245

22. D. A. Outka and R. J. Madix, Surf. Sci., 179 (1987) 361

23. R. W. Joyner and M. W. Roberts, Proc. R. Soc. Lon. A, 350 (1976) 107

24. J. L. Davis and M. A. Barteau, Langmuir, 5 (1989) 1299

25. Q. Gao and J. C. Hemminger, J. Electron Spec., 54/55 (1990) 667

26. Q. Gao and J. C. Hemminger, Surf. Sci., 248 (1991) 45

27. M. R. Columbia and P. A. Thiel, Proc. DOE Workshop -Direct Methanol/Air Fuel Cells, to be published

28. R. C. Millikan and K. S. Pitzer, J. Chem. Phys., 27 (1957) 1305

29. R. C. Millikan and K. S. Pitzer, J. Am. Chem. Soc., 80 (1958) 3515

30. Y. Mikawa, R. J. Jakobsen and J. W. Brasch, J. Chem. Phys., 45 (1966) 4750

31. Y. Mikawa, J. W. Brasch and R. J. Jakobsen, J. Mol. Spectros., 24 (1967) 314

32. M. R. Columbia and P. A. Thiel, Rev. Sci. Instrum., 58 (1987) 309

33. P. K. Leavitt, J. L. Davis, J. S. Dyer and P. A. Thiel, Surf. Sci., 218 (1989) 346

34. A. S. Cooley, J. Am. Chem. Soc., 50 (1928) 2166

35. K. Christmann, G. Ertl and T. Pignet, Surf. Sci., 54 (1976) 365

36. P. Hofmann, S. R. Bare, N. V. Richardson and D. A. King, Surf. Sci., 133 (1983) L459

37. A. Novak, Struct. Bonding (Berlin), 18 (1974) 177

38. F. Holtzberg, B. Post and I. Fankuchen, Acta Cryst., 6 (1953) 127

SECTION III:

THE OVERLAYER STRUCTURE OF WATER AND FORMIC ACID COADSORBED ON PT(111)

The Overlayer Structure of Water and Formic Acid Coadsorbed on Pt(111)

by

M. R. Columbia, A. M. Crabtree, and P. A. Thiel

Department of Chemistry and Ames Laboratory
Iowa State University
Ames, IA 50010 USA

Submitted to *Surface Science*

Abstract

We have studied the interaction of water and formic acid coadsorbed on Pt(111) using thermal desorption spectroscopy (TDS) and high resolution electron energy loss spectroscopy (HREELS). TDS experiments where the exposure of one adsorbate is constant and the other varied indicate water and formic acid undergo mutual displacement from surface sites; upon completion this displacement leaves reproducible amounts of both adsorbates in a "mixed" overlayer suggesting the formation of a stoichiometric complex. TDS experiment that substitute D_2O for H_2O show the existence of hydrogen bonding between formic acid and D_2O. HREEL spectra for the mixed overlayer heated to 150 K show water, molecular acid, and bridging formate are present. Water does not affect the conversion of molecular acid to formate and can probably hydrogen bond to both adspecies. A significant fraction of water molecules in the overlayer undergo reorientation from C_s symmetry to C_{2v} symmetry causing the disappearance of the water librational mode in the HREEL spectra. We discuss models which accommodate this reorientation for overlayer complexes of water and formic acid based on hydrogen bonding between the water molecules which

mimic a bilayer structure and formic acid molecules involved in catameric chains.

1. Introduction

Small oxygen-containing hydrocarbons like formic acid show great promise for their use in fuel cells. In these cells formic acid reacts on an electrode surface to produce CO_2 and H^+. Platinum is an extremely efficient catalyst for this reaction; however, a self-poisoning reaction also occurs which renders the electrode surface incapable of adsorbing formic acid. The nature and prevention of this poisoning reaction are subjects of numerous electrochemical studies [1-21]. The problem has also attracted the attention of the surface science community [22-28], which has focused primarily on the fundamental interactions between formic acid and Pt surfaces in the absence of electrical fields and without the aqueous environment of the fuel cell.

We have studied the interaction of HCOOH with Pt(111) [22-24]. For exposures less than 0.3 L decomposition occurs via dehydrogenation. This produces CO_2 desorption with a peak temperature of 260 K and desorption of H_2 between 300 K and 400 K. We estimate that 0.05-0.1 monolayer of HCOOH decomposes based on comparison of thermal desorption areas of H_2 produced from HCOOH decomposition and an exposure of H_2 sufficient to saturate one monolayer . (We define one monolayer to be equivalent to the number of

surface sites per cm^2.) Avery also reports decomposition via dehydrogenation only [26]; however, Abbas and Madix also observe dehydration as a decomposition pathway [28]. Above this exposure molecular desorption occurs in 3 states: (1) the first is populated between 0.3 L and 0.6 L and has a peak temperature of 200 K; (2) the second is populated between 0.6 L and 1.2 L. Its peak temperature moves from 160 K to 170 K with increasing exposure; and, (3) the third appears above 1.2 L and does not saturate. At 1.2 L its peak temperature is 160 K, but moves to higher values with increasing exposure and eventually merges with the second state.

Our results for desorption from a Pt(111) surface exposed to water reproduce those of Fisher and Gland [29]. Below a water exposure of ca. 1.5 L desorption occurs from a state centered at ca. 180 K. Above this exposure desorption occurs from a second state which first appears at 155-160 K. As exposure increases this state does not saturate and moves to higher peak temperatures.

We have studied the coadsorption of water and formic acid on Pt(111) to gain a better understanding of the influence of an aqueous environment on the interaction between formic acid and the surface. Other studies have probed the effects of water coadsorbed with electrochemically-relevant adsorbates on

transition metals: Dœhl-Oelze et al. report that for coadsorbed nitric acid and water on Ag(110), the primary interaction is solvation of NO_3 adspecies by water molecules as well as solvation of multilayer HNO_3 molecules [30]. Similar solvation also occurs between water and atomic adspecies like Cl, Br, and Cs coadsorbed on various transition metals [31]. Kizhhakevariam et al. show that solvation increases the sticking coefficient of perchloric acid on Ag(110) when water is coadsorbed [32]. Wagner and Moylan's investigation of coadsorbed water and hydrofluoric acid on Pt(111) suggests fluoride ions produced upon adsorption are separated from the surface by a solvation net of water admolecules and are solvated above by a capping water molecule [33].

Our results indicate that a stoichiometric complex forms between the water and formic acid which resembles solvation. Mutual displacement of water and formic acid from the Pt(111) surface produces an overlayer with reproducible amounts of both coadsorbates present in it. Glagoleva reports that in aqueous solutions of formic acid, complexes with the stoichiometry $HCOOH \cdot H_2O$ and $HCOOH \cdot 2H_2O$ can form [34, 35]. We believe that an analogous surface complex forms on Pt(111) with a definite stoichiometry.

2. Experimental Details

The ultrahigh vacuum system, the method of performing thermal desorption experiments, and the Pt(111) crystal used for these experiments have been previously outlined [22, 36, 37]. The exposure units reported in this paper are Langmuir, although the surface is exposed to HCOOH through a directional doser containing a conductance-limiting aperture. We determine the Langmuir equivalence of these exposures based on comparison of CO thermal desorption areas for exposure via the doser with areas for exposure via backfilling.

The high resolution electron energy loss spectrometer has also been described previously [37]. The elastic peaks have intensities between 100 and 350 kHz and full-widths at half-maxima between 8 and 11 meV (65 cm^{-1} to 89 cm^{-1}). For those experiments which probe the effect of temperature on the vibrational spectrum, exposure temperatures are between 80 and 100 K; the surface is then heated to the indicated temperature at ~5 K/s, followed by determination of the loss spectrum while the surface cools. This method of heating differs from the continuous heating performed in TDS experiments. This difference results in

desorption states occuring at temperatures 10- 20 K higher than the corresponding changes in the vibrational spectrum.

3. Results

3.1 Thermal desorption

Fig. 1 shows a series of thermal desorption spectra for water as a function of increasing formic acid exposure. We use H_2O^+ (m/e = 18 amu) to monitor water evolution, and HCO^+ (m/e = 29 amu) to monitor molecular acid evolution. For this series the surface is exposed to sufficient water to saturate the "first layer" desorption state peaked at 180 K (ca. 1.5 L), then the surface is exposed to formic acid. (Reversing the sequence of exposures does not affect the results.) As formic acid exposure increases, a new desorption feature appears at 160 K and grows at the expense of the 180 K state.

Fig. 2 shows the quantitative displacement of water as a function of acid exposure. This quantitative measure is difficult to extract directly from the data of Fig. 1, due to overlap of the 160 K and 180 K states. Therefore, we expose the surface as described above, then heat it to ~150 K. This effectively depopulates

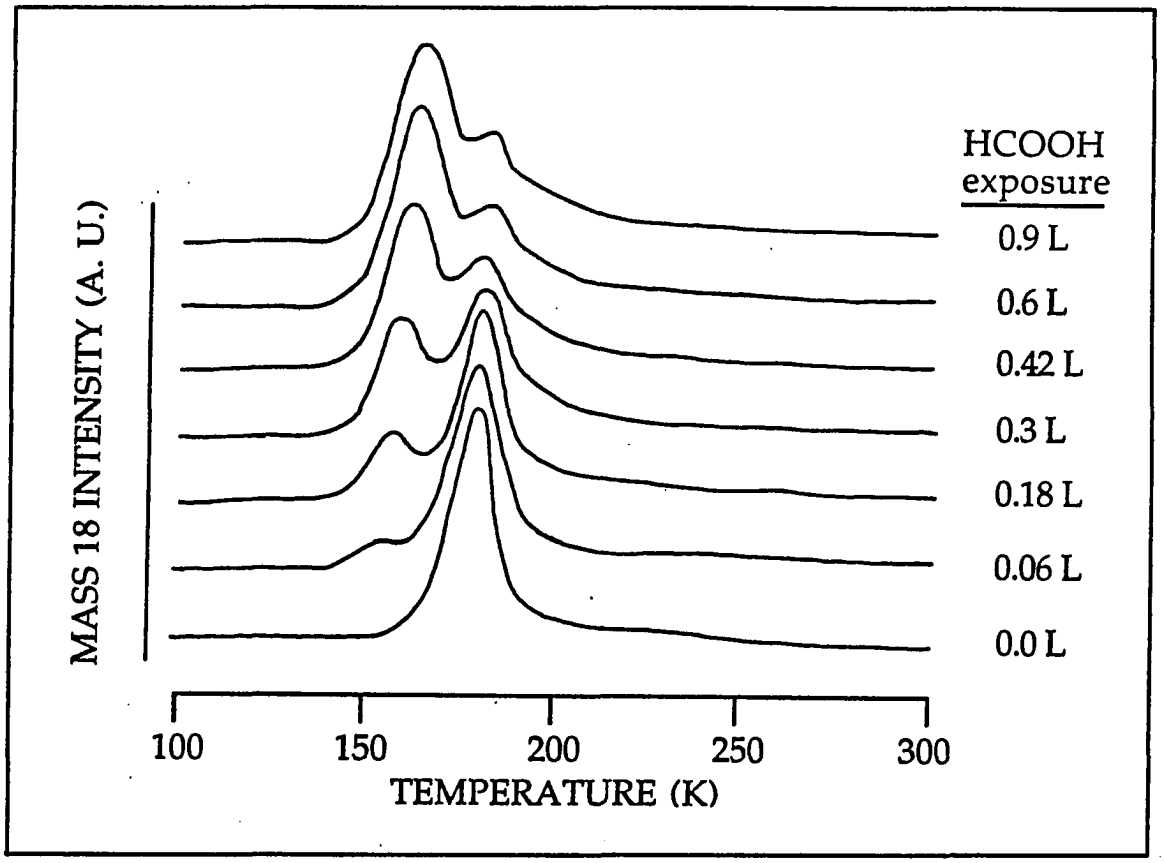

Figure 1. Series of thermal desorption traces of H_2O^+ following exposure of ca. 1.5 L H_2O and the stated exposures of HCOOH at 100 K. The heating rate is 15.6 K/s at 100 K and falls continuously to 6.5 K/s.

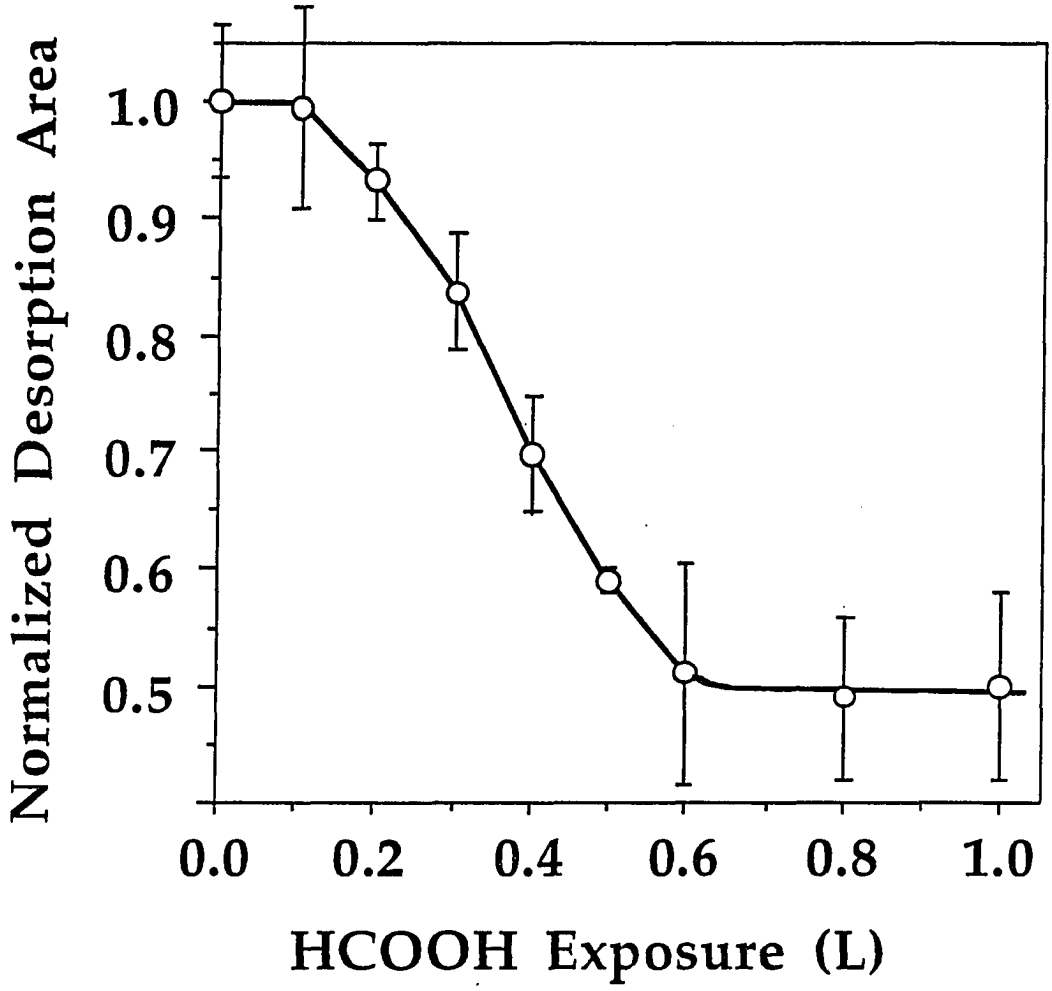

Figure 2. Normalized desorption area of H_2O^+ state at 180 K as a function of HCOOH exposure. H_2O exposure is ca. 1.5 L and surface is heated to 150 K prior to thermal desorption to determine H_2O^+ desorption area. Each normalized value is the average of 3 measurements and the error bars reflect ± one standard deviation.

the 160 K state and allows determination of the amount of water left in the 180 K state. The desorption area of mass 18 as a function of formic acid exposure (Fig. 2) reveals that ca. 50% of the water in the 180 K state is left after displacement is complete. (The extent of displacement is less than we previously reported based on an analysis of relative maximum peak intensities [22].)

This displacement occurs primarily over a range of formic acid exposures, which would populate the first HCOOH molecular desorption state on clean Pt(111). Fig. 3 displays a series of desorption spectra for molecular formic acid as a function of formic acid exposure on clean Pt(111). The appearance of the three desorption states follows the description provided in the introduction. Fig. 4 shows a series of molecular acid desorption for the same experiments which produce the water spectra in Fig. 1; water exposure is at 1.5 L and formic acid exposure is varied. Here we see the simultaneous emergence of *two* acid desorption states at 0.3 L, -at 165 K and 200 K, -followed by a third at 155 K at 0.5 L exposure.

In Fig. 5 we display a series of spectra for formic acid desorption as a function of increasing water exposure. In these experiments the surface is exposed to 0.6 L HCOOH prior to exposure to water. As shown from Fig. 3, this is sufficient to saturate the 200 K state of HCOOH in the absence of water. As

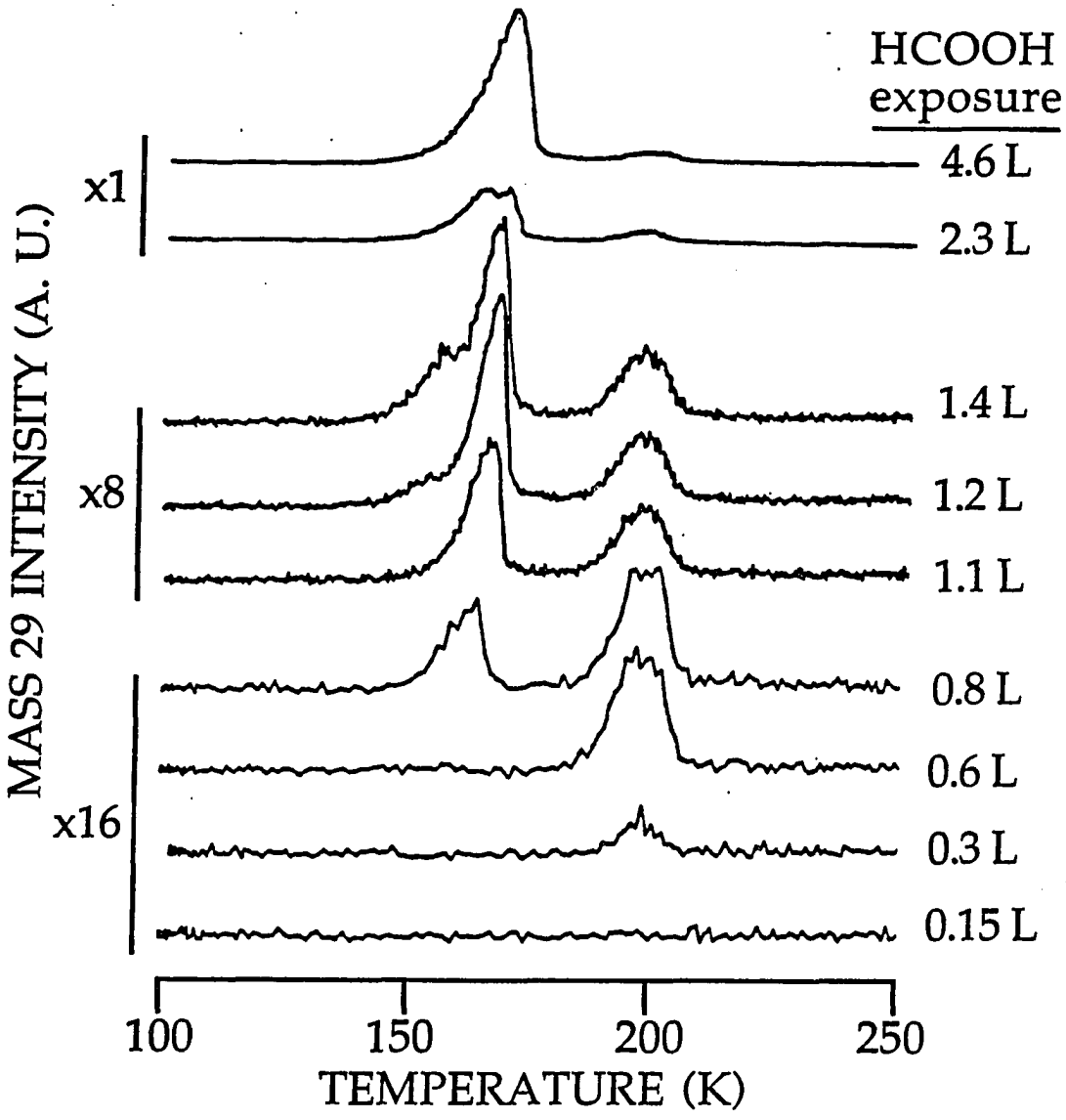

Figure 3. Series of thermal desorption traces for HCO^+ following stated exposures of HCOOH to clean Pt(111) at 100 K. The heating rate is 15.6 K/s at 100 K and drops continuously to 7.1 K/s at 250 K.

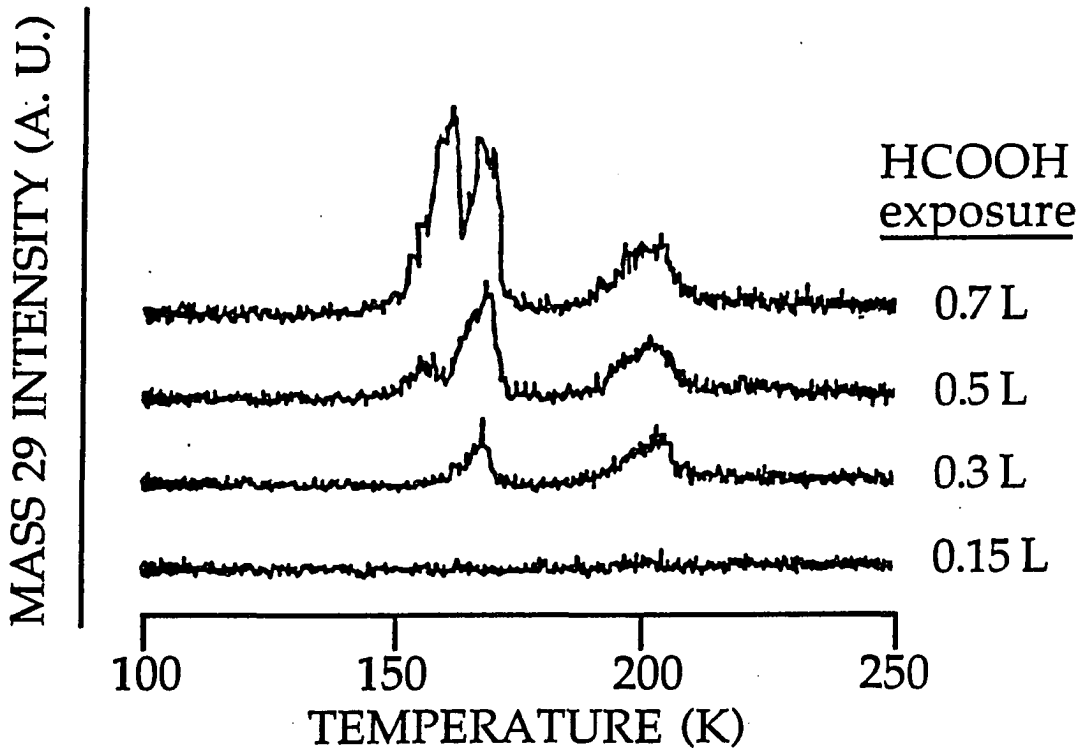

Figure 4. Series of thermal desorption traces for HCO^+ following exposure of HCOOH after 1.5 L H_2O exposure on Pt(111) at 100 K. The heating rate is 15.6 K/s at 100 K and drops continuously to 7.1 K/s at 250 K.

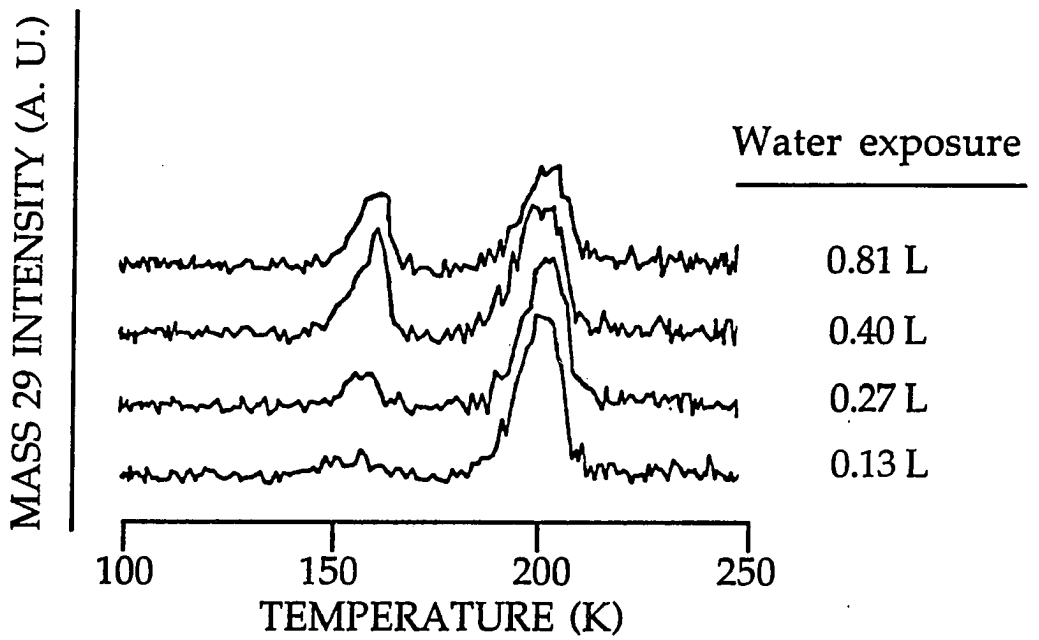

Figure 5. Series of thermal desorption traces for HCO^+ following exposure of 0.6 L HCOOH and stated exposure of water. (Ca. 1.5 L is necessary to saturate water's 180 K desorption state on clean Pt(111) at 100 K.) The heating rate is 15.6 K/s at 100 K and drops continuously to 7.1 K/s at 250 K.

water exposure increases HCOOH is displaced from the 200 K state to the state at 160 K. Fig. 6 depicts this displacement as normalized desorption area of the 200 K state versus water exposure. From this graph we see that at exposures of water greater than 0.4 L, displacement is complete. (This is ca. 25% of the exposure needed to saturate the 180 K desorption state on clean Pt(111).) At completion the desorption area of the 200 K HCOOH molecular state has decreased by 25%. The total area of molecular HCOOH desorption does not remain constant, however, due to differences in desorbing species. Desorption from the 200 K state is dominated by HCOOH monomers, while dimers predominate for desorption states at lower temperatures [24]. Disparity in the HCO^+ produced in the cracking patterns for these two species makes comparison of the desorption areas irrelevant.

In the H_2O^+ spectra in Fig. 1 there is a high temperature shoulder on the 180 K desorption feature; we will treat cracking of molecular acid in the mass spectrometer ionizer as the sole source in order to quantify this shoulder, although we cannot rule out displacement of water from the chamber walls as the origin. (Water is reported as a fragment in the cracking pattern of formic acid with an intensity as high as 0.46 of the parent ion [38].) To determine the contribution of this shoulder to the total water desorption area, we measure the

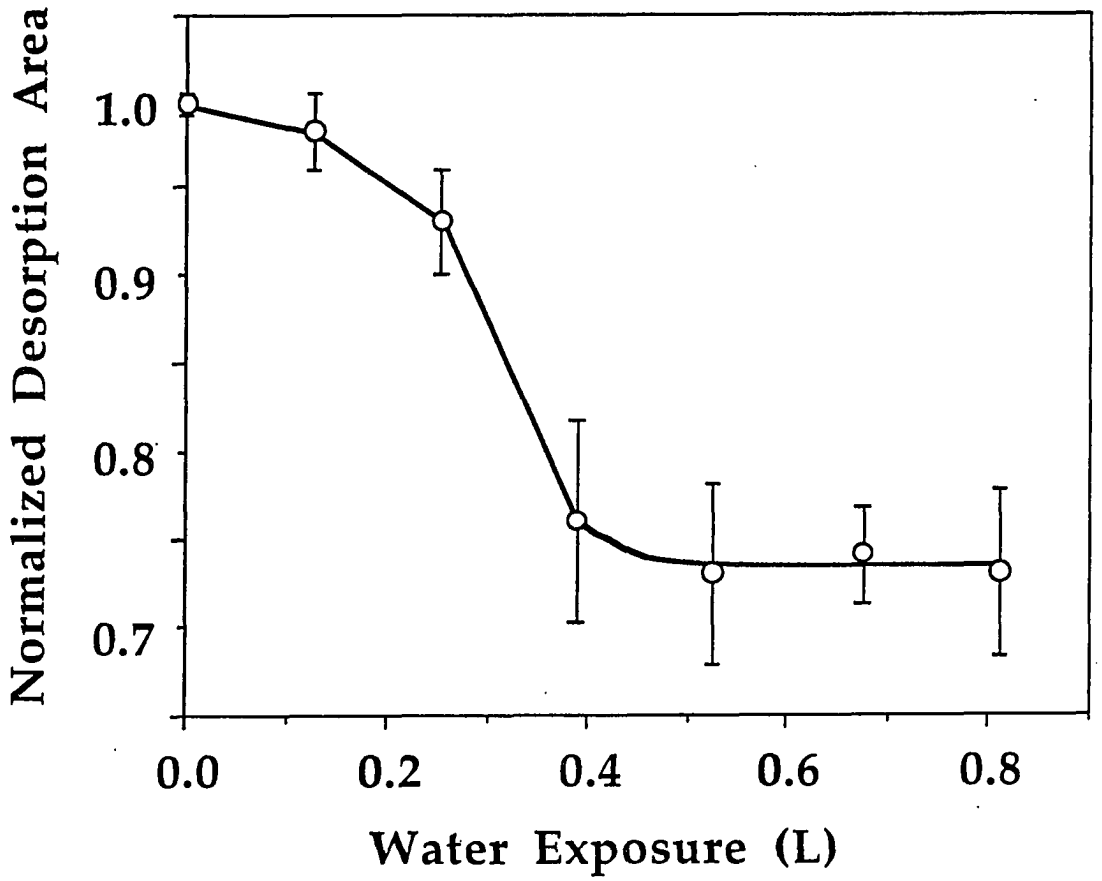

Figure 6. Normalized desorption area of HCO^+ state at 200 K as a function of water exposure The exposure of HCOOH is 0.6 L. Each normalized value is the average of 4-5 measurements and the error bars reflect ± one standard deviation.

water desorption from Pt(111) exposed to 0.6 L HCOOH, then account for mutual displacement in the mixed overlayer by reducing the measured area by 25%. Comparison of this corrected water desorption area to the area produced from a Pt(111) surface exposed to 1.5 L of water reveals that the actual amount of water not displaced from the 180 K desorption state by coadsorbed HCOOH is ca. 45% of the saturated state on the clean Pt(111) surface.

A series of thermal desorption experiments substituting D_2O for H_2O reveal that hydrogen bonding occurs between water and formic acid admolecules. Fig. 7 shows thermal desorption spectra for H_2^+, HD^+, and D_2^+ from a surface exposed to sufficient D_2O to saturate its 180 K desorption state and sufficient formic acid to saturate desorption yields of CO_2 and H_2. (Saturation exposures are determined from the clean surface.) These spectra show desorption features for H_2^+ and HD^+ at ca. 360 K and only a small amount of D_2^+ desorption. (The D_2^+ desorption area is less than 3% of the combined H_2^+ and HD^+ areas.) The HD^+ desorption indicates isotopic exchange between the D_2O and formic acid which we attribute to hydrogen bonding. This produces HCOOD adspecies which decompose to formate and deuterium adatoms. At 260 K, the formate decomposes further, yielding gaseous CO_2 plus H and D adatoms. The lack of D_2^+ desorption indicates that recombination of hydrogen adspecies

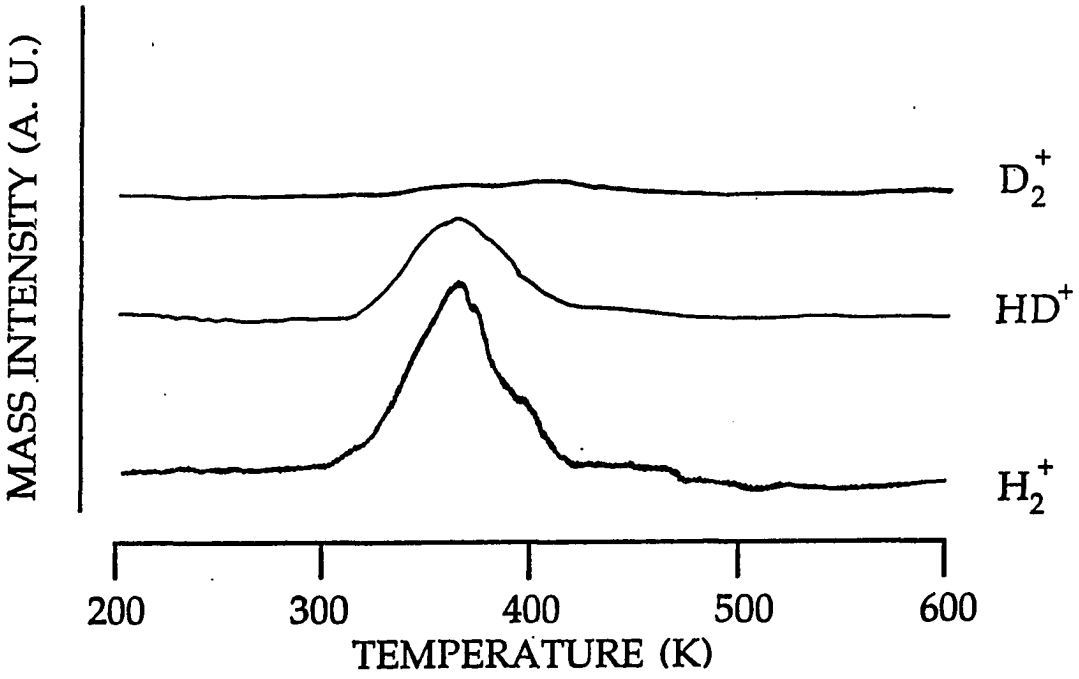

Figure 7. Thermal desorption traces for H_2^+, HD^+, and D_2^+ following exposure of 0.6 L HCOOH and ca. 1.5 L D_2O at 100 K. The heating rate is 15.6 K/s at 100 K and drops continuously to 4.5 K/s at 600 K.

primarily occurs between atoms which originate from the same HCOOH molecule.

The thermal desorption data thus indicate that water and formic acid undergo a mutual depopulation of high-temperature desorption states. This reduction is complete when the water state is reduced to 45% of its clean-surface value, and the acid to 75%. This suggests that the two molecules form a surface complex with a fixed stoichiometry. Isotopic exchange implies that this complex involves hydrogen bonding between the water and formic acid molecules. In an attempt to verify such a complex in the gas phase, masses of possible complexes (e. g., m/e = 64 for $(HCOOH \cdot H_2O)^+$, m/e = 82 for $(HCOOH \cdot 2H_2O)^+$, etc.) were also monitored during thermal desorption. In these experiments the mass spectrometer ionizer voltage was reduced from 70 to 25 volts to minimize cracking of the complex; however, no such complex was observed. Either such a complex is too unstable to survive in the gas phase (up to and past the point of electron-impact ionization), or the complex exists only on the surface and is destroyed upon desorption of water at 180 K.

3.2 High resolution electron energy loss spectroscopy

As we report elsewhere [24] molecular HCOOH can exist in different forms when adsorbed on a solid surface. For all but very low coverages these forms closely resemble the α and β polymorphs observed for solid phase formic acid. Fig. 8 is a typical EEL spectrum for the molecular HCOOH overlayer which resembles the α-polymorph. The most prominent loss in the spectrum occurs at 980 cm^{-1} and is assigned to the out-of-plane OH bend.

Fig. 9 is the loss spectrum for the same overlayer after it is heated to 195 K. This heating is sufficient to desorb all molecular HCOOH and convert the remainder to a bridging formate species. The most prominent loss in this spectrum, assigned to the OCO symmetric stretch, occurs at 1340 cm^{-1}.

In Figs. 10a and 10b are loss spectra for water adsorbed on Pt(111). The spectrum in Fig. 10a is obtained for a surface exposed to sufficient water to saturate its 180 K desorption state. The spectrum in Fig. 10b is obtained for a surface exposed to half that needed to saturate its 180 K state. The features in both spectra agree well with those reported by Sexton [39]. The most intense losses in the spectrum for the saturated surface, at 540 cm^{-1} and 720 cm^{-1}, are assigned to the PtO stretch and a librational mode, respectively. Two other losses are assigned to the HOH scissoring mode (1630 cm^{-1}) and the OH stretch (3400-

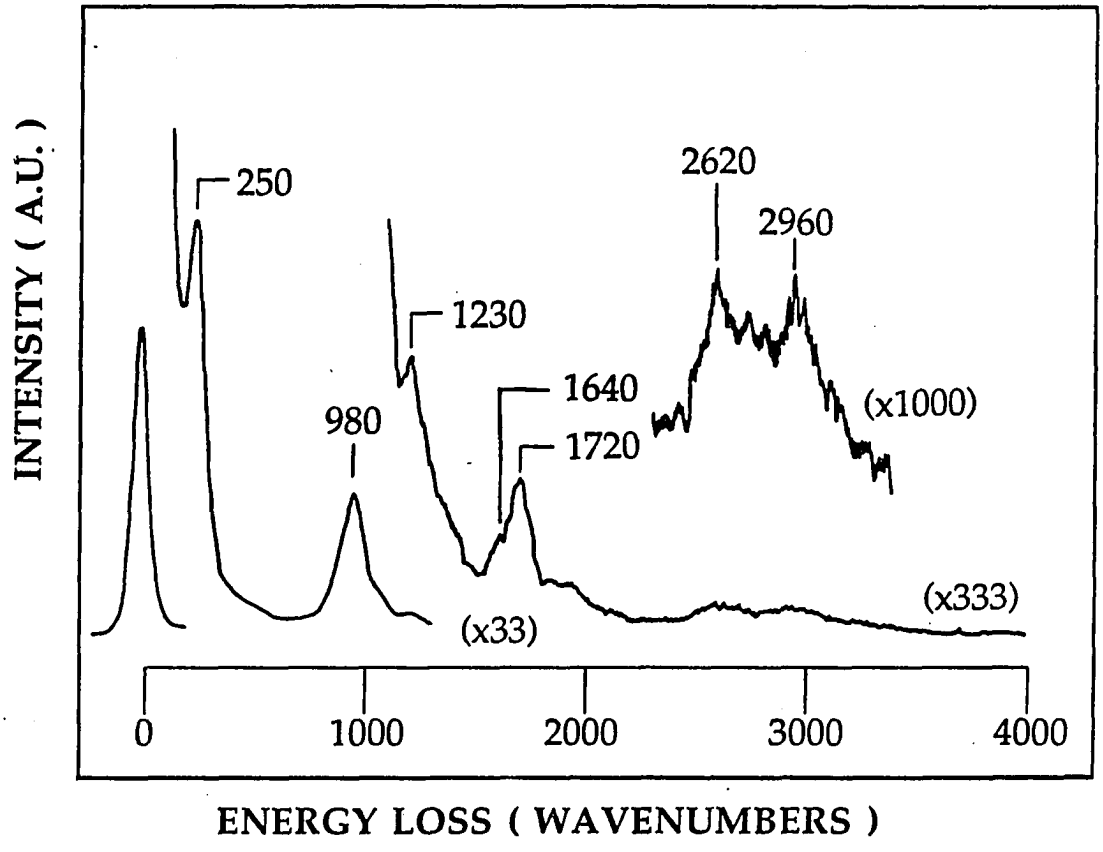

Figure 8. High resolution electron energy loss spectrum following exposure of 0.8 L HCOOH at 100 K followed by heating to 130 K. The elastic peak has an intensity of 350 kHz and a FWHM of 9 mV.

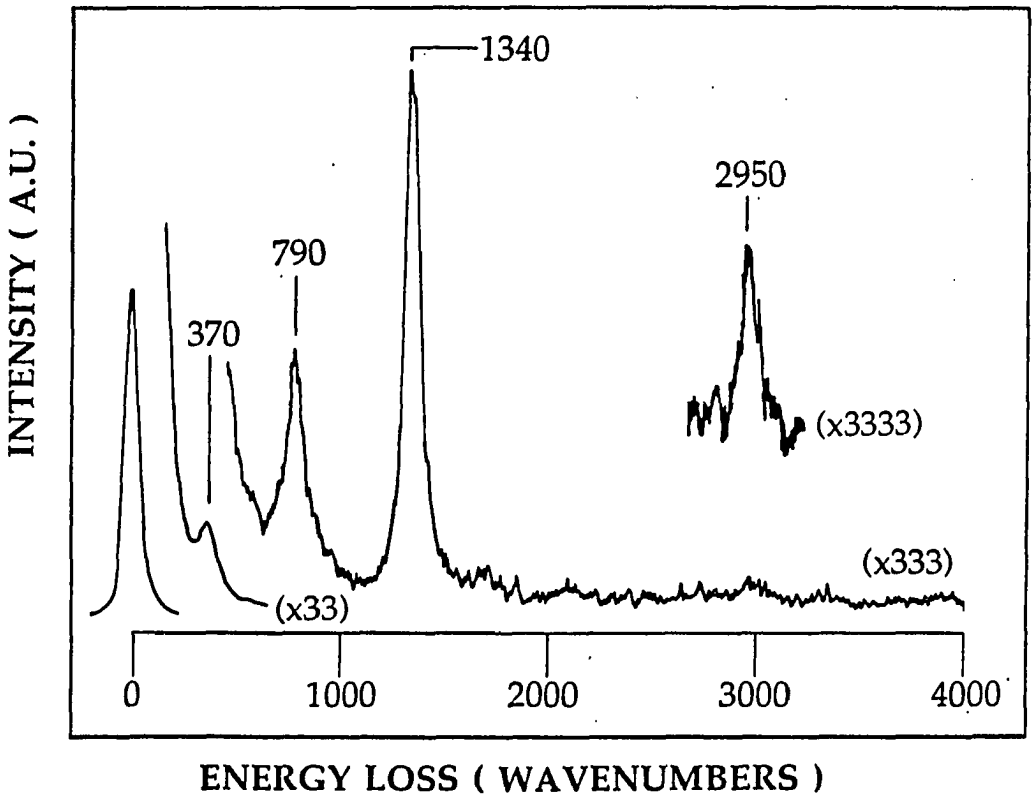

Figure 9. High resolution electron energy loss spectrum following exposure of 0.8 L HCOOH at 100 K and followed by heating to 195 K. The elastic peak has an intensity of 110 kHz and a FWHM of 10 mV.

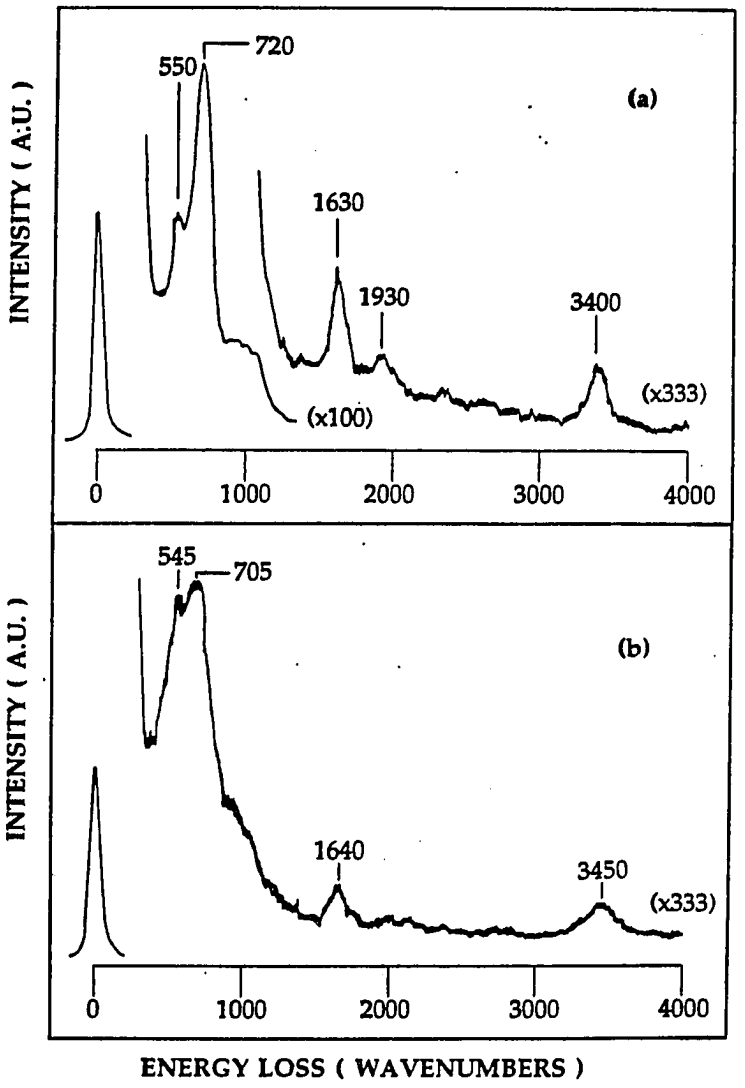

Figure 10. High resolution electron energy loss spectrum following exposure of ca. 1.5 L (a) and 0.7 L (b) H_2O at 100 K. The elastic peaks have intensities of 135 and 100 kHz and FWHM of 9 and 11 mV, respectively.

3450 cm^{-1}). The loss at 1930 cm^{-1} seems to be peculiar to the Pt(111) surface and is assigned to a minority adspecies of water [40]. The primary difference between the two spectra are the intensities of the losses, with the saturated surface exhibiting more intense losses. Notably, the losses due to the PtO stretch and librational modes are approximately equal in intensity for the unsaturated surface (Fig. 10b), but the former loss is much less intense than the latter, for the saturated surface (Fig. 10a).

In Fig. 11 is the loss spectrum for the mixed overlayer produced from exposure to both formic acid and water. To form this overlayer, the surface is exposed to sufficient water (~ 1.5 L) to saturate its 180 K desorption state and sufficient HCOOH (0.6 L) to saturate decomposition and the molecular desorption state at 200 K at 100 K. It is then heated to 150 K to desorb water and HCOOH which were displaced to lower temperature desorption states. This corresponds to the conditions under which the high-exposure plateaus in Fig. 2 and Fig. 5 are obtained.

In Fig. 12 we list all of the losses seen in the spectrum for this mixed overlayer and correlate them with the spectra from Figs. 8-11. The prominent losses for molecular HCOOH (π(OH) at 970 cm^{-1}) and bridging formate (ν_s(OCO) at 1360 cm^{-1} and δ(OCO) at 790 cm^{-1}) appear in this spectrum. The ν(CH) loss at

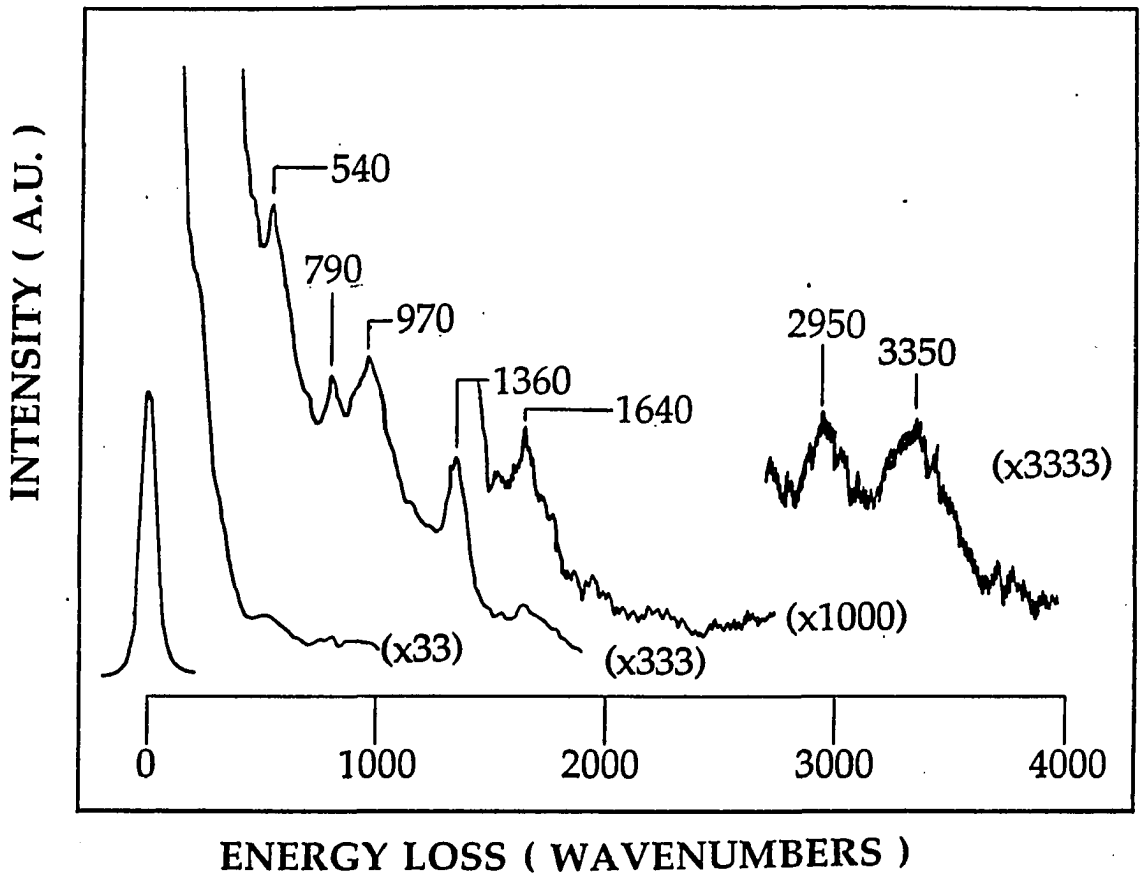

Figure 11. High resolution electron energy loss spectrum following exposure of 0.6 L HCOOH and ca. 1.5 L H_2O and heating to 150 K. The elastic peak has an intensity of 100 kHz and a FWHM of 10 mV.

LOSS FREQUENCY	MOLECULAR HCOOH	BRIDGING FORMATE	WATER	MIXED OVERLAYER
250	lattice			
370		ν (PtO)		
540-550			ν (PtO)	ν (PtO)
705-720			libration	
790		δ (OCO)		δ (OCO)
980	π (OH)			π (OH)
1230	ν (C-O)			
1340-1360		ν_s (OCO)		ν_s (OCO)
1630-1640			δ(HOH)	δ(HOH)
1640 1720 }	ν (C=O)			
2620	ν (OH)			
2950-2960	ν (CH)	ν (CH)		ν (CH)
3350-3450			ν (OH)	ν (OH)

Figure 12. Loss assignments for high resolution electron energy loss spectra of molecular HCOOH (Fig. 8), bridging formate (Fig. 9), water (Fig. 10) and the mixed overlayer (Fig. 11).

2950 cm^{-1} can be attributed to both adspecies. The low frequency losses for the molecular HCOOH and formate (at 250 cm^{-1} and 370 cm^{-1}, respectively) do not appear, perhaps due to increased surface disorder caused by the presence of both adspecies. Losses for water occur at 540 cm^{-1} (ν (PtO)), 1640 cm^{-1} (δ(HOH)), and 3350 cm^{-1} (ν(OH)). The maximum intensity for the ν(OH) loss can occur as low as 3300 cm^{-1} in loss spectra for the mixed overlayer exhibiting a decrease of 100-150 cm^{-1} relative to the water spectrum in Fig. 10b. The most prominent feature missing from the mixed overlayer spectrum is the 720 cm^{-1} loss caused by a water librational mode.

4. Discussion

4.1 The nature of the formic acid and formate adspecies in the mixed overlayer

The HREEL spectrum for the mixed overlayer shows losses for both bridging formate and molecular formic acid. At this exposure molecular formic acid exists in configurations similar to the solid phase, as indicated by the frequencies of the π(OH) loss [24]. In these structures, chains of HCOOH molecules exist with the hydroxyl hydrogen atom of one molecule forming a

hydrogen bond with the carbonyl oxygen atom of the next molecule in the chain. If such catamers remain intact, then it is required that hydrogen bonds between water and acid molecules involve only the water's hydrogen atoms and the acid's oxygen atoms.

The formic acid catamers exhibit two polymorphs with distinctive frequencies for their OH stretching and bending modes. The loss indicative of the molecular acid occurs at 970 cm^{-1} for the OH out-of-plane bend; this is close to the value for the solid phase α-polymorph of formic acid. However, this spectrum is measured for a surface heated to 150 K to desorb all molecular acid and water displaced to lower temperature (< 180 K) desorption states. The molecular acid on clean Pt(111) heated to 150 K exhibits an OH out-of-plane bend at ca. 945 cm^{-1}, closer to the frequency for the same vibration in the β-polymorph. It is difficult, therefore, to conclude which polymorphic form exists under these conditions; we can, however, rule out the presence of HCOOH monomers and dimers. The losses at 790 cm^{-1} and 1360 cm^{-1} reveal the presence of bridging formate along with the molecular acid. Both are also seen in HREEL spectra for Pt(111) heated to 150 K after exposure to only HCOOH. Conversion of molecular acid to formate involves breaking of the acid molecule's O-H bond. This process results in an interruption of the catameric

chain at the point, but it should not eliminate the electron lone pairs on the formic acid oxygen atoms which participate in hydrogen bonding to water admolecules. It is reasonable to posit that the acid-to-formate conversion perturbs the interspecies hydrogen bonding very little.

4.2 Reorientation of water admolecules

The HREEL spectrum for the mixed overlayer reveals two important effects relative to the spectra for water alone: (1) The librational mode at 720 cm^{-1} observed for water on Pt(111) disappears, and (2) the PtO stretch at 540 cm^{-1} remains. We do not believe the disappearance of the librational mode results from a frequency shift which causes overlap of this feature with losses caused by formate of molecular formic acid (i.e., the formate OCO out-of-plane bend at 790 cm^{-1} and the formic acid OH out-of-plane bend at 970 cm^{-1}). The relative intensity of those losses remains unchanged from those produced by similar exposure and temperature conditions on clean Pt(111). Rather, we believe there is a reduction in the intensity of water's librational loss which makes it undetectable on this surface. To understand the implications of these facts, consider the structure proposed for water adsorbed on atomically smooth, (111) faces of fcc transition metals. Thiel and Madey report that the commonly

accepted model for this structure involves a molecular bilayer system with long range order manifested in island formation[41]. Half of the water molecules are involved in direct bonding with the surface via the electron lone pairs on the oxygen atom. The remaining molecules act as hydrogen bonded bridges between those bonded to the surface. This bilayer is illustrated in Fig. 13 and resembles the crystal structure of ice constrained by epitaxy to the (111) substrate lattice.

The vibrational spectra for the bilayer structure commonly exhibit two features not seen for water in the gas phase. These features are assigned to the metal-oxygen stretch (500-550 cm^{-1}) and one or more frustrated rotational modes called librations (600-1000 cm^{-1}). The dipole activity of these librational modes indicates the symmetry of the water admolecules is lower than C_{2v} [42]. This lower symmetry permits the bilayer to exist as closely as possible to the structure of ice with each water molecule in the lower half of the bilayer participating in hydrogen bonding with three molecules in the upper half.

The absence of the librational modes in the loss spectrum for the mixed overlayer reveals that a significant fraction of water molecules which remains in the 180 K desorption state undergo a change in symmetry to C_{2v}. (A configuration for the water molecule orienting its molecular plane parallel to the surface can be ruled out due to enhancement of the dipole activity of the wagging

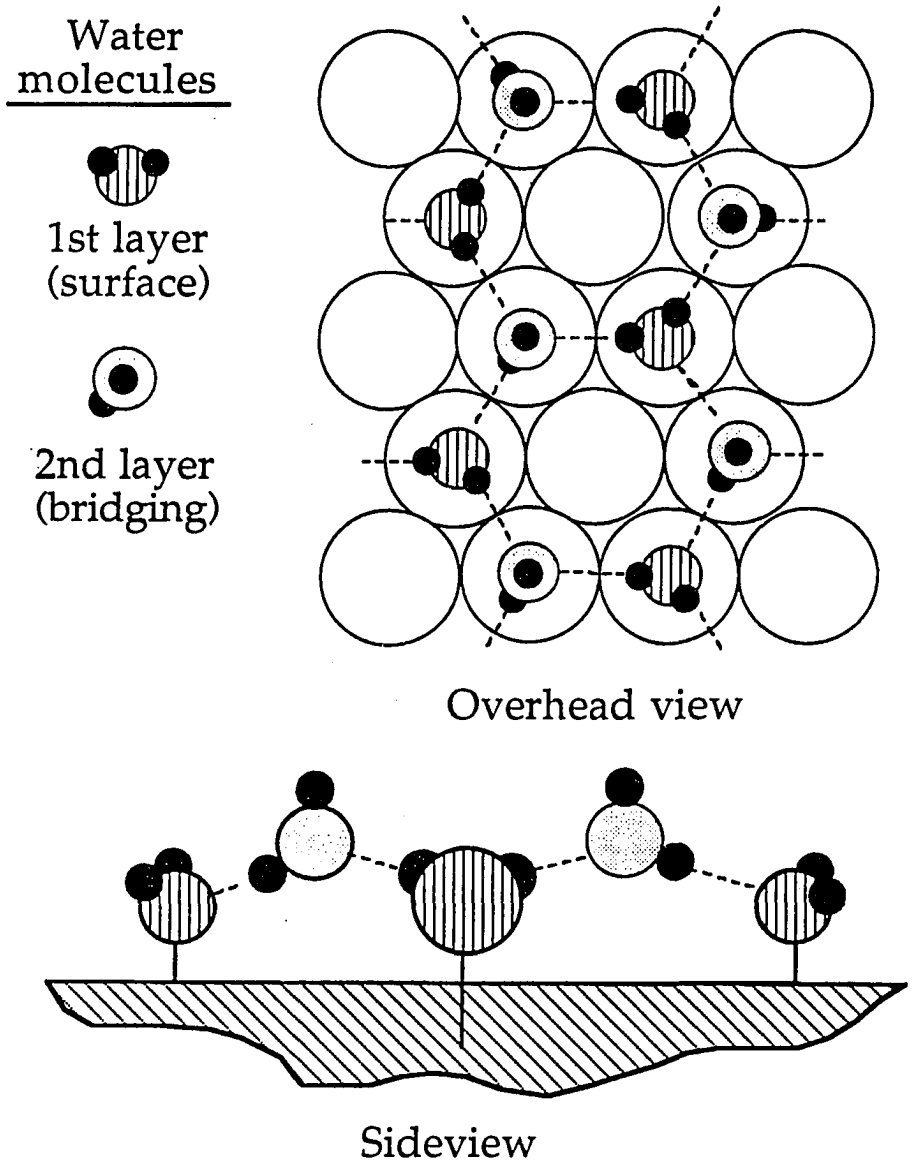

Figure 13. Model of the water bilayer structure on an fcc (111) surface. Taken from Thiel and Madey [41].

libration, which would occur for such a hypothetical orientation. In other words, the wagging mode would become more, not less, intense.) The presence of the PtO stretch shows that there are still water molecules in direct contact with the surface. Should those admolecules involved in direct bonding to the surface possess C_{2v} symmetry the long range order of the bilayer would be significantly altered. This would arise from the reduction in the number of hydrogen bonds those water admolecules can form with the molecules in the upper half of the bilayer (from three to two) and subsequent inability to form an extensive hydrogen-bonded layer. The effects of symmetry on possible interactions between the water bilayer and molecular HCOOH and the formate adspecies are discussed in section 4.3.

4.3 Mutual displacement

The peak temperatures for molecular desorption of water in a bilayer and formic acid in direct contact with the Pt(111) surface differ by only 20 K indicating very little disparity in their respective energies of adsorption. Mutual displacement is then not such a surprise; the surprise is the consistent amounts which are displaced. When water is coadsorbed with HCOOH, water is displaced to its 160 K desorption state. The degree of displacement changes most rapidly at

HCOOH exposures that populate the molecular HCOOH desorption state at 200 K, and, when complete, approximately 55% of the water is displaced.

When HCOOH exposure is constant at 0.6 L (sufficient to saturate its 200 K molecular desorption state) and water exposure increases, HCOOH molecules in the 200 K desorption state are displaced to the state peaked at 160 K. Displacement reaches a maximum beyond 25-30% of the water exposure needed to saturate its 180 K desorption state and at this maximum the desorption area of the 200 K HCOOH desorption state is only 75% of that for clean Pt(111).

Coadsorption of D_2O and HCOOH indicates hydrogen bonding occurs between the two adspecies, based upon the isotopic mixing observed mass spectrometrically. This mixing, taken with the mutual displacement results mentioned above and the downshift in the O-H stretch frequency of water, suggests that a hydrogen-bonded structure of reproducible stoichiometry is produced between water and formic acid molecules. The reorientation of water admolecules observed in the HREEL spectra for the mixed overlayer indicates that the structure produced significantly alters the water bilayer structure which exists in the absence of coadsorbed formic acid. We believe this is accomplished by the "invasion" of the water bilayer by the HCOOH chains which breaks up long range order and leaves only small patches of the bilayer intact. This

structure is illustrated in Fig. 14. Two arrangements of hydrogen bonding between the HCOOH chain and the water admolecules are presented which allow the reorientation of some of the water molecules while leaving others in direct contact with the surface. In one arrangement the bridging water molecule possesses C_{2v} symmetry which allows the water molecule in direct contact with the surface to retain its C_s symmetry; the alternate arrangement allows the bridging water molecule to retain its C_s symmetry which forces the water molecule in direct contact with the surface to adopt C_{2v} symmetry.

4.4 Possible stoichiometries

As a start to determine possible stoichiometries for the hydrogen bonded complex, we consider the coverage of water in the bilayer structure; this is estimated to be 0.67 monolayer [41]. Approximately 55% of this is displaced by the HCOOH, leaving a coverage of ca. 0.3 monolayer. Unfortunately, HCOOH coverages are more difficult to estimate due to lack of long range order in its overlayer structure. As a guideline we estimate the HCOOH coverage to fall between 0.1 and 0.2 monolayer. These limits are based on the amount of HCOOH which decomposes; comparison of the desorption area of H_2 produced from HCOOH decomposition at saturation with that for H_2 desorption from a

saturated surface (one monolayer of H adatoms) gives a range of 0.05-0.1 monolayer for the coverage of HCOOH which decomposes [22, 23]. If the sticking probability remains constant up to an exposure of 0.6 L (the exposure which saturates desorption yields of CO_2 and H_2 and the HCOOH molecular desorption at 200 K), it is reasonable that above 140 K, half of the HCOOH is converted to formate (and, ultimately, to gaseous H_2 and CO_2) while the remainder desorbs molecularly in the state peaked at 200 K. This gives limits which are twice the HCOOH decomposition coverage or 0.1-0.2 monolayer. Considering this range the water-to-HCOOH ratios must fall between 1.5 : 1 and 3 : 1.

One possible structure involves one bridging water molecule between one water molecule in direct contact with the surface and one HCOOH molecule; this gives a 2 : 1 stoichiometry. This is the type of structure shown in Fig. 14. Given the range of water-to-HCOOH ratios a 3 : 1 stoichiometry is also another strong possibility; however, higher stoichiometries, as well as the existence of unhydrated HCOOH molecules cannot be ruled out entirely. The most probable condition is one where the 2 : 1 and 3 : 1 stoichiometries predominate with other stoichiometries being far less common. The average stoichiometry, however,

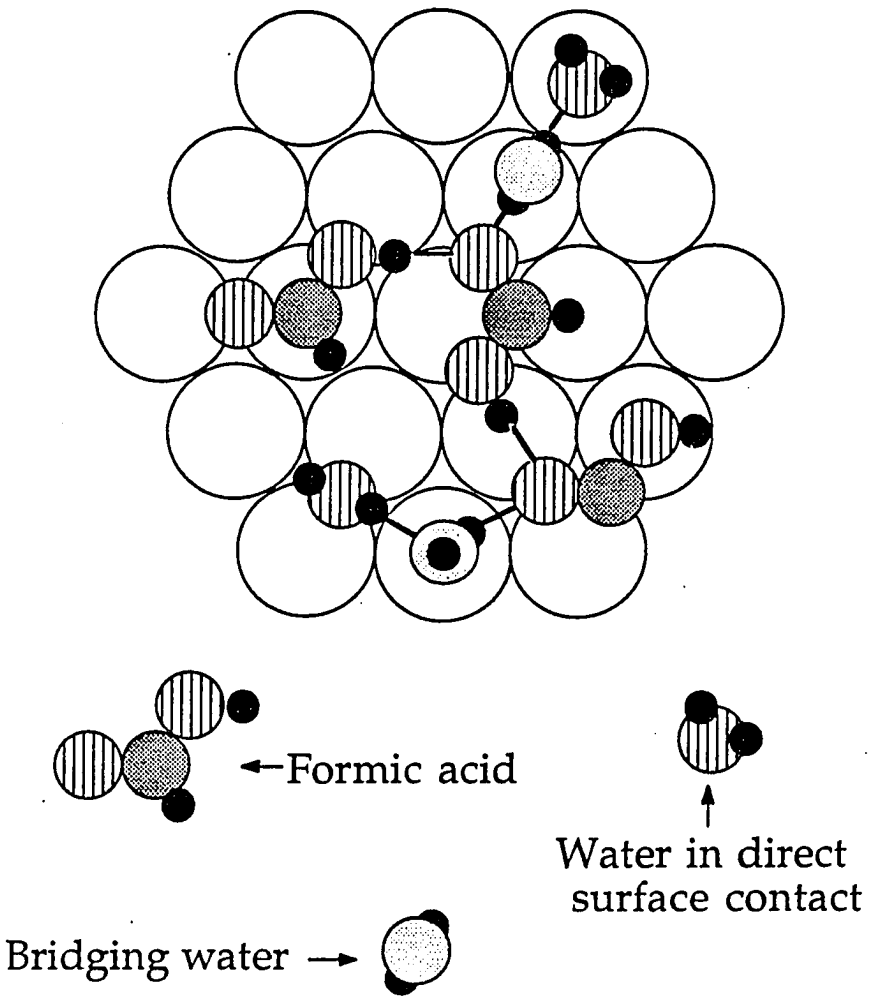

Figure 14. Model of the $2H_2O \cdot HCOOH$ complex

remains a statistically reproducible phenomenon as reflected in the reproducibilty of the amounts of HCOOH and water displaced.

5. Summary

The coadsorption of water and formic acid on Pt(111) produces a mixed overlayer which contains reproducible amounts of the two adsorbates. Formic acid displaces ca. 55% of the water from its 180 K desorption state on the clean surface. Water displaces about 25% of the formic acid from its 200 K desorption state on the clean surface. The consistency of these values, and the fact that they do not depend upon adsorption sequence, suggests that a stoichiometric complex forms between water and formic acid. (Glagoleva suggests the existence of such complexes in aqueous solutions of HCOOH [34, 35].) Thermal desorption from a surface exposed to D_2O and formic acid shows that both H_2 and HD are produced from the decomposition of formic acid. This indicates extensive hydrogen bonding between D_2O and formic acid as a possible driving force behind the complex formation.

HREEL spectra for this mixed overlayer after heating to 150 K indicate the presence of water, molecular acid, and bridging formate. Water does not measurably affect the conversion of molecular acid to formate and has the capacity to participate in hydrogen-bonding with both the molecular acid and the formate. These spectra still exhibit the PtO stretch of water, yet its librational mode has disappeared. We interpret this as due to reorientation of a large fraction of water molecules in the overlayer from C_s to C_{2v} symmetry while allowing a large fraction of the water molecules to remain in direct contact with the surface.

We suggest two possible stoichiometries for the complex ($2H_2O \cdot HCOOH$ and $3H_2O \cdot HCOOH$) based on the coverages which correspond to the amounts of water and formic acid which remain in their high temperature ($T_p > 160$ K) desorption states, 0.3 monolayer and 0.1- 0.2 monolayer, respectively. While both of these stoichiometric complexes agree with the coverages of formic acid and water, the existence of other stoichiometries cannot be ruled out entirely. We will continue study of this system with low energy electron diffraction (LEED) and electron stimulated desorption ion angular distribution (ESDIAD) to augment these models.

Acknowledgements

Acknowledgement is made to the Donors of The Petroleum Research Fund, administered by the American Chemical Society. Some equipment and all facilities are provided by the Ames Laboratory, which is operated for the U. S. Department of Energy by Iowa State University under Contract No. W-7405-ENG-82.

References

1. H. Angerstein-Kozlowska, B. MacDougall and B. E. Conway, J. Electrochem. Soc, 120 (1973) 756

2. R. R. Adzic, D. N. Simic, A. R. Despic and D. M. Drazic, J. Electroanal. Chem., 65 (1975) 587

3. V. E. Kazarinov, R. R. Adzic, V. N. Andreev and A. N. Zhuchkov, J. Electroanal. Chem., 270 (1989) 137

4. J. Clavilier, A. Fernanadez-Vega, J. M. Feliu and A. Aldaz, J. Electroanal. Chem., 261 (1989) 113

5. A. Fernandez-Vega, J. M. Feliu, A. Aldaz and J. Clavilier, J. Electroanal. Chem., 258 (1989) 101

6. J. Clavilier, A. Fernandez-Vega, J. M. Feliu and A. Aldaz, J. Electroanal. Chem., 258 (1989) 89

7. M. Shibata, O. Takahashi and S. Motoo, J. Electroanal. Chem., 249 (1988) 253

8. M. Shibata, N. Furuya, M. Watanabe and S. Motoo, J. Electroanal. Chem., 263 (1989) 97

9. M. Watanabe, M. Horiucchi and S. Motoo, J. Electroanal. Chem., 250 (1988) 117

10. L. V. Minevski and R. R. Adzic, J. Appl. Electrochem, 17 (1987) 240

11. R. W. Tsang, D. C. Johnson and G. R. Luecke, J. Electrochem. Soc., 131 (1983) 2369

12. C. Lamy, J. M. Leger, J. Clavilier and R. Parsons, J. Electroanal. Chem., 150 (1983) 71

13. J. Clavilier, R. Parsons, R. Durand, C. Lamy and J. M. Leger, J. Electroanal. Chem, 124 (1981) 321

14. B. Beden, A. Bewick and c. Lamy, J. Electroanal. Chem., 148 (1983) 147

15. B. Beden, A. Bewick and C. Lamy, J. Electroanal. Chem., 150 (1983) 505

16. S.-C. Chang, L.-W. H. Leung and M. J. Weaver, J. Phys. Chem., 94 (1990) 6013

17. D. S. Corrigan and M. J. Weaver, J. Electroanal. Chem., 241 (1988) 143

18. K. Kunimatsu, J. Electroanal. Chem., 213 (1986) 149

19. K. Kunimatsu and H. Kita, J. Electroanal. Chem., 218 (1987) 155

20. S. G. Sun, J. Clavilier and A. Bewick, J. Electroanal. Chem., 240 (1988) 147

21. O. Wolter, J. Willsau and J. Heitbaum, J. Electrochem. Soc., 132 (1985) 1635

22. M. R. Columbia and P. A. Thiel, Surf. Sci., 235 (1990) 53

23. M. R. Columbia and P. A. Thiel, Proc. DOE Workshop -Direct Methanol/Air Fuel Cells, to be published (1990)

24. M. R. Columbia, A. M. Crabtree and P. A. Thiel, submitted to J. Am. Chem. Soc., (1991)

25. N. Kizhakevariam and E. M. Stuve, J. Vac. Sci. Technol. A, 8 (1990) 2557

26. N. R. Avery, App. Surf. Sci., 11/12 (1982) 774

27. N. R. Avery, App. Surf. Sci, 14 (1982-83) 149

28. N. Abbas and R. J. Madix, App. Surf. Sci., 16 (1983) 424

29. G. B. Fisher and J. L.Gland, Surf. Sci., 94 (1980) 446

30. R. Dœhl-Oelze, C. C. Brown, S. Stark and E. M. Stuve, Surf. Sci., 210 (1989) 339

31. N. Kizhakevariam, E. M. Stuve and R. Dœhl-oelze, J. Chem Phys., 94 (1991) 670

32. N. Kizhakevariam, R. Dœhl-Oelze and E. M. Stuve, J. Phys. Chem., 94 (1990) 5934

33. F. T. Wagner and T. E. Moylan, Surf. Sci, 182 (1987) 125

34. A. A. Glagoleva, J. Gen. Chem. (U. S. S. R.), 11 (1941) 765

35. A. A. Glagoleva, J. Gen. Chem. (U. S. S. R.), 6 (1936) 1769

36. M. R. Columbia and P. A. Thiel, Rev. Sci. Instrum., 58 (1987) 309

37. P. K. Leavitt, J. L. Davis, J. S. Dyer and P. A. Thiel, Surf. Sci., 218 (1989) 346

38. G. A. Ropp and C. E. Melton, J. Am. Chem. Soc., 80 (1958) 3509

39. B. A. Sexton, Surf. Sci., 94 (1980) 435

40. F. T. Wagner and T. E. Moylan, Surf. Sci., 191 (1987) 121

41. P. A. Thiel and T. E. Madey, Surf. Sci. Rep., 7 (1987) 211

42. P. A. Thiel, F. M. Hoffmann and W. H. Weinberg, J. Chem. Phys., 75 (1981) 5556

SECTION IV:

THE EFFECT OF COADSORBED ATOMIC OXYGEN ON THE INTERACTION OF FORMIC ACID WITH PT(111)

The Effect of Coadsorbed Atomic Oxygen on the Interaction of Formic Acid with Pt(111)

by

M. R. Columbia, A. M. Crabtree, and P. A. Thiel

Department of Chemistry and Ames Laboratory
Iowa State University
Ames, IA 50011 USA

To be submitted to *Journal of Chemical Physics*

Abstract

We have studied the influence of atomic oxygen on the interaction between formic acid and the (111) surface of Pt using the techniques of thermal desorption spectroscopy and high resolution electron energy loss spectroscopy. The presence of atomic oxygen enhances the production of formate adspecies. The temperature for complete conversion of molecular formic acid to formate is lowered by as much as 70 K relative to the clean surface; the desorption yields for CO_2 resulting from decomposition of the formate adspecies are increased by factors of four to six. This decomposition occurs at temperatures 25-55 K higher than the clean surface, further indicating stabilization of the formate by atomic oxygen. Water is the other primary decomposition product; this contrasts with the clean surface, which produces only H_2 and CO_2. At low HCOOH exposures water desorbs in two states with peak temperatures of 200-210 K and 285-300 K. The low temperature state is indicative of the presence of hydroxyl adspecies; this is confirmed in the HREEL spectra. With increasing HCOOH exposure, a new water desorption state emerges from the state at 200-210 K. The peak temperature of this new state, probably caused by the desorption of molecular water, moves down with increasing HCOOH exposure to 170-175. At high

HCOOH exposure, the CO_2 desorption at 285 K saturates; simultaneously new features emerge, not observed from the clean surface, in desorption traces both for CO_2 and molecular acid.

1. Introduction

There are many studies of the interaction of formic acid and atomic oxygen on transition metals reported in the surface science literature [1-10]. These studies generally agree that atomic oxygen facilitates the decomposition of molecular formic acid to a formate surface intermediate. On the (110) surfaces of Ag [1, 2] and Au [3] formic acid does not undergo decomposition; however, the presence of atomic oxygen on these surfaces results in the extraction of the acid's hydroxyl proton and the production of surface formate. This formate is stable on the Ag surface to 400 K [1, 2] and on the Au surface to 340 K [3]. At these temperatures the formate decomposes to give gaseous CO_2 and H_2 or H_2O.

On surfaces where decomposition does occur, such as Rh, Ni, and Pt, atomic oxygen can change the reaction pathway. Solymosi et al report that HCOOH on clean Rh(111) produces CO and H_2O (dehydration products), as well as CO_2 and H_2 (dehydrogenation products); atomic oxygen retards desorption of CO and H_2. Thus, oxygen promotes dehydrogenation over dehydration and the atomic hydrogen reacts preferentially with atomic oxygen to yield water (CO_2 yield also increases) [4]. Johnson and Madix report a dramatic change in the decomposition pathway on Ni(110) . Clean Ni(110) produces sharp desorption

features at 400 K for CO_2 and H_2 from formic acid decomposition; this is attributed to an autocatalytic reaction. Atomic oxygen inhibits this reaction and allows decomposition to occur by a nonautocatalytic process, producing relatively broad desorption features for CO_2 and H_2 [5].

Avery reports less drastic changes in the decomposition of HCOOH on Pt(111) as a result of coadsorbed atomic oxygen [6, 7]. Dehydrogenation is the only pathway observed both on the clean and oxygen-covered surfaces giving CO_2 desorption with a peak temperature of 260 K. He estimates that the formate coverage on the oxygen-covered surface is increased by a factor of six or seven relative to the clean surface, based on high resolution electron energy loss intensities. In addition, the clean surface produces H_2, while the oxygen-covered surface gives both H_2 and H_2O as desorption products. (Similar differences are reported for clean and oxygen-covered surfaces of Cu [9, 10].)

We have studied the interaction of atomic oxygen and formic acid on Pt(111) using thermal desorption spectroscopy and high resolution electron energy loss spectroscopy. In a previous paper, we have described the reactions of formic acid on clean Pt(111) [11]. In the present paper, we compare the reactions which formic acid undergoes on Pt(111) in the presence of oxygen. By combining data from thermal desorption spectroscopy and high resolution electron energy

loss spectroscopy, we can develop a detailed reaction scheme which explains the complex influence of atomic oxygen in this system.

2. Experimental Details

The ultrahigh vacuum system, the method of performing thermal desorption experiments, and the Pt(111) crystal used for these experiments have been previously described [11-13]. The exposure units reported in this paper are Langmuir, although the surface is exposed to HCOOH through a directional doser containing a conductance-limiting aperture. We determine the Langmuir equivalence based on comparison of CO thermal desorption areas following exposure via the doser with areas following exposure via backfilling. A saturated layer of atomic oxygen is prepared by exposing the Pt(111) surface to ca. 5 L O_2 at 100 K followed by heating to 180-200 K; this removes oxygen which is adsorbed molecularly and leaves a 0.25 monolayer of atomic oxygen on the surface. (We define one monolayer as the density of atoms at the Pt(111) surface, i.e. 1.50×10^{15} per cm^2.) Auger electron spectroscopy confirms the saturation of the atomic oxygen layer. Gland et al report an Auger ratio of 0.3 for the O(510 eV) peak

height to the Pt(237 eV) peak height for the the saturated layer [14]. We observe a ratio of 0.29 at saturation. (Higher O_2 exposures do not increase this ratio.) Gland et al verify the coverage by LEED [14].

The high resolution electron energy loss spectrometer has also been described previously [13]. The elastic peaks have intensities between 100 and 350 kHz and full-widths at half-maxima between 8 and 11 meV (65 cm^{-1} to 89 cm^{-1}). For those experiments which probe the effect of temperature on the vibrational spectrum, exposure temperatures are between 80 and 100 K; the surface is then heated to the indicated temperature at ~5 K/s, followed by determination of the loss spectrum while the surface cools. This method of heating differs from the continuous heating performed in TDS experiments. This difference results in desorption states occuring at temperatures 10- 20 K higher than the corresponding changes in the vibrational spectrum.

3. Results

3.1 Thermal desorption

For exposures less than 0.3 L HCOOH on clean Pt(111), decomposition occurs exclusively; this produces desorption of CO_2 with a peak temperature of 260 K, and of H_2 with peak temperatures between 350 K and 390 K. The desorption of CO_2 is attributed to the decomposition of bridging formate adspecies, while H_2 desorption resembles that from clean Pt(111) exposed to H_2 only [11, 15, 16]. Coadsorption of atomic oxygen alters this behavior markedly.

Fig. 1 shows a series of thermal desorption spectra for CO_2 from Pt(111) covered with 0.25 monolayer of atomic oxygen prior to HCOOH adsorption. For the lowest exposure of HCOOH (0.08 L), the peak temperature for CO_2 desorption occurs at ca. 315 K and moves down to 280-285 K with increasing exposure. This is 20-55 K higher than the CO_2 peak desorption temperature observed for the clean surface, which is invariant with HCOOH exposure. At exposures of 0.6 L and above, a second desorption feature emerges; it appears at ca. 190 K and moves down in temperature with increasing exposure. (This feature is not observed for the clean surface.) The intensity of this feature increases with exposure up to ca. 1 L, then decreases.

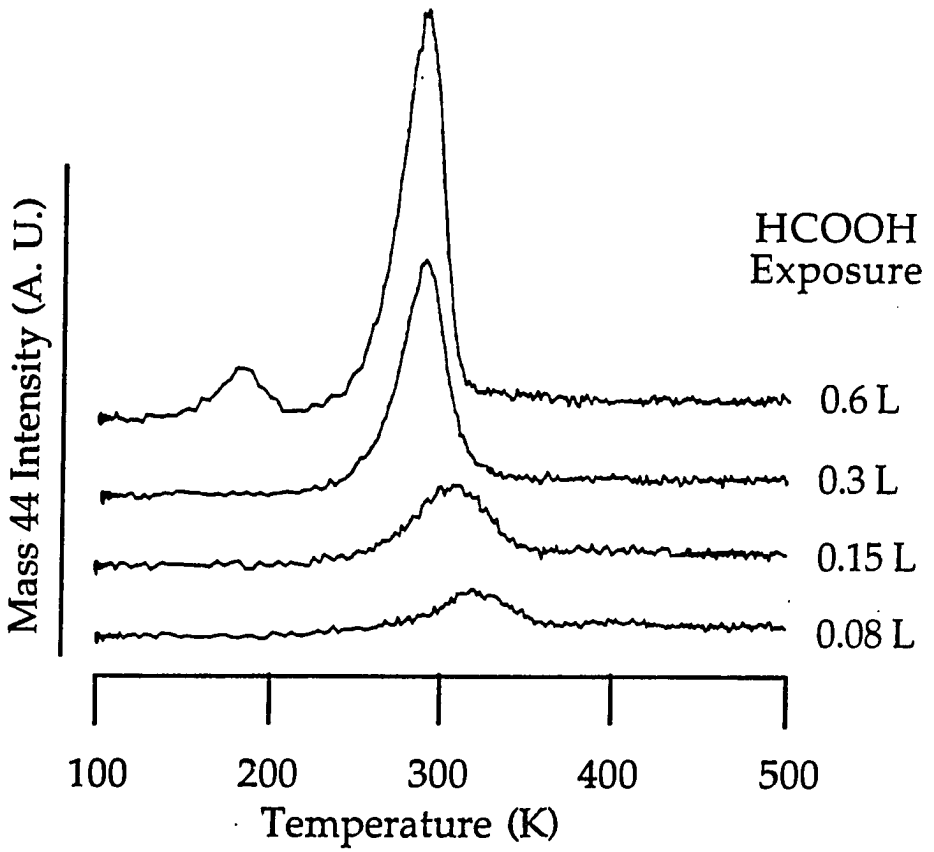

Figure 1. Series of thermal desorption traces for CO_2^+ following stated exposures of HCOOH at 100 K. The Pt(111) surface is exposed to 5 L O_2 at 100 K and heated to 200 K prior to exposure to HCOOH. The heating rate is 15.6 K/s at 100 K and drops continuously to 4.7 K/s at 500 K.

Another dramatic change relative to the clean surface is the increase in desorption yield for CO_2. Fig. 2 shows CO_2 desorption areas (normalized to saturation for the clean surface) for the clean (a) and the oxygen-predosed (b) surfaces vs HCOOH exposure. The inset shows thermal desorption spectra for an exposure (0.6 L) which saturates CO_2 desorption yields from both surfaces. The saturation desorption yield from the oxygen-predosed surface is 4 to 6 times greater than that from the clean surface. There appear to be two factors contributing to this increase: (1) The HCOOH exposure needed for saturation is doubled (0.3 L for the clean surface vs 0.6 L for the oxygen-predosed one). (2) For HCOOH exposures below decomposition saturation (< 0.3 L), the rate of increase in CO_2 desorption as HCOOH exposure increases is 2 to 3 times greater for the oxygen-predosed surface relative to the clean surface; this implies that atomic oxygen enhances the sticking coefficient for HCOOH relative to the clean surface.

The presence of atomic oxygen retards H_2 production from decomposition of HCOOH. Fig. 3 is a series of thermal desorption traces for H_2 from the oxygen-predosed surface. For HCOOH exposures below 0.6 L no H_2 desorption is seen; this is the same exposure range where CO_2 desorption grows. On clean Pt (111), the desorption of CO_2 and H_2 appears and saturates over the same HCOOH

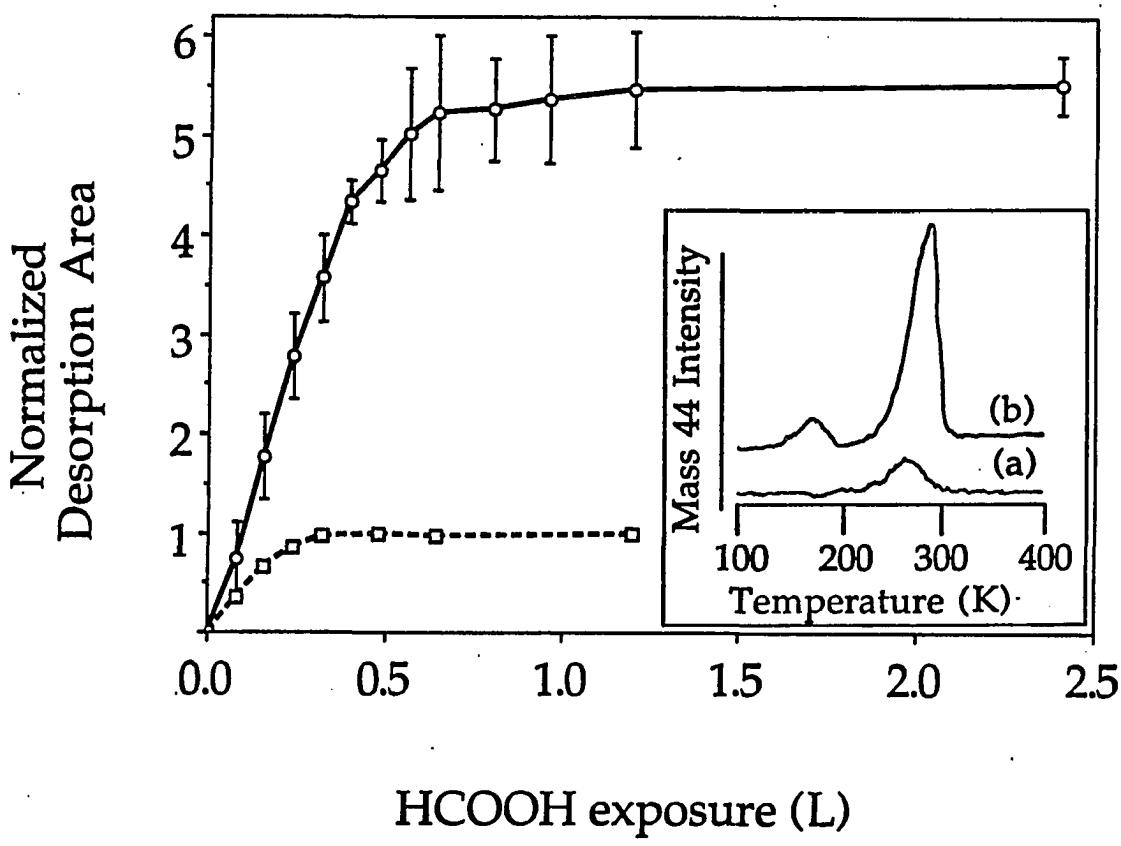

Figure 2. CO_2^+ desorption area as a function of HCOOH exposure for clean Pt(111) and Pt(111) covered with 0.25 monolayer of atomic oxygen. The desorption areas are normalized to the saturated desorption area of clean Pt(111). The inset shows spectra for saturated CO_2^+ desorption areas for (a) clean Pt(111) and (b) Pt(111) covered with 0.25 monolayer of atomic oxygen.

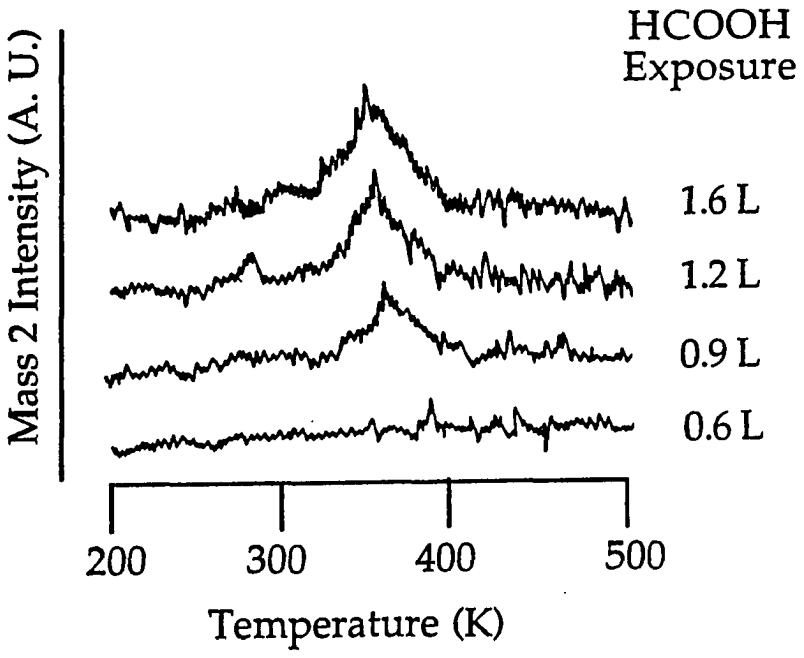

Figure 3. Series of thermal desorption traces for H_2^+ following stated exposures of HCOOH at 100 K. The Pt(111) surface is exposed to 5 L O_2 at 100 K and heated to 200 K prior to exposure to HCOOH. The heating rate is 8.5 K/s at 200 K and drops continuously to 4.7 K/s at 500 K.

exposure range. Above 0.6 L HCOOH, H_2 desorption occurs, and saturates by ca. 1.2 L. This desorption has its maximum at temperatures of 350-380 K, similar to the clean surface.

Water desorption occurs from the oxygen-predosed surface for HCOOH exposures less than 0.3 L; this stands in contrast to the clean surface. The only water observed for the clean surface occurs at the same temperature and exposure conditions as molecular HCOOH desorption. We attribute it to cracking of the acid molecule in the mass spectrometer ionizer, and not to true surface desorption. However, water desorption *is* observed from the oxygen-predosed surface at exposures below the threshold of molecular HCOOH desorption. Fig. 4 displays a series of water thermal desorption spectra for increasing HCOOH exposures. At 0.3 L HCOOH, water desorbs in two broad states: one centered at about 205 K (labeled A1) and the other at 290 K (labelled A2). The peak temperature of A1 is close to that of water desorption resulting from reaction of surface hydroxyl groups [17, 18] and A2's is close to the peak desorption temperature for CO_2 at this exposure. As HCOOH exposure increases, the A1 state broadens further and grows asymmetrically toward lower temperatures.

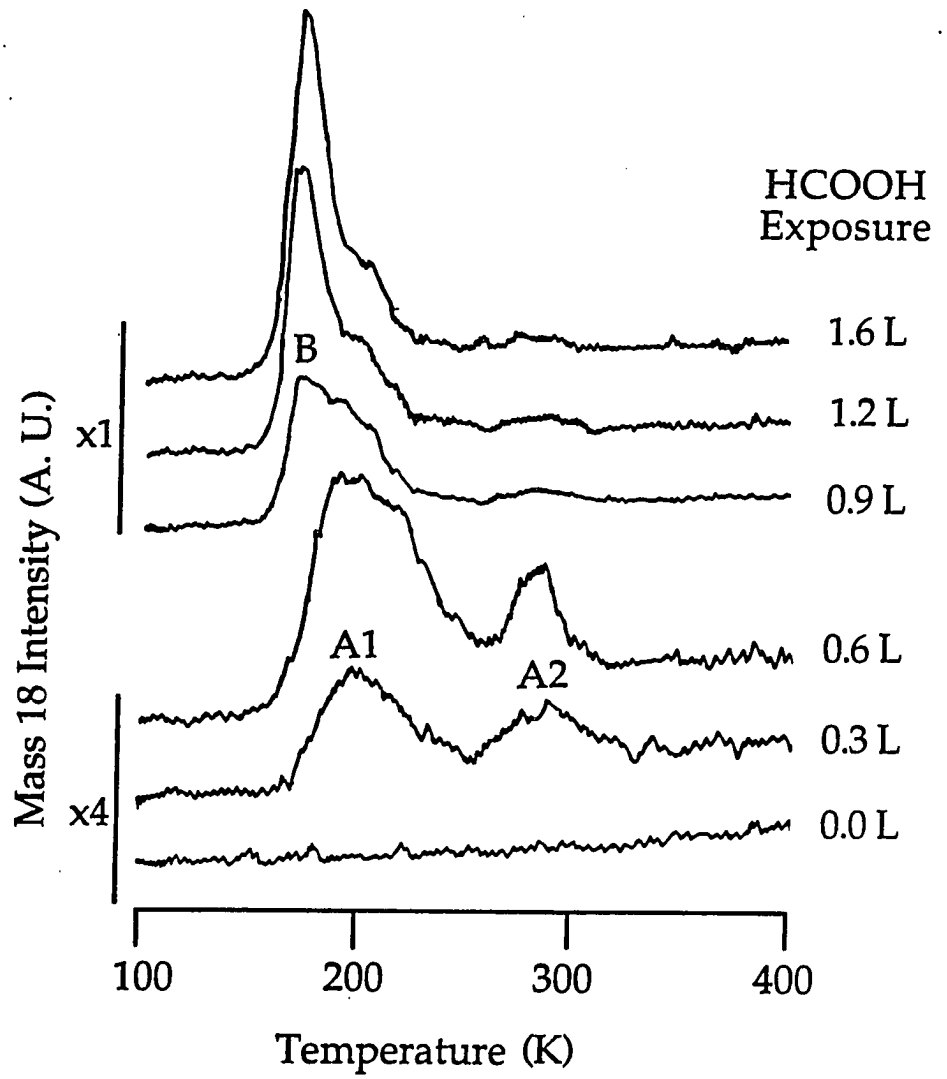

Figure 4. Series of thermal desorption traces for H_2O^+ following stated exposures of HCOOH at 100 K. The Pt(111) surface is exposed to 5 L O_2 at 100 K and heated to 200 K prior to exposure to HCOOH. The heating rate is 8.5 K/s at 200 K and drops continuously to 4.7 K/s at 500 K.

Eventually, a new peak (labelled B) emerges and continues to move lower in temperature; at an exposure of 1.2 L the B-state is at a peak temperature of 170-175 K with the A1-state appearing as a high temperature shoulder. The yield of the A2-state reaches a maximum at 0.6 L and then decreases with increasing exposure, by ca. 33% relative to the maximum.

Molecular HCOOH desorption is also altered by the presence of oxygen adatoms. On clean Pt(111) such desorption begins at exposures above 0.3 L in a state at 200 K [16]. A second state appears at exposures above 0.6 L; simultaneously, the state at 200 K saturates [16]. The second state emerges with a peak temperature of 160 K and moves up with increasing exposure. At an exposure of 1.2 L this peak temperature is 170 K and a third desorption state emerges at 160 K [16]. This third state also moves up in temperature with increasing exposure; it eventually merges with the second desorption feature and this single feature grows without bound. An important distinction between the 200 K state and the two at lower temperature is the nature of the HCOOH molecules desorbing from them. Desorption from the 200 K state is dominated by HCOOH monomers while desorption from the lower temperature states is dominated by HCOOH dimers [16].

Fig. 5 displays a series of thermal desorption spectra for mass 29. (HCO^+, 29 amu, is the most intense fragment produced by cracking of HCOOH in the mass spectrometer ionizer.) The first molecular desorption state (here labelled A) appears at exposures above 0.3 L as on the clean surface; unlike the clean surface, however, this state mimics the CO_2 desorption state at 280-285 K. At 0.8 L HCOOH exposure a second state (labelled B) emerges at 200 K, followed at 0.9 L by a third state (labelled C) emerging at 175-180 K. State C continues to grow and saturates at 1.2-1.4 L; simultaneously, a fourth state (labelled D) appears at 155-160 K. This state moves to higher temperatures with increasing exposure. A fifth state (labelled E) appears as a low temperature shoulder on state D above exposures of 2.3 L; resolution of these two states (D and E) is not always obtained. The combined area of states D and E grows without bound with increasing exposure; this is consistent with desorption from a multilayer.

As previously noted, molecular HCOOH desorption from the clean surface occurs either as monomers or dimers. Fig. 6 displays thermal desorption traces for mass 29, HCO^+, (produced by the cracking of both monomers and dimers) and mass 47, $HCOOH \cdot H^+$, (produced by the cracking of dimers only) from the oxygen-predosed surface exposed to 2.3 L HCOOH at 100 K. While all 5 states (A-

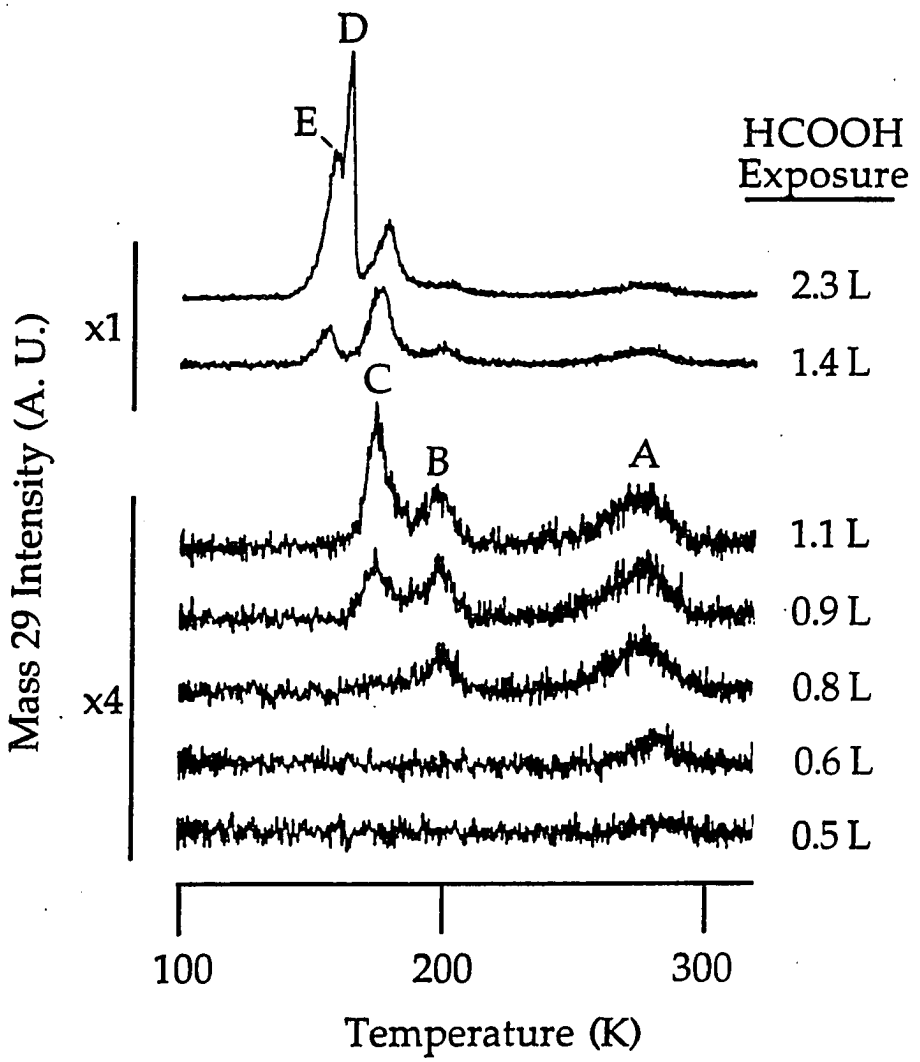

Figure 5. Series of thermal desorption traces for HCO^+ following stated exposures of HCOOH at 100 K. The Pt(111) surface is exposed to 5 L O_2 at 100 K and heated to 200 K prior to exposure to HCOOH. The heating rate is 15.6 K/s at 100 K and drops continuously to 6.5 K/s at 300 K.

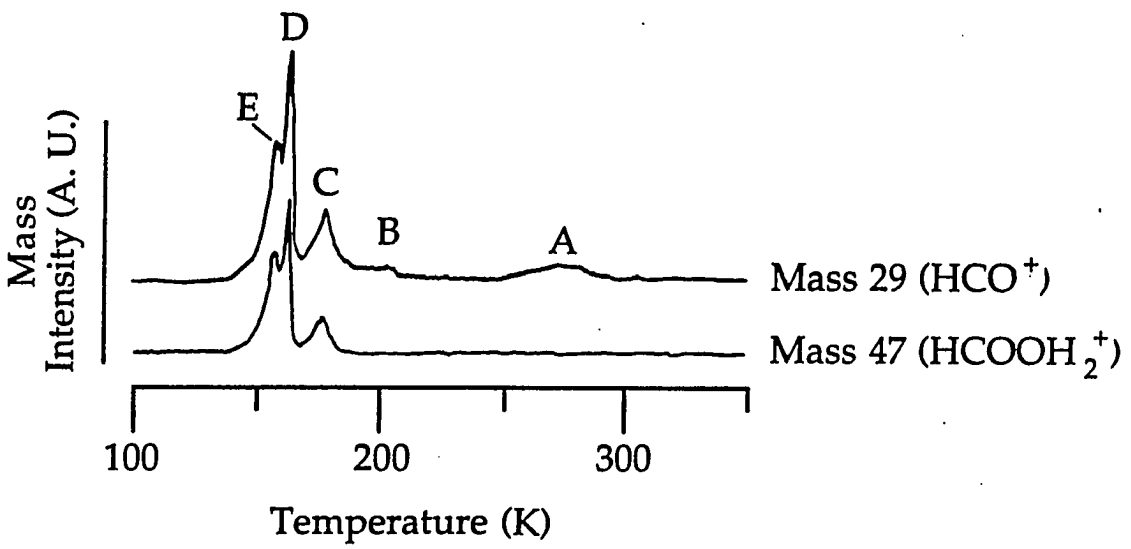

Figure 6. Thermal desorption traces for HCO^+ and $HCOOH_2^+$ following exposure of 2.3 L HCOOH at 100 K. The Pt(111) surface is exposed to 5 L O_2 at 100 K and heated to 200 K prior to exposure to HCOOH. The heating rate is 15.6 K/s at 100 K and drops continuously to 5.3 K/s at 350 K.

E) appear in the trace for mass 29, only states C, D, and E appear in the trace for mass 47. Therefore, desorption from states A and B is dominated by monomers and that from the remaining states is dominated by dimers, based on this comparison.

3.2 High resolution electron energy loss spectroscopy

Fig. 7 displays a HREEL spectrum for a Pt(111) surface covered with 0.25 monolayer of atomic oxygen and subsequently exposed to 0.2 L HCOOH at 80-100 K. At these exposures, the only desorption which occurs (at higher temperature) is due to decomposition, with CO_2 in one state at ca. 300 K and H_2O desorbing in two states at ca. 205 K and 300 K. The spectrum is very similar to one reported by Avery [7], which identifies a monodentate formate adspecies on this surface. Avery attributes losses at 1290 cm^{-1} and 1620 cm^{-1} to the symmetric and asymmetric OCO stretching modes of the formate, respectively. The presence of the asymmetric stretching mode, Avery argues, indicates that the symmetry of the adspecies is lower than C_{2v}, leaving the monodentate configuration as the only feasible formate structure. The same modes appear in Fig. 7 at 1330 cm^{-1} and 1630 cm^{-1}. The symmetric OCO stretching frequency, however, is closer to

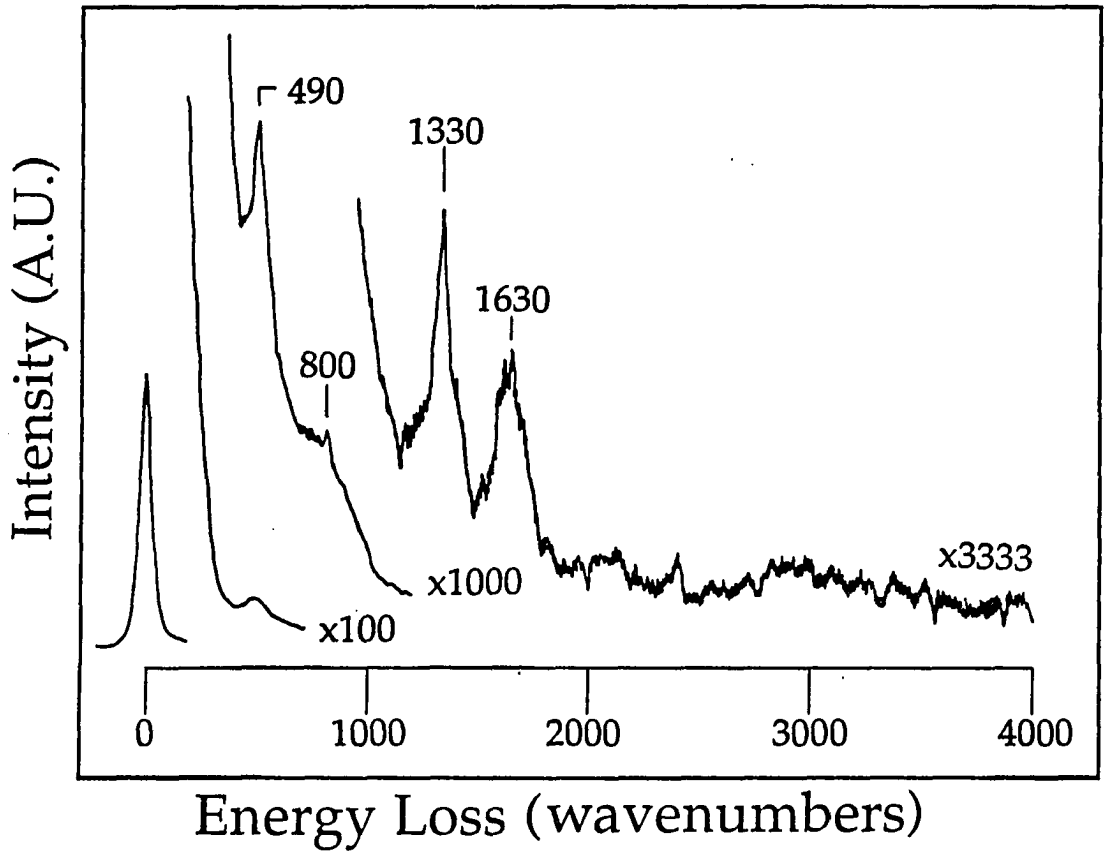

Figure 7. High resolution electron energy loss spectrum following exposure of 0.2 L HCOOH at 100 K. The Pt(111) surface is exposed to 5 L O_2 at 100 K and heated to 200 K prior to exposure to HCOOH. The elastic peak has an intensity of 100 kHz and a FWHM of 10 mV.

the value expected for a "bridging" configuration. Its intensity is roughly twice that of the asymmetric stretching mode unlike Avery's spectrum, where both intensities are approximately equal. This could indicate the coexistence of both configurations on our surface.

This also stands in contrast to our observations for clean Pt(111), which exhibits only bridging formate [16]. Another distinction is the existence of formate at 100 K; on clean Pt(111), the surface must be heated to 170 K to completely convert all molecular HCOOH to formate [16].

Both Avery's spectra [7] and that in Fig. 7 exhibit losses for the PtO stretch for the oxygen adatoms (at 490 cm^{-1} in Fig. 7), but the resolution of the spectrum in Fig. 7 is not sufficient to allow observation of the PtO stretch for the formate adspecies (at 360 cm^{-1} in Avery's spectrum). Fig. 7 exhibits a loss at 800 cm^{-1} not reported by Avery for his spectrum of monodentate formate; however, in a subsequent spectrum taken for a higher exposure of HCOOH, a broad feature appears at 780 cm^{-1} which Avery attributes to two vibrations: the OCO in-plane bend of the formate adspecies and molecular water librations. (At this exposure, Avery contends that formate exists in a bridging configuration as indicated by attenuation of the OCO asymmetric stretch.) Both vibrational modes probably also contribute to the 800 cm^{-1} feature in Fig. 7. The spectrum also exhibits a

slight increase in intensity between 2700 cm^{-1} and 3300 cm^{-1}; this is probably caused by the OH stretching mode of H_2O and the CH stretching mode of formate. The low intensity and broad widths of these features greatly reduces the information extractable from this spectral region.

Fig. 8 shows the results when the surface of Fig. 7 is heated successively to 120 K, 170 K, and 200 K. The 100 K spectrum shows the symmetric and asymmetric OCO stretching modes observed in Fig. 7, as well as the OCO in-plane bending mode. The latter mode is better resolved than in Fig. 7, allowing another mode to emerge at about 680 cm^{-1}. This frequency does not correspond to any observed for formate adspecies, but is close to 700 cm^{-1}, the frequency of the water librational mode on clean Pt(111) [19]. (The presence of two librational modes indicates that the water produced from reaction of HCOOH with oxygen adatoms is oriented differently than molecular water adsorbed on clean Pt(111), where only one librational mode is observed [19, 20].)

Heating the surface to 120 K attenuates the OCO asymmetric stretching mode while the symmetric mode intensifies; the loss at 800 cm^{-1} also intensifies slightly. This reveals a change in formate configuration from monodentate to bridging. Heating to 170 K further intensifies the loss at 800 cm^{-1}, while the

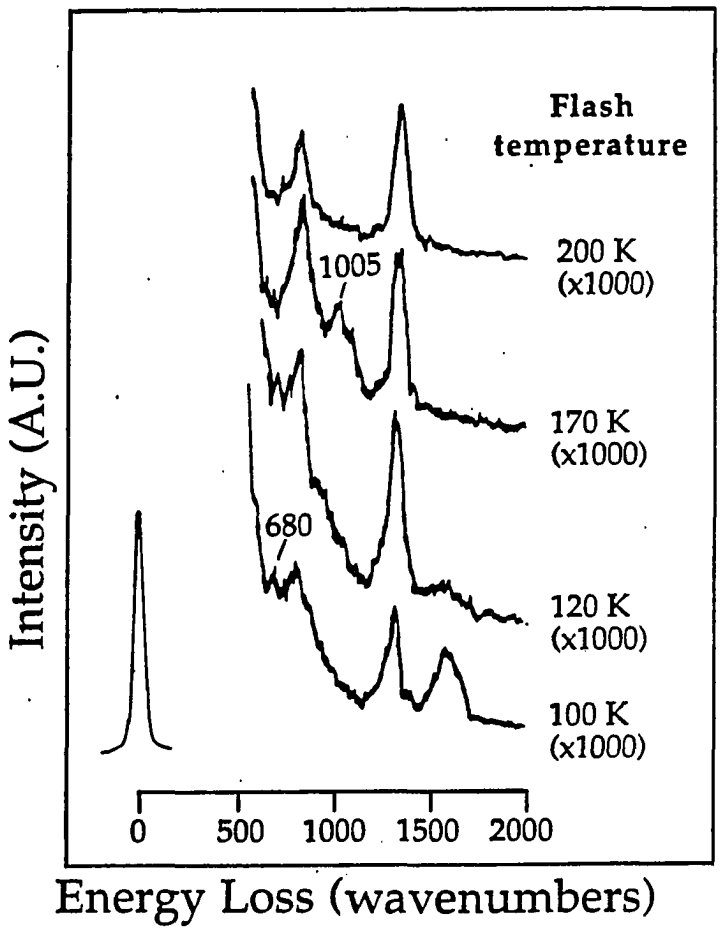

Figure 8. Series of high resolution electron energy loss spectra following exposure of 0.2 L HCOOH at 100 K and heating to 120 K, 170 K, and 200 K, respectively. The elastic peak has an intensity of 110 kHz and a FWHM of 9 mV. Each spectrum is multiplied by 1000 relative to the elastic peak.

loss at 680 cm^{-1} disappears; a new loss appears at ca. 1000 cm^{-1}. This new feature occurs close to the 1015 cm^{-1} frequency assigned by Fisher and Sexton to the PtOH bending mode present for surface hydroxyl groups [17]. (The emergence of this loss is consistent with the 205 K desorption feature for mass 18 discussed earlier.) The 200 K spectrum reveals only losses at 790 cm^{-1} and 1330 cm^{-1} indicating that only bridging formate remains on the surface at this temperature.

Inspection of the 200 K spectrum allows carbonate to be eliminated as a possible intermediate. HREEL spectra have identified carbonate as a product resulting from the reaction of atomic oxygen and carbon dioxide coadsorbed on Ag(110) [21] and Ni(110) [22]. The formation of carbonate is an activated process on both surfaces; several losses attributed to carbonate appear in the HREEL spectra after heating the surface to 200 K, following adsorption of CO_2 on an oxygen-covered surface at 150 K or below. Although some of these losses occur close to the vibrational frequencies associated with formate, a loss unique to carbonate is observed between 1000 and 1050 cm^{-1}. This is attributed to the C-O stretch and is clearly not observed in the 200 K spectrum displayed in Fig. 8.

To summarize the low-exposure data of Figs. 7 and 8, adsorption at 80-100 K on an oxygen-covered surface produces a mixture of monodentate and

bridging formate, and molecular water. Upon heating, the monodentate converts to the bridging form, and surface hydroxyl appears. By 200 K, only the bridging formate remains.

Fig. 9 displays a HREEL spectrum for a Pt(111) surface covered with 0.25 monolayer of atomic oxygen and subsequently exposed to 0.8 L HCOOH at 100 K. At this exposure CO_2 desorption saturates in both its low (below 200 K) and high (above 250 K) temperature states, the water B-state emerges from the A1-state, and molecular HCOOH occurs in the A and B states. The losses for the OCO symmetric (1340 cm^{-1}) and asymmetric (1665 cm^{-1}) stretches are still observed, with the asymmetric loss greatly broadened and shifted up in frequency by 35 cm^{-1}. Also present is the PtO stretching mode for the oxygen adatoms at 470 cm^{-1}. Two modes not seen in the spectrum in Fig. 7 appear at 928 cm^{-1} and 2974 cm^{-1}; the mode at lower frequency is due to the OH out-of-plane bend of molecular HCOOH and the mode at higher frequency is caused by the CH stretch of both the formate and molecular HCOOH. The latter feature is broader than that observed for HCOOH adsorbed on clean Pt(111); it possibly contains contribution from the OH stretching mode of HCOOH.

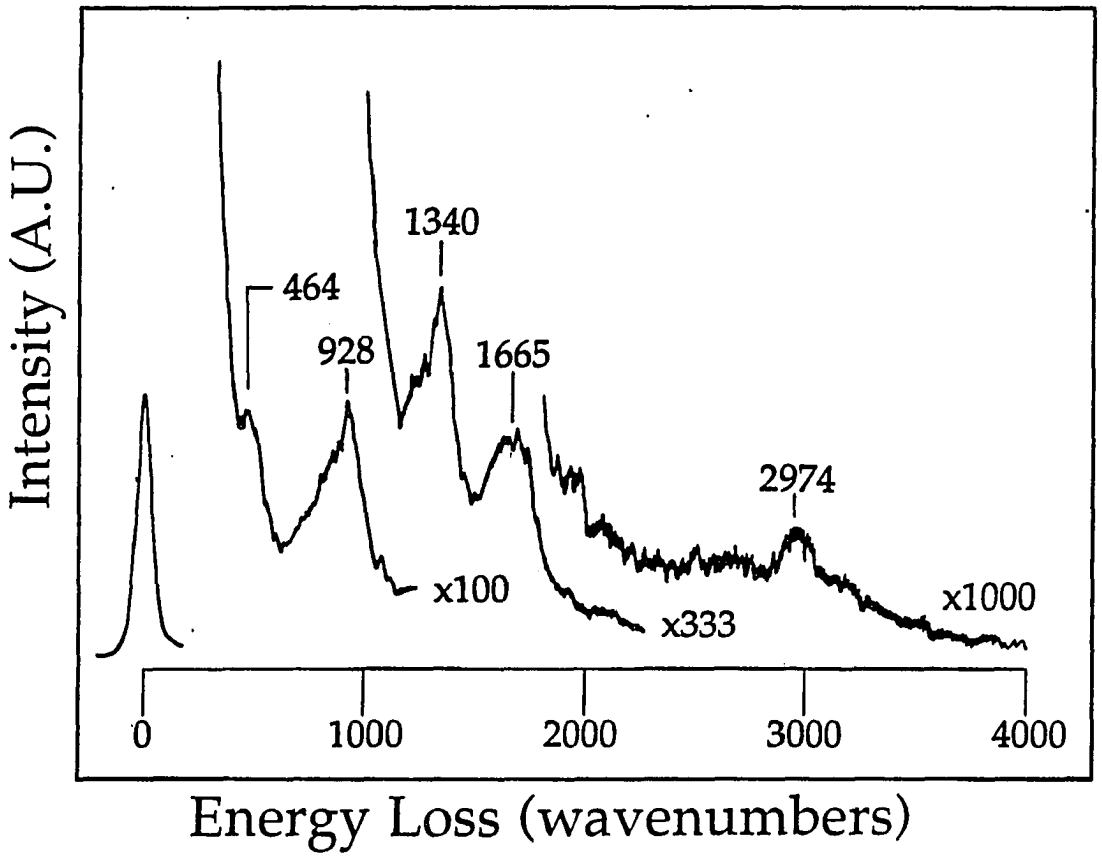

Figure 9. High resolution electron energy loss spectrum following exposure of 0.8 L HCOOH at 100 K. The Pt(111) surface is exposed to 5 L O_2 at 100 K and heated to 200 K prior to exposure to HCOOH. The elastic peak has an intensity of 100 kHz and a FWHM of 9 mV.

The OH out-of-plane bend is the most intense loss in this spectrum, indicating that molecular HCOOH is much more abundant on the surface than monodentate and bridging formate. The carbonyl CO stretch of molecular HCOOH occurs at 1690 cm^{-1} [23-25] and possibly explains the broadening of the formate OCO asymmetric stretching mode and its shift to a higher frequency.

Fig. 10a shows the first two spectra in a series which starts from the surface of Fig. 9. These spectra are produced by heating to 130 K, 160 K, 180 K, and 220 K, respectively. The 100 K spectrum exhibits the same major loss features as the spectrum in Fig. 9. Heating the surface to 130 K intensifies the formate symmetric OCO stretch and causes the broad feature assigned to the asymmetric OCO stretch to split into 3 low-intensity features at 1520 cm^{-1}, 1630 cm^{-1}, and 1710 cm^{-1}. The molecular acid OH out-of-plane bending mode disappears, indicating that *all* the molecular acid reacts to produce formate. On the clean surface, the same OH out-of-plane bend persists to 180 K [16]. A new feature emerges at 1005 cm^{-1}; this feature is close in frequency to that of the OH bend described previously for surface hydroxyl groups [17]. A very intense new feature appears at 840 cm^{-1} with possible contributions from the formate OCO in-plane bending and water librational modes. Finally, the PtO stretching mode broadens and shifts up to 550 cm^{-1}.

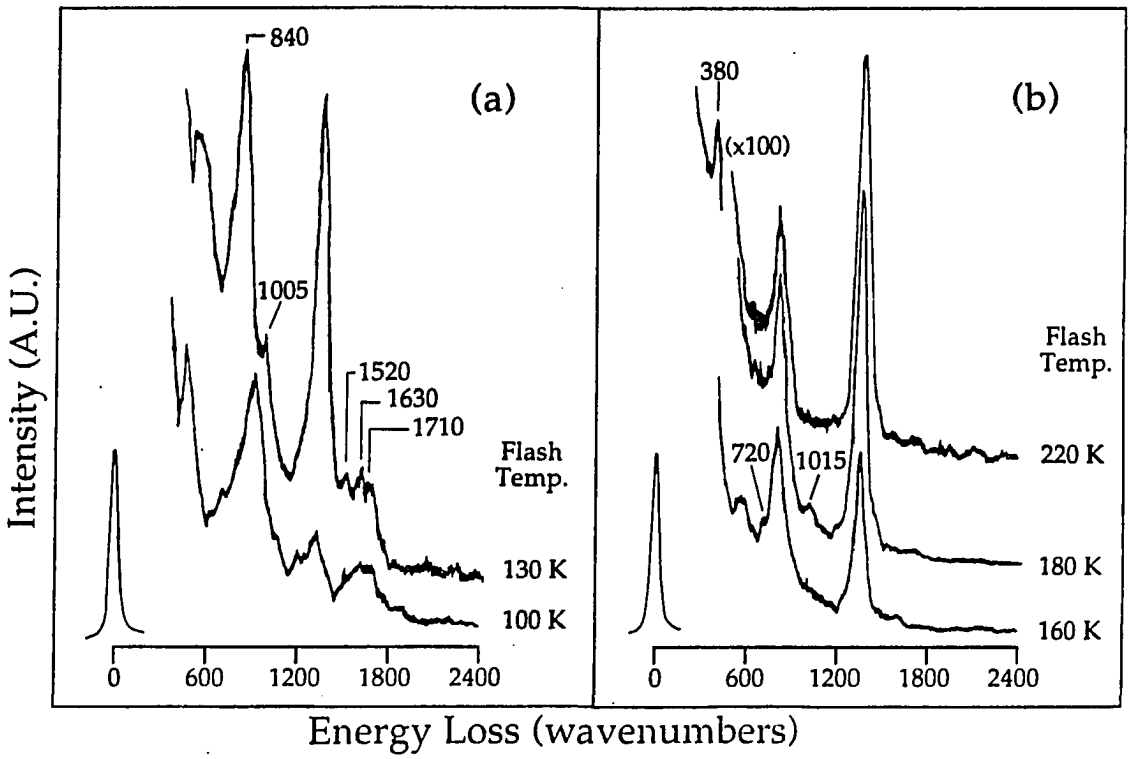

Figure 10. Series of high resolution electron energy loss spectra following exposure of 0.2 L HCOOH at 100 K and heating to 130 K, 160 K, 180 K and 220 K, respectively. (The 100 K and 130 K spectra are displayed in (a) and the 160 K, 180 K, and 220 K spectra are displayed in (b).) The elastic peak has an intensity of 110 kHz and a FWHM of 10 mV. Each spectrum is multiplied by 333 relative to the elastic peak.

Fig. 10b displays the last three spectra in the series for this surface. Heating to 160 K causes the features at 1005 cm^{-1}, 1520 cm^{-1}, and 1710 cm^{-1} to disappear and attenuates the remaining features. Also the feature at 840 cm^{-1} moves down to 790 cm^{-1} and develops a low frequency shoulder at 720 cm^{-1}. This is consistent with a surface that contains a bridging formate adspecies, as well as water admolecules. The intensity of the 1330 cm^{-1} feature is reduced by ca. 50% relative to the other spectra in the series; this could possibly be attributed to a reorientation of formate at this temperature which causes its molecular plane to cant towards the surface. Heating to 180 K causes the features at 540 cm^{-1} and 720 cm^{-1} to disappear and the remaining features to intensify; a small feature appears at 1015 cm^{-1}, revealing the presence of hydroxyl adspecies. Heating to 220 K causes a feature at 380 cm^{-1} to emerge (at a multiplication of 100). This is most probably the PtO stretch of the bridging formate.

To summarize the high-exposure data of Figs. 9 and 10, adsorption at 80-100 K on an oxygen-covered surface produces a mixture of monodentate formate, molecular acid, and molecular water. Upon heating, the molecular acid reacts completely to produce formate; simultaneously, hydroxyl appears. By 160 K, water molecules also appear. Above 180 K molecular water desorbs leaving only the hydroxyl adspecies, which combine to to form water and desorb above 200 K.

4. Discussion

The thermal desorption data provide information about the coverage- and temperature-dependence of the gas-phase product distribution. The electron energy loss spectra provide information about the surface species from which these products originate. Combining these two sets of information, we can develop a plausible set of elementary reactions which explains all the observed phenomena.

4.1 Reactions occurring at low HCOOH exposures (< 0.6 L HCOOH)

Several researchers [1-4, 6, 7] have suggested that oxygen facilitates the conversion of formic acid to formate resulting in the overall reaction:

$$2\,HCOOH_{ad} + O_{ad} \text{-------} > 2\,HCOO_{ad} + H_2O_{ad} \qquad (1)$$

Barteau et al. [1] and Solymosi et al. [4] suggest that this reaction proceeds by sequential hydrogenation of the oxygen adatom:

$$HCOOH_{ad} + O_{ad} \text{-------} > HCOO_{ad} + OH_{ad} \qquad (1a)$$

$$HCOOH_{ad} + OH_{ad} \text{-------} > HCOO_{ad} + H_2O_{ad} \qquad (1b)$$

Our TDS and HREELS data for HCOOH exposures less than 0.6 L indicate this to be the primary reaction on Pt(111). At 80-100 K formate produced from

reaction (1) exists both in monodentate and bridging configurations; heating to 120 K converts all monodentate adspecies to the bridging configuration. The existence of two water librational modes in the HREEL spectrum at these temperatures indicates the water admolecules formed from this reaction are configured differently than water molecules adsorbed alone on Pt(111). The HREEL spectrum for water adsorbed on clean Pt(111) shows only one broad feature at 700 cm^{-1} for librations [19]. The common viewpoint is that water molecules form a hydrogen-bonded bilayer, which resembles a truncation of the I_h structure of ice [26]. The water admolecules formed from the reaction of HCOOH and oxygen adatoms probably exist as isolated monomers strongly interacting with the formate adspecies and oxygen adatoms and might even be oriented with their molecular planes parallel to the surface.

As the surface temperature rises to 170 K, the water admolecules react with oxygen adatoms to form hydroxyl adspecies:

$$H_2O_{ad} + O_{ad} \text{ -------> } 2\,OH_{ad} \qquad (2)$$

This is supported by the presence of the 1000 cm^{-1} feature in the HREEL spectrum for this temperature, as well as the 200-210 K peak temperature for the A1 water desorption state observed for this exposure range, where the reverse of reaction (2) occurs. (See Figs. 4 and 8.)

As surface temperature increases past 250 K the formate decomposes, resulting in concurrent desorption of carbon dioxide and water according to the reaction:

$$2\,HCOO_{ad} + O_{ad} \text{ -------> } 2\,CO_{2\,g} + H_2O_g \qquad (3)$$

The oxygen adatoms increase the stability of the formate relative to the clean surface, requiring temperatures 20-55 K greater than the clean surface to reach maximum CO_2 desorption rate. The effect is most pronounced at lower exposures of HCOOH.

Above 0.3 L HCOOH molecular desorption of HCOOH accompanies formate decomposition. One possible reaction which could explain this phenomenon is:

$$2\,HCOO_{ad} \text{ -------> } HCOOH_g + CO_{2\,g} \qquad (4)$$

4.2 Reactions occurring at high HCOOH exposures (> 0.6 L HCOOH)

As HCOOH exposure exceeds 0.6 L, several changes and new features are observed in thermal desorption spectra for H_2O (mass 18), CO_2 (mass 44) and HCOOH (mass 29): (1) The peak temperature of the A1/B state in the mass 18 spectrum decreases from 205 K to 170-175 K as the B-state emerges from the A1-state; (2) The desorption area of the A2-state in the mass 18 spectrum decreases by

ca. 33% relative to its maximum value attained at 0.5-0.6 L HCOOH; (3) A second desorption state appears below 200 K in the mass 44 spectrum. Its desorption area increases to a maximum at 1-1.2 L HCOOH and then decreases; and, (4) The desorption area of the A-state in the mass 29 spectrum continues to increase, reaching a plateau at 1-1.2 L HCOOH. Fig. 11 summarizes these observations.

Additionally, several states appear in the mass 29 desorption spectra. The B-state appears at 200 K, the C-state at 180 K, and the D-state at 160 K, above HCOOH exposures of 0.8, 0.9 L, and 1.2-1.4 L, respectively. This contrasts with molecular desorption from the clean surface which occurs in three states: at 200 K, 160-170 K, and 160 K with onset exposures of 0.3, 0.6, and 1.2 L, respectively. The two surfaces do exhibit the same behavior regarding monomeric vs dimeric desorption; on both surfaces, the states at 200 K or above are dominated by monomeric desorption, while all states at lower temperatures are dominated by dimeric desorption. Monomeric desorption on the clean surface results from HCOOH molecules in direct surface contact and dimeric desorption from HCOOH in a multilayer, or HCOOH in direct surface contact which is displaced by a polymorphic transition [16].

Finally, hydrogen desorption occurs above 0.6 L HCOOH exposure and saturates by 1.2 L. The lack of desorption below 0.6 L is attributable to the creation

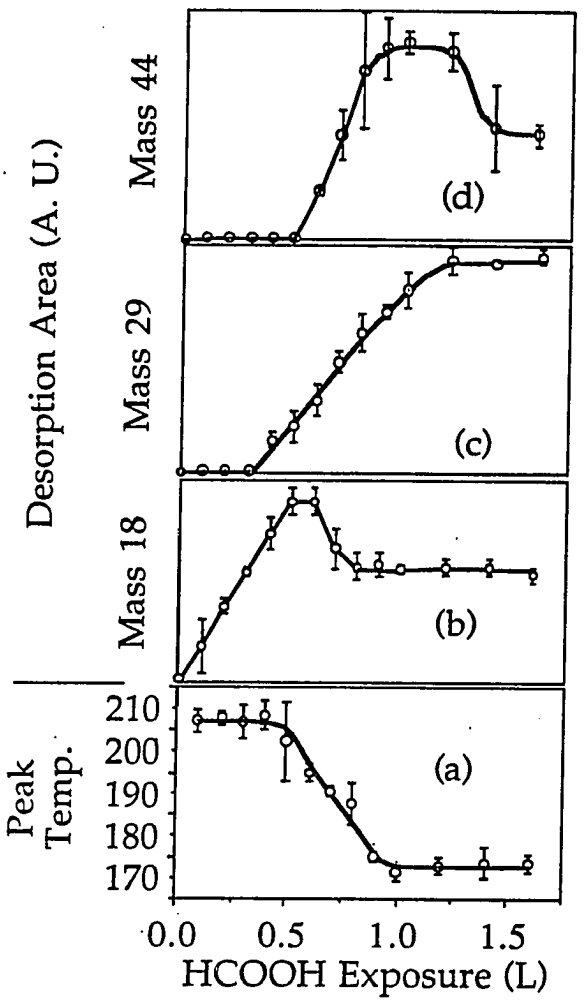

Figure 11. (a). Peak temperature for the H_2O A1/B desorption state as a function of HCOOH exposure. (b). Desorption area of the H_2O A2-state as a function of HCOOH exposure. (c). Desorption area of the HCOOH A-state as a function of HCOOH exposure. (d). Desorption area of the low temperature CO_2 state as a function of HCOOH exposure.

of water from atomic oxygen and hydrogen. The desorption of hydrogen beyond this exposure must result from depletion of oxygen adatoms. This results in inadequate local oxygen adatom coverages to react with all the hydrogen adatoms produced from formate decomposition.

The HREEL spectral series for 0.8 L HCOOH exposure (see Figs. 10a and 10b) shows the existence of monodentate and bridging formate and molecular HCOOH at 80-100 K; however, at 130 K the surface is covered with water, bridging formate and hydroxyl groups. Heating to 160 K causes the hydroxyl band at 1005 cm^{-1} to disappear and above 160 K the water modes also disappear.

We can deduce several elementary reactions by noting that some reaction phenomena are correlated as follows: (1) Hydrogen desorption begins at HCOOH exposures greater than 0.6 L while the desorption area of the molecular HCOOH A-state continues to increase. These two phenomena reflect that sufficient depletion of oxygen adatoms occurs above 0.6 L to allow recombination of formate and atomic hydrogen, as well as combination of atomic hydrogen to produce molecular hydrogen, i. e.

$$H_{ad} + HCOO_{ad} \text{ -------> } HCOOH_g \quad \text{(Desorption @ 280-285 K)} \qquad (5)$$

$$2\,H_{ad} \text{ -------> } H_{2\,g} \quad \text{(Desorption @ 350-380 K)} \qquad (6)$$

Both of these desorption features saturate at ca. 1.2 L (See Figs. 3 and 11c) . (2) As HCOOH exposure exceeds 0.6 L the surface coverage of formate reaches a level where reaction between the formate (produced in reaction (1)) and hydroxyl groups (produced in reaction (2)) occurs giving water and carbon dioxide desorption at temperatures below 200 K.

$$HCOO_{ad} + OH_{ad} \text{ -------> } CO_{2\,g} + H_2O_g \qquad (7)$$

This reaction results in the low temperature CO_2 desorption state and the B-state in water desorption. Additionally, the decrease in peak temperature for the water B-state is consistent with the 2nd order nature of this reaction (see Fig. 11a). (The peak temperature for the low temperature CO_2 desorption state also follows this trend.) (3) The desorption area of the water A2 state reaches a maximum at 0.5-0.6 L HCOOH then drops to a plateau value beyond 0.8 L (see Fig. 11b). The areas at the plateau are 60-70% of the maximum. In the same exposure range the B and C molecular HCOOH desorption states appear and the low temperature CO_2 state (produced by reaction (7)) reaches a maximum desorption area. The HREEL spectrum for oxygen-covered Pt(111) exposed to 0.8 L HCOOH at 80-100 K followed by heating to 160 K shows evidence for the presence of water, not hydroxyl groups; however, the 180 K spectrum in this series indicates the presence of hydroxyl adspecies. These collective facts indicate that, beyond 0.8 L

HCOOH, formate undergoes new reactions which produce molecular HCOOH and maintain the level of atomic oxygen sufficient to produce water desorption in the A2-state at 60-70% of its maximum desorption yield. The molecular acid B-state is produced from a new reaction between formate and hydroxyl adspecies.

$$HCOO_{ad} + OH_{ad} \text{ -------> } HCOOH_g + O_{ad} \qquad (8)$$

This reaction reflects the monomeric nature of the desorption from the B-state and agrees with the 180 K HREEL spectrum from Fig. 10b, indicating the presence of hydroxyl adspecies at this temperature, and the 200 K peak temperature of the B-state. The fact that a new reaction between formate and hydroxyl groups occurs at this exposure indicates that the amount of these two adspecies consumed by reaction (7) is limited; therefore, reaction (7) is dependent on some surface condition, possibly needing a given ensemble of sites or minimum local coverage of atomic oxygen.

The molecular acid C-state is produced from a reaction between formate and molecular water.

$$2\,HCOO_{ad} + H_2O_{ad} \text{ -------> } (HCOOH)_{2\,g} + O_{ad} \qquad (9)$$

This reaction reflects the dimeric desorption of the C-state and agrees with the predominance of water, not hydroxyl, on the surface at this temperature. The intensity of the C-state increases between 0.9 L and 1.4 L HCOOH; this is

reasonable considering the reduction in atomic oxygen coverage caused by reaction (1) as more HCOOH adsorbs on the surface. The result is a decrease in the amount of hydroxyl adspecies produced from reaction (2) and explains the decrease in the low temperature CO_2 desorption area beyond 1.2 L (see Fig. 11d). The desorption area of the water B-state, in contrast, continues to increase, swelled by reaction (1).

5. Summary

The presence of atomic oxygen greatly enhances the tendency of molecular HCOOH to produce a formate adspecies on Pt(111). This is reflected in two observations: (1) HREEL spectra show that at a low exposure (0.2 L HCOOH) molecular HCOOH produces formate upon adsorption at 80-100 K. At a higher exposure (0.8 L HCOOH) all molecular HCOOH is converted to formate by 130 K. The clean surface requires temperatures of 170-180 K to complete conversion from acid to formate. (2) The desorption yields for CO_2 resulting from formate decomposition are increased by four to sixfold for the oxygen-covered surface

relative to the clean surface. Additionally, the peak temperature for CO_2 desorption is increased by 25-55 K in the presence of atomic oxygen.

Coadsorbed oxygen retards the desorption of hydrogen observed from the clean surface. Instead, the hydrogen, released upon formate formation, reacts with the atomic oxygen to form molecular water. At HCOOH exposures below 0.6 L this water also interacts with atomic oxygen to produce hydroxyl adspecies; these react to desorb water between 200 and 210 K. The decomposition of the formate also produces water desorption peaked at 285-300 K. HCOOH exposures beyond 0.6 L produce a third water desorption state which emerges from the low temperature side of the water desorption at 200-210 K and moves down in temperature with increasing exposure. This desorption results from a reaction between formate and hydroxyl adspecies releasing H_2O and CO_2, as well as desorption of molecular water which has not reacted with atomic oxygen. (The CO_2 released by the reaction of formate and hydroxyl appears as a low-temperature feature in the CO_2 desorption spectrum.)

Molecular desorption occurs above 0.3 L HCOOH exposure in a state centered at 285-300 K. This desorption is attributed primarily to recombination of formate and atomic hydrogen. Two more states appear with onset exposures of 0.8 and 0.9 L, respectively. The former appears at 200 K and results from a

reaction between formate and hydroxyl adspecies to give monomeric desorption; the latter appears at 200 K and results from a reaction between formate and molecular water to give dimeric desorption. Molecular desorption states which appear above exposures of 1.2-1.4 L HCOOH do not saturate with increasing exposure and are attributed to multilayers.

Acknowledgments

Acknowledgement is made to the Donors of The Petroleum Research Fund, administered by the American Chemical Society. Some equipment and all facilities are provided by the Ames Laboratory, which is operated for the U. S. Department of Energy by Iowa State University under Contract No. W-7405-ENG-82.

References

1. M. A. Barteau, M. Bowker and R. J. Madix, Surf. Sci., 94 (1980) 303
2. B. A. Sexton and R. J. Madix, Surf. Sci., 105 (1981) 177
3. D. A. Outka and R. J. Madix, Surf. Sci., 179 (1987) 361
4. F. Solymosi, J. Kiss and I. Kovacs, Surf. Sci., 192 (1987) 47
5. S. W. Johnson and R. J. Madix, Surf. Sci., 66 (1977) 189
6. N. R. Avery, App. Surf. Sci., 11/12 (1982) 774
7. N. R. Avery, App. Surf. Sci, 14 (1982-83) 149
8. N. Kizhakevariam and E. M. Stuve, J. Vac. Sci. Technol. A, 8 (1990) 2557
9. M. Bowker and R. J. Madix, Surf. Sci., 102 (1981) 542
10. S. A. Isa, R. W. Joyner, M. H. Matloob and M. W. Roberts, Appl. Surf. Sci., 5 (1980) 345
11. M. R. Columbia and P. A. Thiel, Surf. Sci., 235 (1990) 53
12. M. R. Columbia and P. A. Thiel, Rev. Sci. Instrum., 58 (1987) 309
13. P. K. Leavitt, J. L. Davis, J. S. Dyer and P. A. Thiel, Surf. Sci., 218 (1989) 346
14. J. L. Gland, B. A. Sexton and G. B. Fisher, Surf. Sci., 95 (1980) 587
15. M. R. Columbia and P. A. Thiel, Proc. DOE Workshop -Direct Methanol/Air Fuel Cells, to be published (1990)

16. M. R. Columbia, A. M. Crabtree and P. A. Thiel, submitted to J. Am. Chem. Soc., (1991)

17. G. B. Fisher and B. A. Sexton, Phys. Rev. Lett., 44 (1980) 683

18. G. B. Fisher and J. L.Gland, Surf. Sci., 94 (1980) 446

19. B. A. Sexton, Surf. Sci., 94 (1980) 435

20. M. R. Columbia, A. M. Crabtree and P. A. Thiel, submitted to Surf. Sci., (1991)

21. E. M. Stuve, R. J. Madix and B. A. Sexton, Chem. Phys. Lett., 89 (1982) 48

22. H. Lindner, D. Rupprecht, L. Hammer and K. Mueller, J. Electron Spectros., 44 (1987) 141

23. R. C. Millikan and K. S. Pitzer, J. Am. Chem. Soc., 80 (1958) 3515

24. Y. Mikawa, R. J. Jakobsen and J. W. Brasch, J. Chem. Phys., 45 (1966) 4750

25. Y. Mikawa, J. W. Brasch and R. J. Jakobsen, J. Mol. Spectros., 24 (1967) 314

26. P. A. Thiel and T. E. Madey, Surf. Sci. Rep., 7 (1987) 211

SECTION V:

THE INFLUENCE OF COADSORBED CARBON MONOXIDE ON THE DECOMPOSITION OF FORMIC ACID ON PT(111)

The Influence of Coadsorbed Carbon Monoxide on the Decomposition of Formic Acid on Pt(111)

by

M. R. Columbia, A. M. Crabtree, and P. A. Thiel

Department of Chemistry and Ames Laboratory
Iowa State University
Ames, IA 50011 USA

To be submitted to *Journal of Electroanalytical Chemistry and Interfacial Phenomena*

Abstract

We have studied the influence of coadsorbed CO on the decomposition of HCOOH on Pt(111) utilizing the techniques of thermal desorption spectroscopy and high resolution electron energy loss spectroscopy. We find that HCOOH decomposes to CO_2 and H_2 for HCOOH exposures less than 0.3 L; this decomposition proceeds via a formate intermediate bonded to the surface through both of the oxygen atoms. The coadsorption of CO retards the conversion of molecular HCOOH to the formate adspecies. This causes the desorption yields of CO_2 and H_2 to decrease with increasing CO coverage; however, CO_2 desorption does not occur beyond a CO coverage of ca. 0.35 monolayer, while H_2 desorption persists up to a coverage of 0.5 monolayer. This discrepancy in desorption behavior suggests that CO produces a new decomposition pathway for the formate adspecies. As the decomposition yields decrease with increasing CO coverage, molecular desorption occurs and increases accordingly. Initial molecular desorption occurs at a peak temperature of 195-200

K and is monomeric. Increasing CO coverage decreases this peak temperature in a linear manner to 170 K at 0.5 monolayer CO. This decrease is accompanied by a shift to dimeric desorption.

1. Introduction

Small oxygen-containing hydrocarbons like formic acid hold potential for their use in fuel cells utilizing Pt as the electrode material. Formic acid undergoes electrochemical decomposition in the fuel cell to produce CO_2 and H^+ accompanied by the release of electrons. This reaction proceeds with nearly 100% efficiency [1-3]. A competing reaction is also known to occur, which poisons the electrode [4]; the prevailing explanation, summarized by several reviewers [5-8], relies on the production of different intermediates for the two reactions. One intermediate reacts to form CO_2, which desorbs from the electrode surface; the other intermediate is unreactive and remains adsorbed. Accumulation of the latter intermediate eventually prevents adsorption of HCOOH and poisons the electrode surface. Studies utilizing electrochemical techniques suggest several possible intermediates with COH and COOH being the most likely [8]; COOH is believed to readily decompose to CO_2, while COH adsorbs more strongly, ultimately poisoning the electrode [8]. Shibata et al have reported that the two reaction pathways require different ensembles of sites to proceed [9, 10].

The development of in situ infrared spectroscopic techniques in the last decade has revitalized the discussion of these intermediates. Beden et al report the first in situ infrared spectrum of a polycrystalline Pt electrode surface poisoned by oxidation of HCOOH [11]. Their spectra reveal the presence of only CO, adsorbed predominantly in a linear configuration; these observations are also report by Kunimatsu [12] and Corrigan and Weaver [13]. Sun et al, however, report a vibrational feature produced by HCOOH oxidation on low-index faces of single crystal Pt electrodes not observed on the polycrystalline electrodes [14]. They attribute this feature at ca. 1780 cm^{-1} to the intermediate which readily decomposes to CO_2 (possibly COOH).

Considering that in situ infrared techniques identify CO as the primary surface species produced from HCOOH oxidation on Pt electrodes , we have studied the effect of coadsorbed CO on the interaction of HCOOH with a Pt(111) surface in ultrahigh vacuum. Madix et al report the only ultrahigh vacuum study of CO and HCOOH coadsorption, using a Ni(110) surface [15]. They observe that the decomposition of HCOOH on clean Ni(110) produces bridging formate adspecies and CO (the latter results from the decomposition of HCO intermediates); the presence of coadsorbed CO stabilizes the formate adspecies and alters its decomposition kinetics.

We observe a different effect on Pt(111). We report elsewhere [16, 17] that, for exposures less than 0.3 L, HCOOH decomposes exclusively to form H_2 and CO_2 (the latter results from the decomposition of bridging formate). The presence of CO retards this by preventing the deprotonation of HCOOH to produce formate; however, some evidence suggests that CO alters the decomposition pathway of the formate which is produced.

2. Experimental Details

The ultrahigh vacuum system, the method of performing thermal desorption experiments, and the Pt(111) crystal used for these experiments have been previously outlined [16, 18, 19]. The dosing of the surface is performed as follows: (1) The surface is exposed to CO at 80-100 K. (2) The surface is heated to ~260 K, then cooled back down to 80-100 K. (3) The crystal is exposed to 0.3 L HCOOH at 80-100 K.

The exposure units reported in this paper for HCOOH are Langmuir, although the surface is exposed to HCOOH through a directional doser containing a conductance-limiting aperture. We determine the Langmuir

equivalence based on comparison of CO thermal desorption areas following exposure via the doser with areas following exposure via backfilling. We convert CO exposures via a second doser directly to coverage values based on two comparisons: (1) A plot of mass 28 (CO^+) thermal desorption area vs CO exposure produces a plateau region beyond 700-800 Torr-sec CO (Torr-sec units are defined as the CO pressure behind the doser's conductance-limiting aperture multiplied by the time of the exposure). Such a plateau occurs at a CO coverage of 0.5 monolayer, where the sticking coefficient approaches zero [20-22]. (2) A CO exposure of 250 Torr-sec is needed to produce a loss in HREEL spectra at ca. 1850 cm^{-1}, following adsorption at 100 K and heating to 260 K. Steininger et al attribute this loss to the CO stretch of a CO admolecule which occupies a 2-fold bridge site and this is not observed for CO coverages less than 0.17 monolayer, following adsorption at 92 K and heating to 260 K [22]. Taken together, these two correlations provide a basis for the assignment of CO coverage as a function of CO exposure.

The high resolution electron energy loss spectrometer has also been described previously [19]. The elastic peaks have intensities between 100 and 350 kHz and full-widths at half-maxima between 8 and 11 meV (65 cm^{-1} to 89 cm^{-1}). For those experiments which probe the effect of temperature on the vibrational

spectrum, exposure temperatures are between 80 and 100 K; the surface is then heated to the indicated temperature at ~5 K/s, followed by determination of the loss spectrum while the surface cools. This method of heating differs from the continuous heating performed in TDS experiments. This difference results in desorption states occurring at temperatures 10- 20 K higher than the corresponding changes in the vibrational spectrum.

3. Results

3.1 Thermal desorption

On clean Pt (111) HCOOH decomposes exclusively, at exposures less than 0.3 L, resulting in hydrogen adatoms and a formate adspecies [16, 17]. The formate adspecies decomposes above 200 K producing desorption of CO_2 peaked at 260 K and more hydrogen adatoms. These adatoms combine above 300 K giving H_2 desorption peaked between 350 and 400 K . To probe the effect of CO coadsorption, the Pt(111) surface is exposed to varying amounts of CO followed by an exposure of HCOOH slightly greater than 0.3 L. (This HCOOH exposure saturates the desorption yields of CO_2 and H_2 and produces the onset of the first

molecular desorption state at 200 K.) Fig. 1 displays typical CO_2, H_2, and CO thermal desorption traces for these overlayers. The most noticeable change produced by increasing CO coverage is the decrease in the desorption yields for both CO_2 and H_2. The peak temperature for CO_2 desorption remains constant, while that for H_2 desorption decreases. The latter effect is in agreement with the repulsive interaction observed between coadsorbed CO and atomic hydrogen on close-packed faces of many transition metals [23]. The desorption behavior of CO is not measurably affected by coadsorption of HCOOH; the dependences of peak desorption temperatures and desorption areas on CO exposure are the same as for clean Pt(111).

Fig. 2 shows the decrease of these desorption yields (normalized to the saturation yield from the clean surface) as a function of CO coverage. The decrease in the normalized H_2 desorption yield is linear from 1 on the clean surface to 0 at a CO coverage of 0.5 monolayer. The decrease in the CO_2 desorption yield, however, is nonlinear; it drops off more quickly than the H_2 desorption yield at CO coverages below 0.2 monolayer, but more slowly above 0.2 monolayers. It reaches extinction between 0.35 and 0.4 monolayer CO coverage. This difference in behavior implies that CO induces an alternate route to

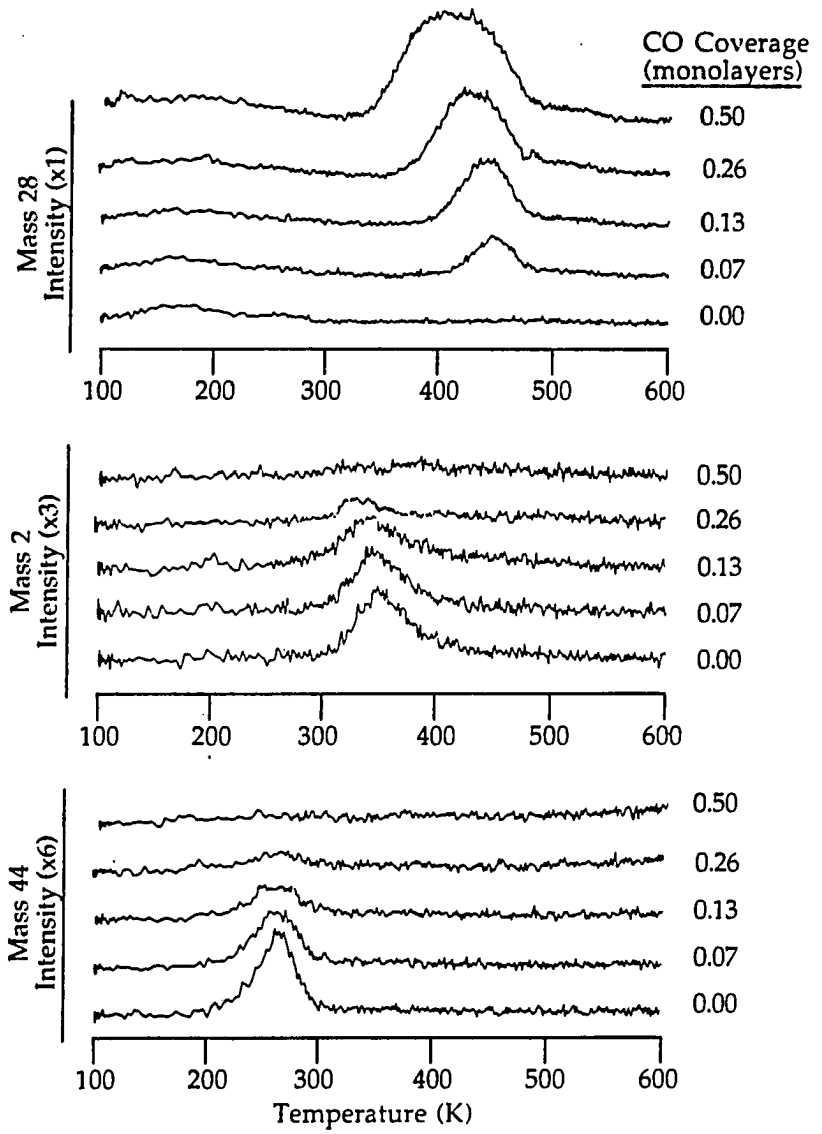

Figure 1. Thermal desorption series for mass 28 (CO^+), mass 2 (H_2^+) and mass 44 (CO_2^+) as a function of CO coverage. The heating rate is 15.6 K/s at 100 K and falls continuously to 4.7 K/s at 500 K.

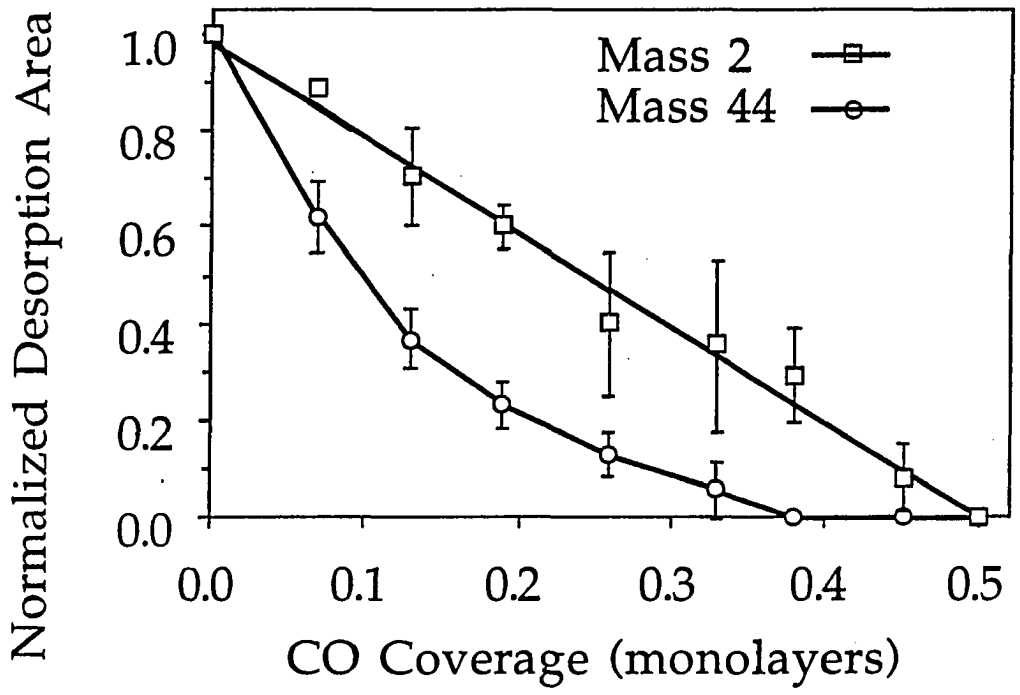

Figure 2. Normalized desorption areas for mass 2 (H_2^+) and mass 44 (CO_2^+) vs. CO coverage. The desorption area measured for a CO coverage of zero is defined as unity. Each normalized value is the average of 3-5 measurements made at the stated temperature and the error bars reflect ± one standard deviation.

decomposition for the formate adspecies which does not result in CO_2 desorption.

At the HCOOH exposure used in these thermal desorption experiments, the molecular desorption state at 200 K has just emerged. The effect of CO coadsorption on molecular desorption is revealed in Fig. 3. This displays two series of desorption traces: mass 29 (HCO^+) monitors monomeric molecular desorption and mass 47 ($HCOOH_2^+$) monitors dimeric molecular desorption. The mass 29 desorption traces show an increase in monomeric molecular desorption with increasing CO coverage up to 0.33 monolayer; beyond this coverage, the desorption yield remains constant, while the peak shape broadens. The mass 47 desorption traces show that dimeric molecular desorption commences at a CO coverage of 0.13 monolayer and follows the general trend of the monomeric desorption traces.

Another important observation is the downward shift of molecular desorption peak temperature with increasing CO coverage. This proceeds in a linear manner as depicted in Fig. 4. The peak temperature decreases from 200 K on the clean surface to 170 K at a CO coverage of 0.5 monolayer. This downward shift in peak temperature is consistent with the dimeric desorption observed for higher CO coverages. On the clean surface molecular desorption occurs in three

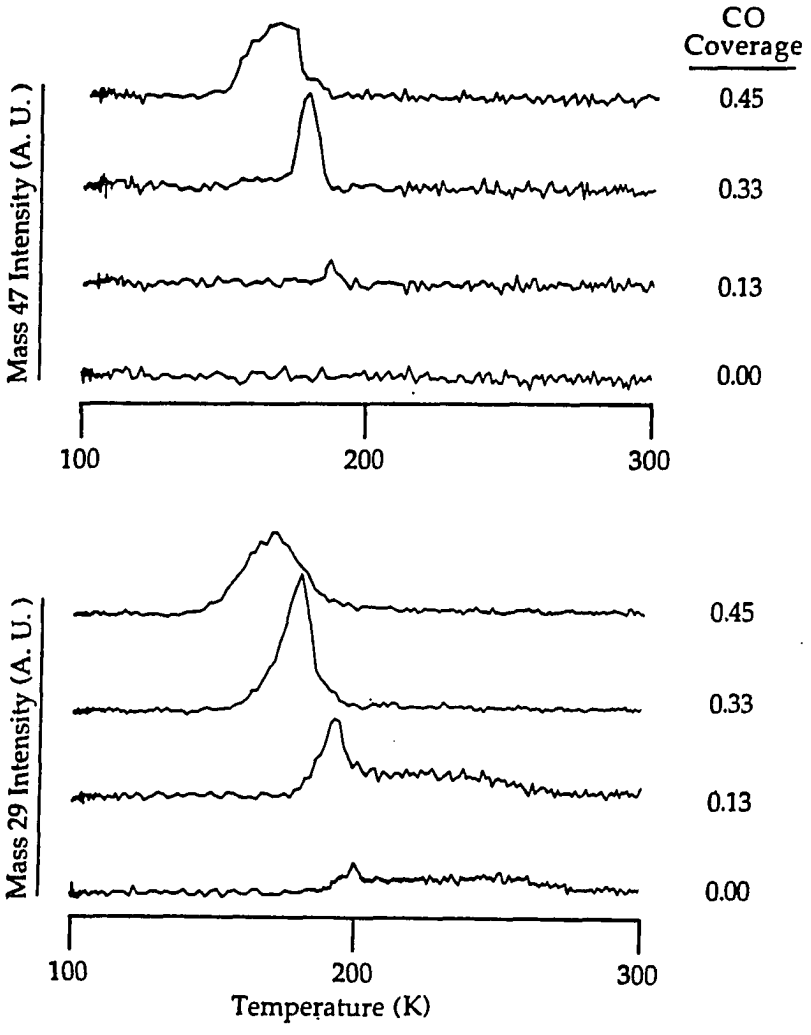

Figure 3. Thermal desorption series for mass 29 (HCO^+) and mass 47 ($HCOOH_2^+$) as a function of CO coverage. The heating rate is 15.6 K/s at 100 K and falls continuously to 6.5 K/s at 300 K.

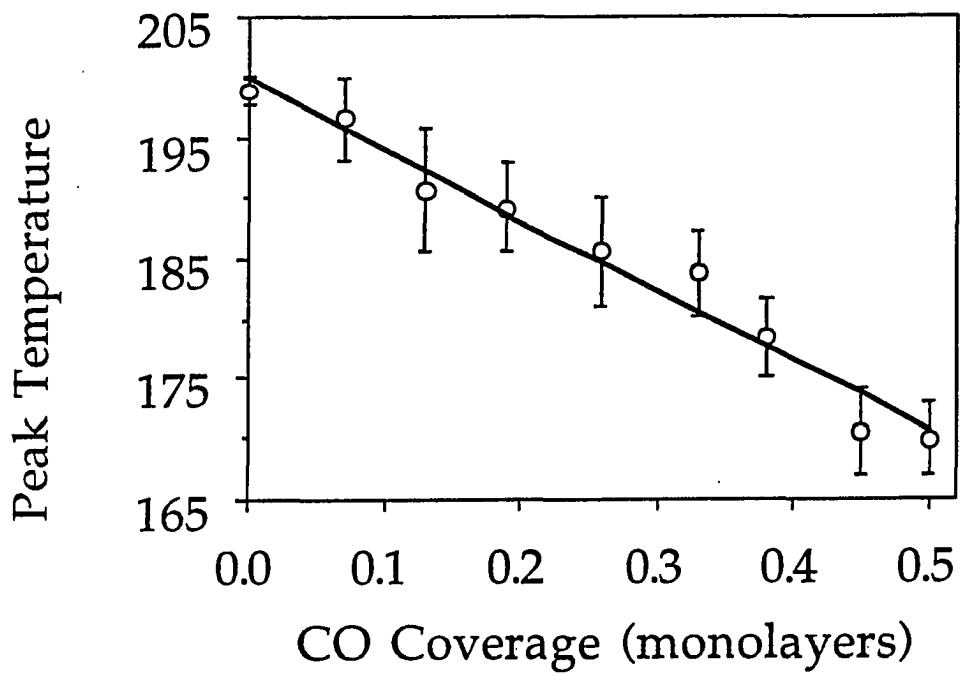

Figure 4. Peak desorption temperature for mass 29 (HCO^+) vs. CO coverage. Each normalized value is the average of 3-5 measurements made at the stated temperature and the error bars reflect ± one standard deviation.

states [17]: the first appears at exposures greater than 0.3 L HCOOH and is centered at 200 K; desorption from this state is monomeric. A second state appears at exposures greater than 0.6 L; at the onset its peak temperature is 160 K and with increasing exposure this value increases. A third state appears above 1.2 L HCOOH and displays the same peak temperature position and shift as the second state; both of these states exhibit dimeric desorption. Apparently, molecular desorption changes from monomeric to dimeric with increasing CO coverage; this results in the linear decrease in the peak temperature as the CO coverage increases.

3.2 High resolution electron energy loss spectroscopy

Fig. 5 displays a series of high resolution electron energy loss spectra produced by Pt(111) exposed to 0.3 L HCOOH at 100 K. Heating to 130 K improves the ordering of the HCOOH overlayer; the spectrum obtained from this overlayer exhibits a loss at 940 cm^{-1}. This loss is assigned to the OH out-of-plane bend of the molecular acid, indicating that HCOOH is adsorbed with the molecular plane nearly parallel to the surface. Heating to 150 K attenuates this loss and produces new losses at 790 cm^{-1} and 1330 cm^{-1}. These new losses reveal the presence of formate adspecies in a bridging configuration (bonding through both

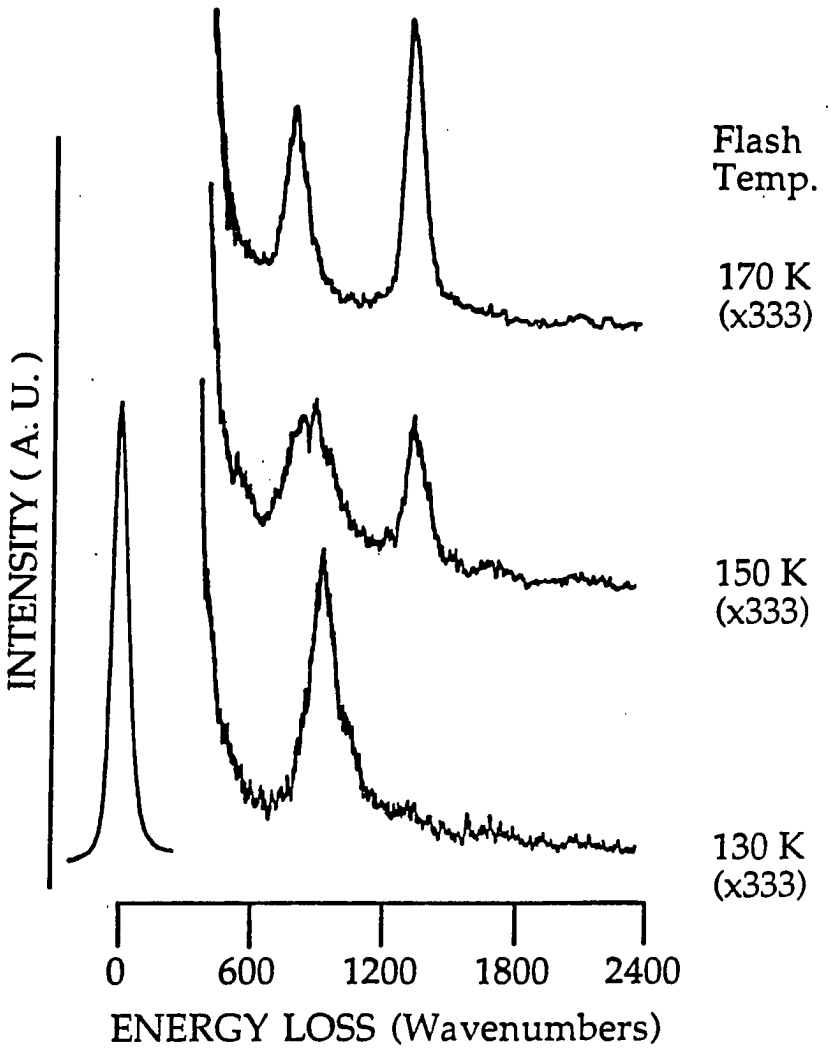

Figure 5. Series of high resolution electron energy loss spectra following exposure of 0.2 L HCOOH at 100 K and heating to 130 K, 150 K, and 170 K, respectively. The elastic peak has an intensity of 50 kHz and a FWHM of 11 mV.

oxygen atoms to two surface sites) with its molecular plane now oriented perpendicularly to the surface. Heating to 170 K eliminates the molecular acid loss and increases the intensities of the formate losses. This spectral series shows the conversion of molecular HCOOH to formate via reaction with the clean surface as it is heated from 130 K to 170 K, as we have reported elsewhere [17].

Fig. 6 displays a spectral series similar to Fig. 5; this one is produced from Pt(111) exposed to CO sufficient to produce a coverage of ca. 0.08 monolayer followed by exposure to 0.3 L HCOOH at 100 K. A loss at ca. 2100 cm^{-1}, appearing in all three spectra, is due to the C-O stretch of CO bonded in an atop surface site. Heating this overlayer to 150 K leaves the loss for the OH out-of-plane of the molecular acid (at 930 cm^{-1}) very intense relative to the formate loss at 1330 cm^{-1}. Heating to 170 K intensifies the formate loss, as well as attenuating and broadening the molecular acid loss. (Presumably the emergence of the formate loss at 790 cm^{-1} contributes to the broadening.) Heating to 190 K eliminates the molecular acid loss and allows the formate loss at 790 cm^{-1} to emerge clearly. This behavior follows that exhibited in Fig. 5, but requires temperatures 20 K higher to be realized.

Fig. 7 shows a spectral series for a coadsorbed overlayer formed by sufficient CO exposure to produce a coverage of 0.35 monolayer followed by

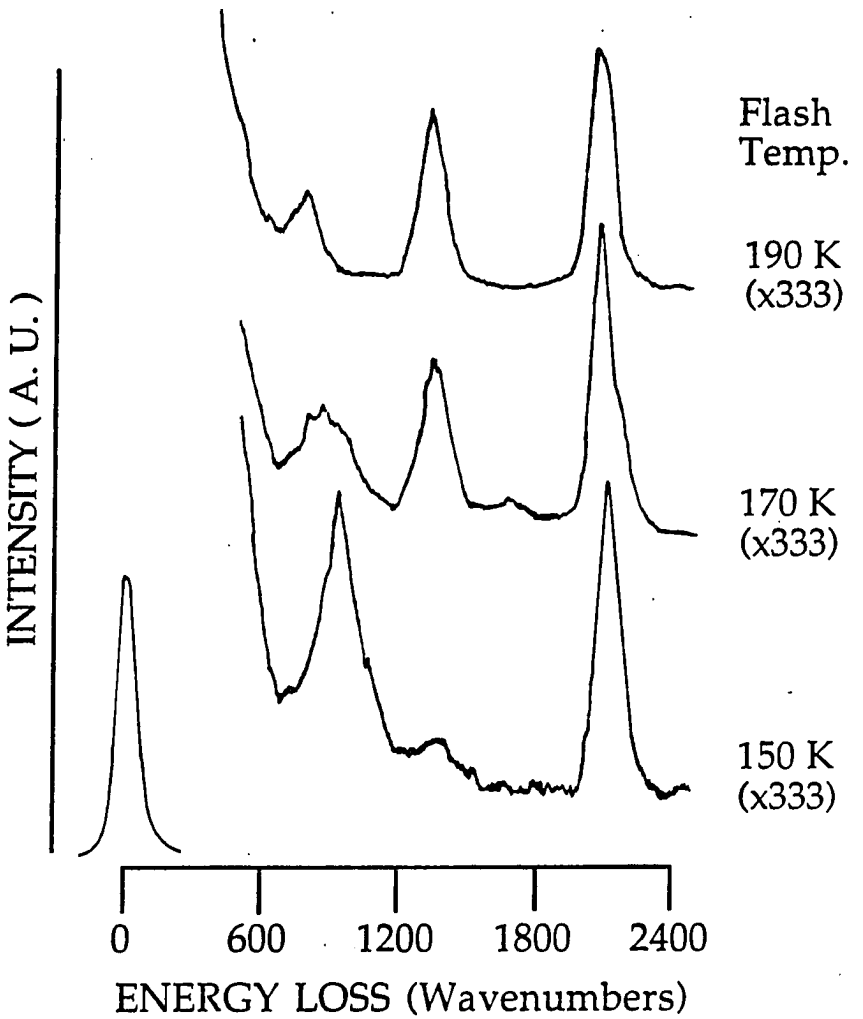

Figure 6. Series of high resolution electron energy loss spectra following exposure of 0.2 L HCOOH at 100 K and heating to 130 K, 150 K, and 170 K, respectively. The surface had been exposed to sufficient CO to produce a coverage of ca. 0.07 monolayer prior to exposure to HCOOH. The elastic peak has an intensity of 110 kHz and a FWHM of 12 mV.

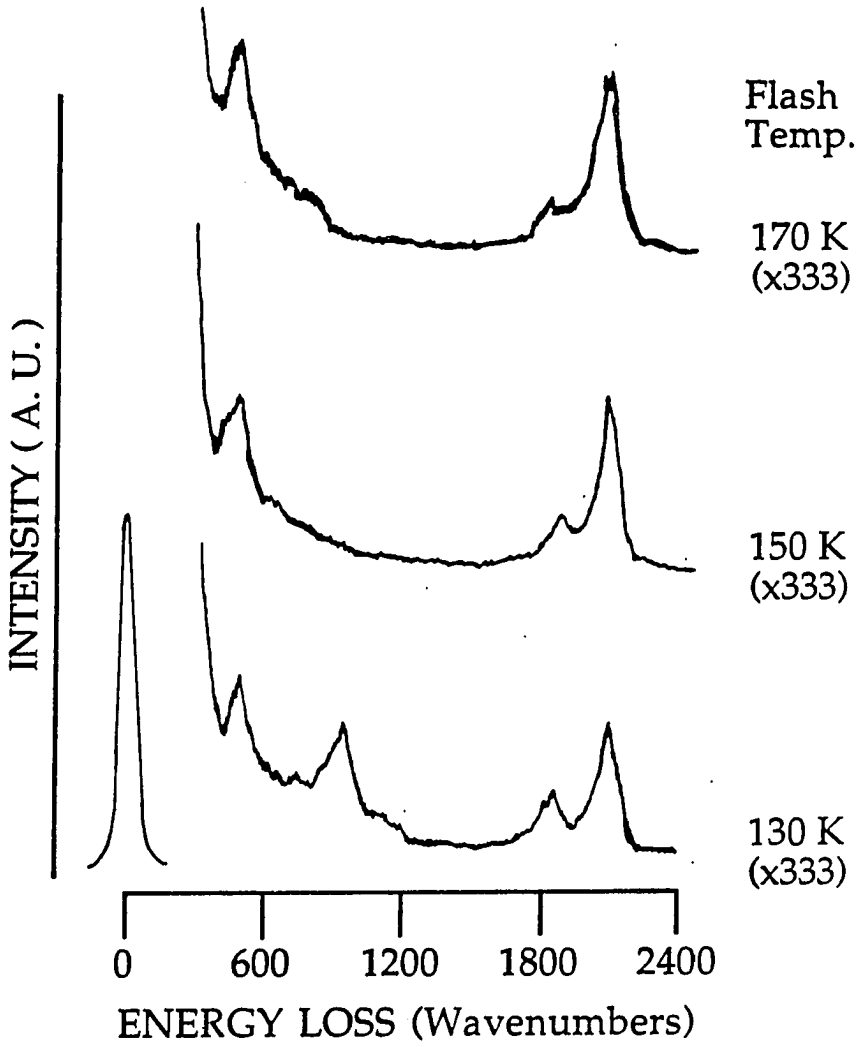

Figure 7. Series of high resolution electron energy loss spectra following exposure of 0.2 L HCOOH at 100 K and heating to 130 K, 150 K, and 170 K, respectively. The surface had been exposed to sufficient CO to produce a coverage of ca. 0.35 monolayer prior to exposure to HCOOH. The elastic peak has an intensity of 120 kHz and a FWHM of 11 mV.

exposure to 0.3 L HCOOH at 100 K. All three spectra exhibit losses at 490 cm^{-1}, 1865 cm^{-1}, and 2100 cm^{-1}; these are assigned to the CO vibrations: the Pt-C stretch of atop CO, the C-O stretch of bridging CO, and the C-O stretch of atop CO, respectively. The spectrum for the overlayer heated to 130 K exhibits the molecular acid loss at 935 cm^{-1} for the O-H out-of-plane bend. Heating to 150 K eliminates this loss; however, no losses appear for a formate adspecies. Heating to 170 K produces the same basic spectrum; however, the resolution between the two losses due C-O stretches has degraded and a broad, low intensity feature appears on the high energy side of the loss for Pt-C stretch. The intensity of this feature has proved difficult to reproduce and sometimes approaches that of the loss for the Pt-C stretch.

An interesting comparison between the spectral series in Figs. 6 and 7 reveals the attenuation of all features in Fig. 7 relative to those in Fig. 6. This is unexpected considering the CO coverage in Fig. 7 series is five times that of the series in Fig. 6. A possible explanation for this observation is the tilting of the CO bond axis away from the surface normal. Such tilting would suggest an electrostatic attraction between CO and formic acid or its decomposition products.

4. Discussion

Two phenomena emerge from the data acquired from thermal desorption and high resolution electron energy loss spectroscopy which demonstrate the influence of CO on the decomposition of HCOOH on Pt(111). One is readily apparent, the arrest of formic acid conversion to formate, while the other is more subtle and difficult to characterize; this is the difference between the decreasing desorption yields of the CO_2 and H_2 caused by increasing CO coverage.

These decreasing yields and the disappearance of formate vibrational bands in the HREEL spectra obtained from surfaces covered by more than 0.35 monolayer CO attest to the decrease in conversion of formic acid to formate. Even at lower CO coverages, higher surface temperatures are required to accomplish the conversion. As this reaction is retarded, molecular HCOOH desorption increases. An interesting aspect of this process is the behavior of the molecular desorption peak temperature; as the yield of molecular desorption increases, the peak temperature moves linearly from 200 K to 170 K with CO coverages increasing from 0 to 0.5 monolayer. This shift is consistent with the appearance of dimeric desorption above 0.13 monolayer CO; on the clean surface,

the molecular desorption state at 200 K is predominantly monomeric, while dimeric desorption dominates for the states at lower temperature.

Both these CO coverage-dependent observations, the increasing preference of molecular desorption over formate production and the shift from monomeric to dimeric desorption, suggest the role of CO as a site blocker. The decreasing amount of formate produced as CO coverage increases can be attributed to the destruction of ensembles needed for the molecular acid to lose its hydroxyl proton to the surface. This also allows the maintenance of the hydrogen bonds which exist between the HCOOH molecules, thus leading to the desorption of dimers, and possibly even higher-numbered oligomers. On clean Pt, we attribute dimer desorption to a polymorphic transition of the hydrogen-bonded HCOOH chains induced by increasing HCOOH exposure. This is evidenced by a ca. 40 cm^{-1} shift in the frequency of the OH out-of-plane bend of the molecular acid. No shift is seen under the conditions reported in this study, however, indicating no such transition occurs. This supports the role of CO as a site blocker, possibly interspersed among the HCOOH chains. (Formation of discrete islands of HCOOH and CO would increase the local HCOOH coverages and lead to the polymorphic transition.)

The ability of CO to prevent the deprotonation of HCOOH via siteblocking explains how it acts as a poison on a Pt surface in ultrahigh vacuum. This fact, in general, reinforces the in situ studies of Shibata et al which involved the control of ensemble size and geometry on a Pt electrode [9, 10]. They revealed that the oxidation pathway HCOOH undergoes is sensitive to both factors.

The more subtle phenomenon is the difference in the decreases of the CO_2 and H_2 desorption yields with increasing CO coverage. The H_2 desorption yield decreases linearly as a function of CO coverage reaching extinction at 0.5 monolayer. This is similar to the dependence of the molecular desorption peak temperature on CO coverage. The parallel behavior suggests that the two are linked and lends more support to the connection of deprotonation and the shift in the nature of molecular desorption. As deprotonation is reduced by increasing CO coverage, molecular desorption becomes more dimeric.

The CO_2 desorption yield drops off much more sharply than the H_2 desorption yield and reaches extinction at CO coverages of 0.35-0.4 monolayer. This distinction, in conjunction with the absence of formate vibrational losses in HREEL spectra for CO coverages greater than 0.35 monolayer, signifies an alternate decomposition pathway. This pathway is initiated by deprotonation but does not lead to the production of formate adspecies with its molecular plane

oriented perpendicularly to the surface. The reorientation might be prevented either through blocking of sites by CO admolecules or through some electrostatic interaction between the two which stabilizes the parallel orientation following deprotonation. A parallel orientation could lead to an alternate reaction pathway between the formate and the surface.

Attempts to characterize this other decomposition pathway have proved problematic, even though as much as 0.03-0.04 monolayer of the alternate intermediate might be produced. (This amount is based on the point of greatest deviation between the H_2 and CO_2 desorption areas and assumes that 0.1 monolayer HCOOH decomposes in the absence of CO [16].) HREEL spectra from coadsorbed overlayers of HCOOH and CO, which are heated to temperatures sufficient to decompose formate, show broad loss features below 1000 cm^{-1}. These spectra also exhibit spurious noise and a degradation in the elastic condition not observed in spectra obtained from adsorption of HCOOH or CO on Pt(111) alone. Such effects are normally associated with the presence of carbonaceous contaminants on the Pt surface; however, attempts to verify the presence of atomic carbon via Auger electron spectroscopy after CO desorbs have failed. Additionally, comparison of CO desorption areas from the clean surface with those produced from coadsorption of CO and HCOOH shows no statistical

differences between the two. The lack of corroborative evidence makes a determination of a mechanism for this alternate pathway difficult and highly speculative; however, such a problem is not unexpected taking into account the differing conclusions reached by those in the electrochemical community who have studied this system.

5. Summary

The presence of coadsorbed CO reduces the ability of Pt(111) to convert molecular HCOOH to formate. This is demonstrated by decreases in the desorption yields of CO_2 and H_2 as CO coverage increases, as well as the lack of any formate vibrational features in HREEL spectra produced by coadsorbed overlayers containing CO coverages greater than 0.35 monolayer. This is an important consequence considering in situ infrared studies of electrooxidation of HCOOH at Pt electrodes which identify CO as the primary candidate for the species responsible for poisoning the electrode surface [11-13].

As the production of formate becomes more difficult, molecular desorption of HCOOH increases. At lower CO coverages this desorption is

monomeric and reaches maximum intensity at 190-200 K. Increasing CO coverage decreases this peak temperature in a linear manner, reaching a value of 170 K at a CO coverage of 0.5 monolayer; the appearance and growth of dimeric desorption accompanies this, as well. These CO coverage-dependent changes indicate that CO blocks sites necessary to the deprotonation of the molecular acid. Such a result is consistent with the sensitivity of the oxidation of HCOOH at Pt electrodes to the availability of specific ensembles of surface sites [9, 10].

There is a difference in the way CO_2 and H_2 desorption yields decrease with increasing CO coverage. H_2 desorption drops off linearly, reaching extinction at 0.5 monolayer of CO; CO_2 desorption drops off more quickly and is completely absent above 0.35-0.4 monolayer CO. This suggests that a new decomposition pathway occurs as a result of interaction between the formate and CO which prevents the reorientation of the molecular plane of the adspecies from parallel to perpendicular to the surface following deprotonation. The characterization of this pathway has proved elusive due to lack of definitive identification of the reaction products; this difficulty is not surprising considering the controversy surrounding the reaction intermediates and pathways produced in the oxidation of HCOOH at Pt electrodes.

Acknowledgments

Acknowledgement is made to the Donors of The Petroleum Research Fund, administered by the American Chemical Society, for the support of this research. Some equipment and all facilities are provided by the Ames Laboratory, which is operated for the U. S. Department of Energy by Iowa State University under Contract No. W-7405-ENG-82.

References

1. E. Mueller, Z. Elektrochem., 29 (1923) 264

2. E. Mueller, Z. Elektrochem., 33 (1927) 561

3. E. Mueller and S. Tanaka, Z. Elektrochem., 34 (1928) 256

4. K. Schwabe, Z. Elektrochem., 61 (1957) 744

5. M. W. Breiter, *Electrochemical Processes in Fuel Cells*, Springer-Verlag, Berlin, 1969

6. W. Vielstich, *Fuel Cells*, Wiley-Interscience, London, 1970

7. B. B. Damaskin, O. A. Petrii and V. V. Batrakov, *Adsorption of Organic Compounds on Electrodes*, Pllenum Press, New York, 1971

8. A. Capon and R. Parsons, J. Electroanal. Chem., 44 (1973) 1

9. M. Shibata, O. Takahashi and S. Motoo, J. Electroanal. Chem., 249 (1988) 253

10. M. Shibata, N. Furuya, M. Watanabe and S. Motoo, J. Electroanal. Chem., 263 (1989) 97

11. B. Beden, A. Bewick and c. Lamy, J. Electroanal. Chem., 148 (1983) 147

12. K. Kunimatsu, J. Electroanal. Chem., 213 (1986) 149

13. D. S. Corrigan and M. J. Weaver, J. Electroanal. Chem., 241 (1988) 143

14. S. G. Sun, J. Clavilier and A. Bewick, J. Electroanal. Chem., 240 (1988) 147

15. R. J. Madix, J. L. Gland, G. E. Mitchell and B. A. Sexton, Surf. Sci., 125 (1983) 481

16. M. R. Columbia and P. A. Thiel, Surf. Sci., 235 (1990) 53

17. M. R. Columbia, A. M. Crabtree and P. A. Thiel, submitted to J. Am. Chem. Soc., (1991)

18. M. R. Columbia and P. A. Thiel, Rev. Sci. Instrum., 58 (1987) 309

19. P. K. Leavitt, J. L. Davis, J. S. Dyer and P. A. Thiel, Surf. Sci., 218 (1989) 346

20. G. Ertl, M. Neumann and K. M. Streit, Surf. Sci., 64 (1977) 393

21. C. T. Campbell, G. Ertl, H. Kuipers and J. Segner, Surf. Sci., 107 (1981) 207

22. H. Steininger, S. Lehwald and H. Ibach, Surf. Sci., 123 (1982) 264

23. J. M. White and S. Akhter, CRC Crit. Rev., 14 (1988) 130

CONCLUSIONS

This dissertation details the interaction of formic acid with Pt(111) as studied in ultrahigh vacuum with thermal desorption spectroscopy (TDS) and high resolution electron energy loss spectroscopy (HREELS). Formic acid adsorbs molecularly at 100 K with its molecular plane oriented almost parallel to the surface. The OH out-of-plane bend is the most prominent loss in HREEL spectra for the molecular adspecies; the frequency of this vibration indicates that formic acid forms hydrogen-bonded chains which resemble those of solid state formic acid. At low coverages the chains resemble the beta polymorphic form of solid formic acid; as the surface temperature is raised to 150 K the chains convert to discrete dimer pairs which decompose to produce formate and atomic hydrogen. HREEL spectra reveal that the formate adspecies is bonded to equivalent surface sites via both oxygen atoms with its molecular plane oriented perpendicular to the surface; this is referred to as a bridging configuration. TDS identifies the decomposition of formate above 200 K, resulting in CO_2 desorption peaked at 260 K. Atomic hydrogen combines and desorbs as H_2 above 300 K.

At coverages near saturation of the first layer, the hydrogen-bonded chains resemble the alpha polymorphic form of solid formic acid. As the surface

temperature is raised to 150 K, HREEL spectra identify the loss of alpha polymorphic formic acid and the simultaneous appearance of beta polymorphic formic acid and bridging formate. This is tied to a molecular desorption state centered at 160-170 K; the connection of these two phenomena suggests the alpha polymorphic chains convert to beta polymorphic chains producing molecular desorption. The OH out-of-plane bend of beta polymorphic formic acid persists in HREEL spectra to 180-190 K; its disappearance coincides with a second molecular desorption state peaked at 200 K. The formate left on the surface following molecular desorption decomposes in the same manner as before.

This dissertation also outlines the effects of coadsorbates commonly encountered in fuel cell environments on the interaction of formic acid and Pt(111). TDS shows that the coadsorption of water causes mutual displacement of formic acid and water from first layer desorption states to multilayer desorption states; these displacements prove very reproducible. TDS results for coadsorption of HCOOH and D_2O reveal that extensive hydrogen bonding occurs between the water and formic acid molecules. These facts suggest that water and formic acid molecules left in contact with the Pt surface might form a stoichiometric complex. HREEL spectra for this mixed overlayer do not exhibit librational losses for water suggesting that water in this complex is oriented

differently than in its own bilayer adstructure. Water is not found to affect the decomposition of formic acid in any measurable way.

The presence of atomic oxygen dramatically enhances the decomposition of formic acid on Pt(111). Saturation areas of CO_2 desorption measured from TDS experiments of formic acid exposed to a Pt(111) surface covered with 0.25 monolayer of atomic oxygen are four to six times the same areas measured for clean Pt(111); this desorption occurs at higher temperatures than on the clean surface as well. The other principal product resulting from decomposition is water, not hydrogen, as observed in the absence of oxygen. Desorption of water occurs in three states: (1) Molecular desorption, centered at 180 K, produced from initial deprotonation of formic acid. (2) Combination of hydroxyl adspecies produced from the same deprotonation process; the peak desorption temperature is 200-210 K. (3) Combination of atomic oxygen with hydrogen adatoms produced by formate decomposition; peak desorption temperatures follow that for CO_2; HREEL spectra show that atomic oxygen significantly lowers the surface temperature required for deprotonation of formic acid to produce formate. They also provide vibrational evidence for the existence of hydroxyl adspecies. A reaction scheme is developed involving formate and hydroxyl adspecies and

molecular water and formic acid to explain new states in the CO_2 and molecular formic acid thermal desorption spectra.

Coadsorbed CO diminishes the decomposition of formic acid; this is strongly supported by the decreasing of CO_2 and H_2 desorption areas as CO coverage increases. The reduction of H_2 desorption is fairly linear to extinction at 0.5 monolayer of CO; over the same CO coverage range molecular desorption appears and shifts down in temperature. These phenomena are attributed to the increasing difficulty of formic acid to deprotonate on the increasingly "crowded" surface. The decline in CO_2 desorption is observed to occur at a faster rate than that of H_2 with extinction occurring between 0.35 and 0.4 monolayer CO. HREEL spectra reveal no formate is produced above these CO coverages. This indicates that an alternate decomposition pathway exists which does not result in formate as an intermediate; the identity of the new intermediate remains undetermined.

REFERENCES

1. P. Mars, J. J. F. Scholten and P. Zwietering, Advan. Cat., 14 (1963) 35
2. J. M. Trillo, G. Munuera and J. M. Craido, Cat. Rev., 7 (1972) 51
3. J. McCarty, J. Falconer and R. J. Madix, J. Cat., 30 (1973) 235
4. E. Mueller, Z. Elektrochem., 29 (1923) 264
5. E. Mueller, Z. Elektrochem., 33 (1927) 561
6. E. Mueller and S. Tanaka, Z. Elektrochem., 34 (1928) 256
7. K. Schwabe, Z. Elektrochem., 61 (1957) 744
8. M. W. Breiter, Electrochemical Processes in Fuel Cells (Springer-Verlag, Berlin, 1969)
9. B. B. Damaskin, O. A. Petrii and V. V. Batrakov, Adsorption of Organic Compounds on Electrodes (Plenum Press, New York, 1971)
10. W. Vielstich, Fuel Cells (Wiley-Interscience, London, 1970)
11. A. Capon and R. Parsons, J. Electroanal. Chem., 44 (1973) 1
12. R. Parsons and T. VanderNoot, J. Electroanal. Chem., 257 (1988) 9
13. N. R. Avery, App. Surf. Sci., 11/12 (1982) 774
14. P. Hofmann, S. R. Bare, N. V. Richardson and D. A. King, Surf. Sci., 133 (1983) L459

15. R. J. Madix, Adv. Cat., 29 (1980) 1

16. B. A. Sexton and R. J. Madix, Surf. Sci., 105 (1981) 177

17. D. A. Outka and R. J. Madix, Surf. Sci., 179 (1987) 361

18. M. Bowker and R. J. Madix, Surf. Sci., 102 (1981) 542

19. B. E. Hayden, K. Prince, D. P. Woodruff and A. M. Bradshaw, Surf. Sci., 133 (1983) 589

20. F. C. Henn, J. A. Rodriguez and C. T. Campbell, Surf. Sci., 236 (1990) 282

21. W. Erley and D. Sander, J. Vac. Sci Technol. A, 7 (1989) 2238

22. J. L. Falconer and R. J. Madix, J. Catal., 51 (1978) 47

23. E. I. Ko and R. J. Madix, Appl. Surf. Sci., 3 (1979) 236

24. N. Kizhakevariam and E. M. Stuve, J. Vac. Sci. Technol. A, 8 (1990) 2557

25. N. Abbas and R. J. Madix, App. Surf. Sci., 16 (1983) 424

26. M. R. Columbia and P. A. Thiel, Surf. Sci., 235 (1990) 53

27. F. Solymosi, J. Kiss and I. Kovacs, Surf. Sci., 192 (1987) 47

28. Y.-K. Sun and W. H. Weinberg, J. Chem. Phys., 94 (1991) 4587

29. L. A. Larson and J. T. Dickinson, Surf. Sci., 84 (1979) 17

30. R. W. Joyner and M. W. Roberts, Proc. R. Soc. Lon. A, 350 (1976) 107

31. F. Holtzberg, B. Post and I. Fankuchen, Acta Cryst., 6 (1953) 127

32. R. C. Millikan and K. S. Pitzer, J. Am. Chem. Soc., 80 (1958) 3515

33. Y. Mikawa, R. J. Jakobsen and J. W. Brasch, J. Chem. Phys., 45 (1966) 4750

34. Y. Mikawa, J. W. Brasch and R. J. Jakobsen, J. Mol. Spectros., 24 (1967) 314

35. B. A. Sexton, Surf. Sci., 88 (1979) 319

36. M. R. Columbia, A. M. Crabtree and P. A. Thiel, submitted to J. Am. Chem. Soc., (1991)

37. M. Chtaib, P. A. Thiry, J. J. Pireaux, J. P. Delrue and R. Caudano, Surf. Sci., 162 (1985) 245

38. R. J. Madix, J. Falconer and J. McCarty, J. Catal., 31 (1973) 316

39. J. L. Falconer, J. G. McCarty and R. J. Madix, Surf. Sci., 42 (1974) 329

40. J. L. Falconer and R. J. Madix, Surf. Sci., 46 (1974) 473

41. R. J. Madix and J. L. Falconer, Surf. Sci., 51 (1975) 546

42. J. McCarty and R. J. Madix, J. Catal., 38 (1975) 402

43. J. L. Falconer and R. J. Madix, Surf. Sci., 48 (1975) 393

44. S. W. Johnson and R. J. Madix, Surf. Sci., 66 (1977) 189

45. J. B. Benziger and R. J. Madix, Surf. Sci., 79 (1979) 394

46. J. B. Benziger and G. B. Schoofs, J. Phys. Chem., 88 (1984) 4439

47. R. J. Madix, J. L. Gland, G. E. Mitchell and B. A. Sexton, Surf. Sci., 125 (1983) 481

48. T. S. Jones, N. V. Richardson and A. W. Joshi, Surf. Sci., 207 (1988) L948

49. T. S. Jones, M. R. Ashton and N. V. Richardson, J. Chem. Phys., 90 (1989) 7564

50. D. H. S. Ying and R. J. Madix, J. Cat., 61 (1980) 48

51. L. H. Dubois, T. H. Ellis, B. R. Zegarski and S. D. Kevan, Surf. Sci., 172 (1986) 385

52. B. A. Sexton, J. Vac. Sci. Technol., 17 (1980) 141

53. B. E. Hayden, K. Prince, D. P. Woodruff and A. M. Bradshaw, Phys. Rev. Lett., 51 (1983) 475

54. J. Stœhr, D. A. Outka, R. J. Madix and U. Dœbler, Phys. Rev. Lett., 54 (1985) 1256

55. D. A. Outka, R. J. Madix and J. Stœhr, Surf. Sci., 164 (1985) 235

56. A. Puschmann, J. Haaase, M. D. Crapper, C. E. Riley and D. P. Woodruff, Phys. Rev. Lett., 54 (1985) 2250

57. M. D. Crapper, C. E. Riley, D. P. Woodruff, A. Puschmann and J. Haase, Surf. Sci., 171 (1986) 1

58. M. D. Crapper, C. E. Riley and D. P. .Woodruff, Phys. Rev. Lett, 57 (1986) 2598

59. M. D. Crapper, C. E. Riley and D. P. Woodruff, Surf. Sci., 184 (1987) 121

60. D. P. Woodruff, C. F. McConville, A. L. D. Kilcoyne, T. Linder, J. Somers, M. Surman, G. Paolucci and A. M. Bradshaw, Surf. Sci., 201 (1988) 228

61. E. G. Seebauer, A. C. F. Kong and L. D. Schmidt, Appl. Surf. Sci., 29 (1987) 380

62. M. R. Columbia, A. M. Crabtree and P. A. Thiel, submitted to J. Chem. Phys., (1991)

63. M. R. Columbia, A. M. Crabtree and P. A. Thiel, to be submitted to J. Electroanal. Chem., (1991)

64. N. R. Avery, App. Surf. Sci, 14 (1982-83) 149

65. N. R. Avery, B. H. Toby, A. B. Anton and W. H. Weinberg, Surf. Sci., 122 (1982) L574

66. B. H. Toby, N. R. Avery, A. B. Anton and W. H. Weinberg, J. Electron Spec., 29 (1983) 317

67. S. W. Jorgensen and R. J. Madix, J. Am. Chem. Soc., 110 (1988) 397

68. D. Sander and W. Erley, J. Vac. Sci. Technol., A8 (1990) 3367

69. C. Egawa, I. Doi, S. Naito and K. Tamaru, Surf. Sci., 176 (1986) 491

70. F. Solymosi, J. Kiss and I. Kovacs, J. Vac. Sci. Technol., A5 (1987) 1108

71. F. Solymosi, J. Kiss and I. Kovacs, J. Phys. Chem., 92 (1988) 796

72. M. A. Barteau, M. Bowker and R. J. Madix, Surf. Sci., 94 (1980) 303

73. P. A. Stevens, R. J. Madix and J. Stœhr, Surf. Sci., 230 (1990) 1

74. M. Chtaib, P. A. Thiry, J. P. Delrue, J. J. Pireaux and R. Caudano, J. Electron Spec., 29 (1983) 293

75. J. B. Benziger and R. J. Madix, J. Catal., 65 (1980) 49

76. J. B. Benziger and R. J. Madix, J. Catal., 74 (1982) 67

77. J. B. Benziger, E. I. Ko and R. J. Madix, J. Catal., 58 (1979) 149

78. A. K. Bhattacharya, J. Chem. Soc.-Farad. Trans. 1, 75 (1979) 863

APPENDIX I:

DESIGN PARAMETERS FOR DIFFERENTIALLY PUMPED ROTATING PLATFORMS

Design Parameters for Differentially Pumped Rotating Platforms

by

M. R. Columbia and P. A. Thiel

Department of Chemistry and Ames Laboratory
Iowa State University
Ames, Iowa 50011 USA

Published in *Review of Scientific Instrumentation*, 58 (1987) 309

Abstract

We have constructed a large differentially pumped platform for use in ultrahigh vacuum. The design utilizes spring-loaded Teflon seals to permit differential pumping between two horizontal stainless-steel disks. This allows the rotation of the upper disk and the items built into it directly inside a vacuum chamber while maintaining a pressure of 2×10^{-10} Torr. The following design parameters are discussed: conductance across the seals, deflection of the seals, rotational friction, and differential thermal expansion during bakeout.

We have recently constructed a large differentially pumped platform for sample manipulation in ultrahigh vacuum. Although differentially pumped rotating stages are currently used in ultrahigh vacuum in many laboratories, particularly those in which molecular beam experiments are underway, we found that several critical design parameters were completely absent both from the scientific literature and the vendor's literature. This information was also unavailable or confusingly inconsistent when we attempted to extract it from users of existing equipment. The purpose of this note is to describe these parameters for our design, based on its actual performance, in order to facilitate future uses of spring-loaded seal technology. These parameters will also be compared with those of a smaller commercial device in our laboratory.

The platform is shown schematically in Fig. 1. It is a variant of the differentially pumped elastomer seal design originally published by Wilson [1]. It consists of two flat stainless-steel disks separated by three concentric, differentially pumped, spring-loaded Teflon seals [2] across which the top stainless-steel plate (62.5 cm diameter) can rotate. The bottom plate (69.85 cm diameter) is stationary, as are the connections to the pumps. The use of spring-loaded Teflon seals in this type of application was originally described by Auerbach [3]. The advantage of this general design is that the entire upper plate

and the items built into it can rotate directly inside the vacuum chamber. The cumbersome alternative is to achieve rotation of items within the chamber via indirectly coupled feedthroughs. In our application, the items built into the upper stage are three sample manipulators on 15-cm-diam flanges, each of which is directly above the chamber's circle of focal points, and which can be themselves mounted on smaller differentially pumped stages [4]. The stage need only be rotated slowly (< 0.1 rotation s^{-1}) and infrequently (< 20 times daily). We shall describe the following important operating parameters for this device: conductance across the seals, deflection of the seals, rotational friction, and the effects of differential thermal expansion during bakeout.

We have found that conductance across the seals improves (decreases) significantly with use. This is due to visible transfer of Teflon from the seal to the metal surfaces, which effectively smooths both the seal and the metal. For this reason, it appears that conductance across the seal per unit length is not a strong function of the smoothness of the contacting metal, within reasonable limits. The large stage shown in Fig. 1 operates with a No. 16 finish on the plates, which is the best finish commonly available direct from the machine-shop lathe. (The large stainless-steel plates were stress relieved prior to lathing and welding, thus ensuring the waviness of the polished surface is no greater

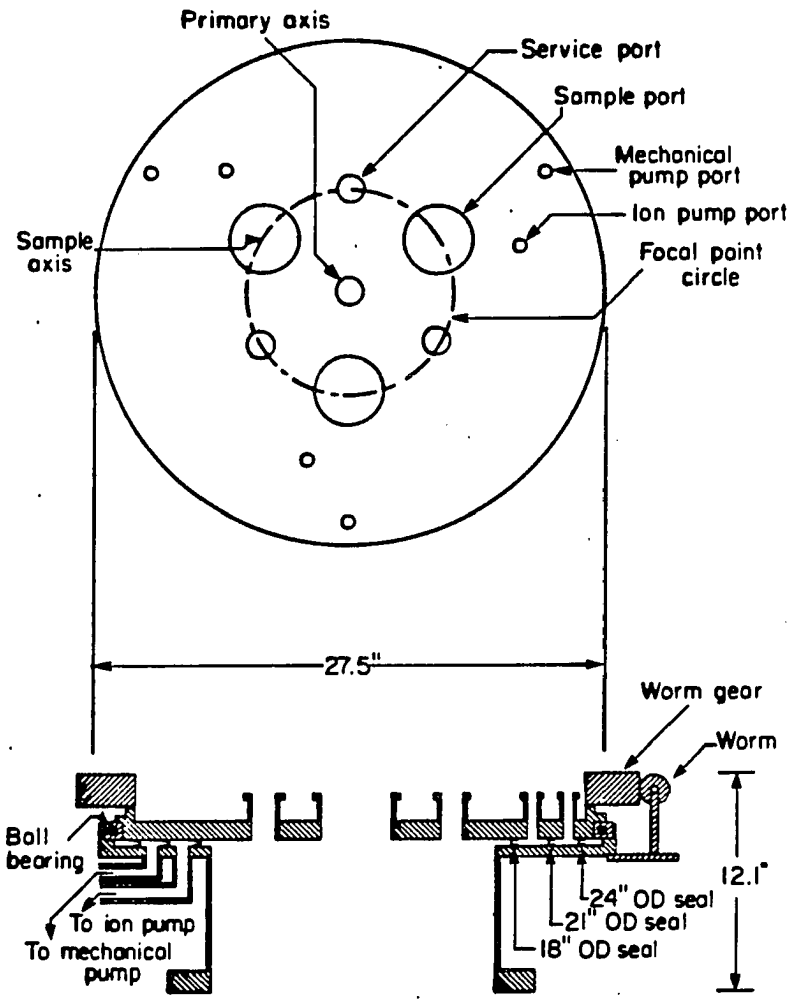

Figure 1. Schematic drawings of the rotatable platform: Top view is shown at the top; a linear cross section is shown at the bottom. Dimensions are given in centimeters. The diameter of the bottom steel plate is 69.9 cm. The sample axis and the primary axis are both perpendicular to the plane of the figure.

than the surface roughness.) Our pressures and pumping speeds allow us to calculate that the seal conductance is 1×10^{-8} l s^{-1} cm^{-1} across the first seal (which stands against atmospheric pressure) and 3×10^{-8} l s^{-1} cm^{-1} across the middle seal. A smaller commercial device of a similar coplanar-seal design,[4, 5] with polished No. 4 metal finishes, yields values for the conductance which are within a factor of two of the average value for the large stage.

One advantage of the design shown in Fig. 1, with concentric coplanar seals, is the ease of assembly and disassembly. Assembly consists of simply dropping the top plate in place. Atmospheric pressure (approximately 2720 kg on a device of the size shown with the chamber evacuated) provides the force to deflect the seals. This is in contrast to a device with stacked seals, where loading (compression) must be forced during assembly by positioning the seals in the fixed space between a pair of concentric cylinders. This can be difficult.

The seals in our device deflect only 0.022 cm upon pumpdown. This deflection is adequate to obtain the conductances described in the previous section, in spite of the fact that the vendor recommends use of higher deflections [2]. He recommends that a 1.044-cm seal be compressed to 0.953 cm [2], so our deflection is only one-quarter of that specified. The bearing [6] does not support

the weight of the top plate as we had anticipated, but only serves as a low-friction positioner.

Based upon vendors' literature [7], we estimate that a breakout force of roughly 286 kg and a moving force of 230 kg would be necessary to turn the platform at the recommended seal loading. Since our seal deflection is considerably less than recommended, we had expected to encounter less resistance in turning the stage. However, our actual turning force (indistinguishable from the breakout force for our device) is 283 kg, which indicates a force of 0.59 kg per cm of seal length or diameter. For the smaller commercial platform, whose top plate is held in place by atmospheric pressure, we measure a force of 0.50 kg/cm. The values for the two devices are thus identical within 20%. Since the smaller stage has a polished No. 4 metal surface whereas the large stage has a No. 16 finish, we conclude that the coefficient of friction is independent of the metal finish within these limits. Again, this is reasonable in view of our observation that some Teflon always transfers from the seal to the metal, so that the main source of friction is Teflon moving on Teflon, rather than Teflon on metal. For the large stage shown in Fig. 1, a gear is necessary to achieve convenient rotation whereas the smaller stage is readily

turned by hand. Knowledge of the turning force is obviously necessary for selection of an appropriate gear.

To achieve ultrahigh vacuum, it is necessary to bake the stage to at least 400 K. (The seals are rated to 500 K [2].) This may potentially lead to pressure on the bearing assembly (with 52 100 steel races [6]) exerted by the 304 stainless-steel plates enclosed within it. We calculated that differences in the coefficient of thermal expansion would cause the rotatable upper plate to exert pressure on the inner race of the bearing, the thermally induced difference in radius between the two pieces being 0.053 cm (0.08%) at 500 K. We have baked the stage several times to 400 K with no apparent loss of function.

The large rotatable stage described herein and depicted in Fig. 1 is entirely compatible with ulltrahigh vacuum, the ultimate base pressure being 4×10^{-11} Torr with the stage immobile and 2×10^{-10} Torr during rotation. The conductance across the seals averages 2×10^{-8} l cm^{-1} s^{-1}. Within a factor of two, the conductance is insensitive to the finish on the metal surfaces, at least between No. 4 (polished) and No. 16 (carefully lathed) surfaces. The seals are deflected (due to atmospheric pressure) by 0.022 cm, about one-quarter of the deflection nominally recommended by their manufacturer [2]. The force of friction is 0.6 kg cm^{-1}. Differential thermal expansion between the bearing races

[6] and stage body does not present a problem. We believe that these parameters will be valuable in future efforts to design differentially pumped stages for ultrahigh vacuum applications.

Acknowledgements

We acknowledge important and fruitful discussion about the design with R. J. Behm, M. Ricks, N. Shinn, and R. Struss. K. Mogard and C. Burg skillfully machined and welded the components of the large stage and P. K. Leavitt assisted us generously during assembly and testing. This work has been supported by the Director for Energy Research, Office of Basic Energy Sciences. Ames Laboratory is operated for the U. S. Department of Energy by Iowa State University under Contract W-7405-ENG-82.

References

1. R. R. Wilson, Rev. Sci. Instrum., 12 (1941) 91

2. We purchased 15% graphite-filled TFE EnerSeals, Mark 1 face type, with 0.95-cm cross section. The part numbers are EAE-017000-06-02-1 (45.7 cm o.d.), EAE-020000-06-02-1 (53.3 cm o.d.), and EAE-023000-06-02-1 (61.0 cm o.d.) from Advanced Products Company, 33 Defco Park Rd., North Haven, CT 06473

3. D. J. Auerbach, C. A. Becker, J. P. Cowin and L. Wharton, Rev. Sci. Instrum., 49 (1978) 1518

4. Devices with a coplanar seal design similar to Fig. 1 are available for use on 15- and 7-cm-o.d. flanges from Thermionics Laboratories Incorporated, 22815 Sutro St., P. O. Box 3711, Hayward, CA 94540

5. P. A. Thiel and J. W. Anderegg, Rev. Sci. Instrum., 55 (1984) 1669

6. We used KG250XPO, 64-cm-i.d x 69-cm-o.d. bearings from Kaydon Corporation, 2860 McCracken St., Muskegon, MI 49443

7. Based on product information from Fluorocarbon Mechanical Seal Division, 10871 Kyle St. Box 520, Los Alamitos, CA 90720

APPENDIX II:

TDS CALIBRATION PROCEDURES

Introduction

The thermal desorption experiments reported in this dissertation are performed with a UTI 100C mass spectrometer and Herz temperature controller interfaced with an IBM AT personal computer. The program and interface that allow the computer to control and acquire data from these components during the TDS experiments are detailed in the Ph. D. thesis of P. K. Leavitt (Iowa State University, 1990). It is the purpose of this appendix to outline calibration procedures for two of the subroutines in that program. One of these subroutines (SLOTA1P) allows the computer to control the mass selection on the quadrupole during the TDS experiment; this subroutine is calibrated on a daily basis. The other subroutine (T2TP) permits the computer to monitor the crystal temperature via the temperature controller; it requires calibration periodically, but not as often as SLOTA1P.

Overview of computer control of mass selection on UTI 100C

Fig. 1 is a schematic outline of the connections which allow computer control of mass selection on the UTI 100C mass spectrometer during the data acquisition of a thermal desorption experiment. The SLOWTDS program converts the AMU values input via the program menu to a digital signal in the SLOTA1P subroutine. This subroutine contains two equations, one for AMU values of 5 and less and one for values greater than 5, which produce digital values of 0 to 4096 for an input range of 0 to 300 AMU. This digital signal is fed to a 12 bit digital-to-analog converter. The converter puts out a voltage range of 0 to 10 volts for digital values of 0 to 4096. This voltage is fed to the "EXTERNAL PROGRAM" BNC terminal on the rear of the UTI 100C controller. (The "EXT" pushbutton on the front of the controller must be depressed for the controller to accept this voltage.) This voltage allows the AMU value on the mass spectrometer to be set over a range of 0 to 300 AMU.

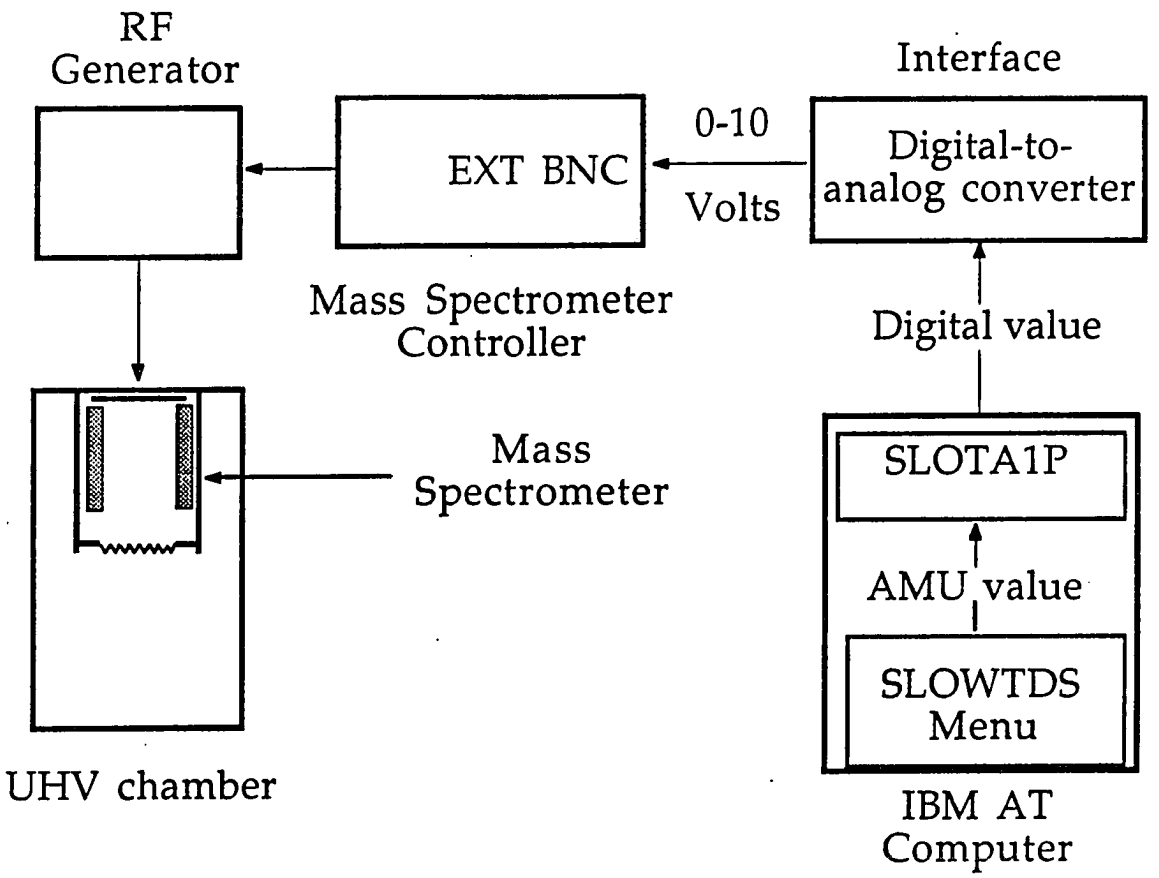

Figure 1. Schematic outline of the connections which allow computer control of mass selection on the UTI 100C mass spectrometer during the data acquisition of a thermal desorption experiment.

Calibration of SLOTA1P subroutine

The equations in the SLOTA1P subroutine which convert the menu AMU values to appropriate digital values are of the y = mx + b type, where x is the AMU value and y is the digital value. The values of m and b must be calibrated often (usually on a daily basis) to ensure proper correlation. The calibration procedure is performed as follows:

1) Set the controls on the mass spectrometer controller to the appropriate settings: PROGRAM selection-depress EXT; FUNCTION selection-depress ON/STBY.

2) Access the DACSWEEP program in the BASICPGM directory by typing in CD\BASICPGM. Load the DACSWEEP by typing in BASICA\DACSWEEP (This program allows manual control of the digital output to the D-to-A converter.) After the program is loaded several options will be offered; Choose "TUNE" by hitting the F6 function key. Enter the desired digital value (e.g., AMU = 2 (H_2) corresponds to digital values of ~ 27). Observe the right panel meter on the front of the mass spectrometer controller

(picoammeter output); adjust the RANGE selection to give the greatest sensitivity without going off-scale. Adjust the digital value up and down using the F9 and F10 function keys, respectively, to determine the digital value which gives the most intense picoammeter signal. Record this value. Adjust the digital value above, then below, this recorded value to observe where the picoammeter signal drops off greatly. Record the upper and lower limits of this range. (Typically, this range extends over 3-5 digital values with the value giving the largest picoammeter intensity at the range's center.) Repeat this procedure for the other primary background gases like H_2O (18 AMU with a digital value of ~ 244), CO (28 AMU with a digital value of ~ 380), and CO_2 (44 AMU with digital value of ~ 600), as well as any AMU values pertinent to gases used in the day's TDS experiments (e,g., AMU values of 29 and 46 for formic acid.) The F8 function button allows selection of a new digital value.

3) Utilizing a calculator with a linear regression program (e.g., TI-55III) determine the slope and y-intercept for a line of AMU values vs digital values of maximum picoammeter intensity for AMU > 5. Record these values. (If possible, check the digital value produced by this equation for each

of the AMU values of interest. The digital value for each should fall within the range produced for each from Step #2.) For AMU < 5 repeat the determination utilizing only the AMU values of 2 and 18. Record the slope and y-intercept values for this line.

4) Exit the DACSWEEP program by pushing the "CONTROL" and "BREAK" buttons simultaneously. Return to the BASICPGM directory by entering SYSTEM. Change directories by entering CD\TDS-NOW. From this directory the text of the SLOTA1P subroutine can be accessed by entering WORD SLOTA1P.FOR. After accessing, press the "ESC" button to display the editing options. Choose the SEARCH option, then enter DOUT; this is the variable name for the y-value produced from the two equations. The editor will locate this term, allowing the two equations to be found easily. The first equation is the one which governs conversion for AMU values less than 5. Change the slope and y-intercept values in this equation to match those from Step #3. Similarly, change the slope and y-intercept values in the second equation to those determined for AMU values greater than 5 in Step #3.

5) Hit "ESC" key again to return to the editor options. Choose TRANSFER; choose SAVE from the options listed; choose UNFORMATTED from the SAVE options by hitting the "TAB" key, followed by "ENTER". Hit "ESC" again and choose QUIT. This returns the display to the TDS-NOW directory.

6) The altered subroutine must now be compiled and linked. Type in F SLOTA1P to compile. (F is a batch file.) Wait until the computer has finished and given a "0 warnings, 0 errors" indication, then link by typing in LINK @SLOWTDS.LNK. The subroutine is now calibrated and ready to use.

Overview of temperature measurement utilizing SLOWTDS program

Fig. 2 is a schematic outline of the components involved in measuring the temperature of the Pt(111) crystal used in the thermal desorption experiments described in this dissertation. The measurement involves a series of conversions: (1) The crystal temperature is monitored by a pair of thermocouple wires (W-5% Re vs W-26% Re) spotwelded directly to the back of the crystal. They produce a temperature-dependent junction potential which is relayed to a Herz temperature controller (HTC) via a special UHV feedthrough. The potential (multiplied by 100) is displayed on the HTC panel meter (absolute range is -1 V to +5 V), as well as output to two separate sockets on the HTC: The DVM socket outputs the bipolar voltage range displayed on the panel meter, and the I/O socket outputs a corresponding voltage based on a unipolar voltage range (0 to +10 V).; (2) The voltage output from the I\O socket (measures at pin #4 of the socket) is input to a voltage-to-frequency converter mounted inside the HTC chassis. This unipolar voltage range is chosen due to the input requirements of the converter. This converter produces a pulse train of 0 Hz to 65 kHz scaled to an input of 0 to 10 Volts.; (3) A counter in the interface samples the pulse train producing a digital value of the frequency. This value is fed to an IBM AT where

the T2TP subroutine in the SLOWTDS program contained on the computer's hard drive converts the digital value into a voltage value via an empirically derived polynomial equation.; and, (4) The voltage value determined from the pulse train frequency is changed to a Kelvin temperature by the T2TP subroutine before storage with other pertinent data for each experimental cycle.

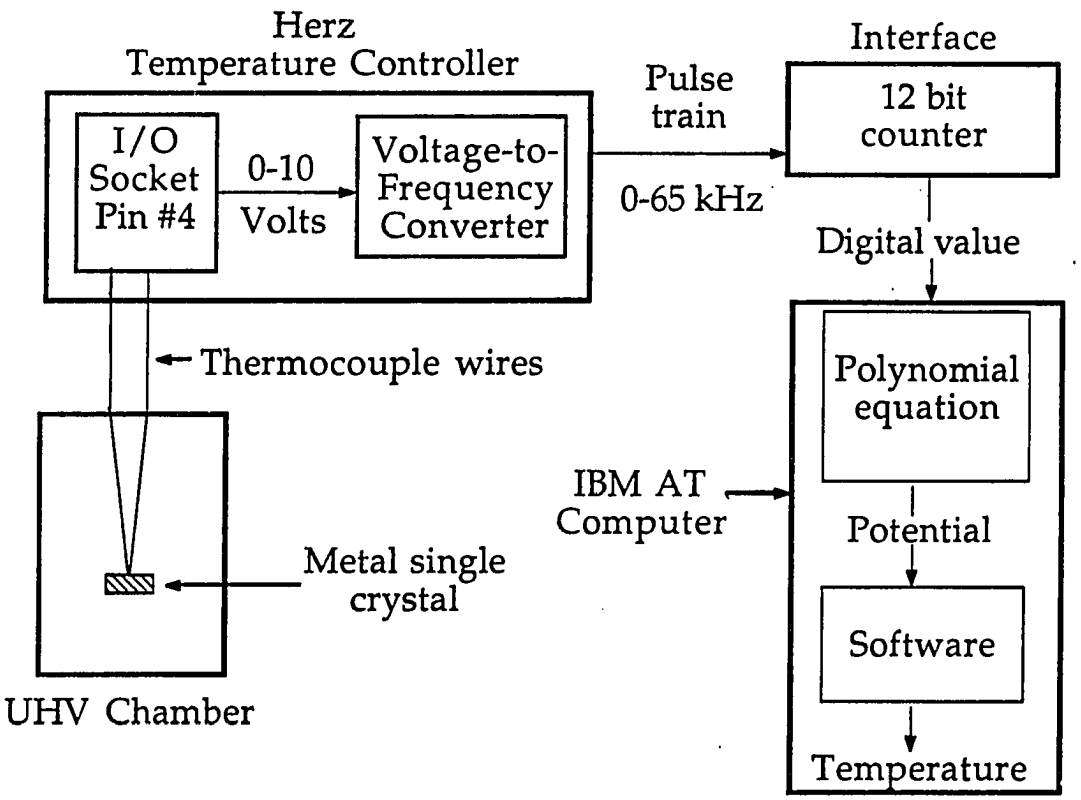

Figure 2. Schematic outline of the components involved in measuring the temperature of the Pt(111) crystal used in the thermal desorption experiments described in this dissertation.

Calibration of the T2TP subroutine

The coefficients in the polynomial equation responsible for converting the pulse train from the HTC to a voltage value must be periodically calibrated to ensure proper correlation of the actual thermocouple junction potential with that produced by the conversion. To accomplish this a reference voltage source can be used to replace the thermocouple junction potential. Fig. 3 displays such a source utilizing a 9V transistor battery and a variable resistor network. The calibration procedure is performed as follows:

1) Adjust the output voltage from the battery to be ~ -2.5 mV by monitoring it with an external digital voltmeter while adjusting the variable resistor. Record this voltage value. Input this voltage into the HTC thermocouple socket. Enter CD\FORTRAN\OLDFORT to access that directory on the computer hard drive, then enter TEMPS to load that program. (This program determines the frequency output from the voltage-to-frequency converter for a given input voltage.) The program offers options of conversion, dwell time, and quitting; choose conversion. This will give the frequency of the converter's pulse train produced for the voltage input from the battery.

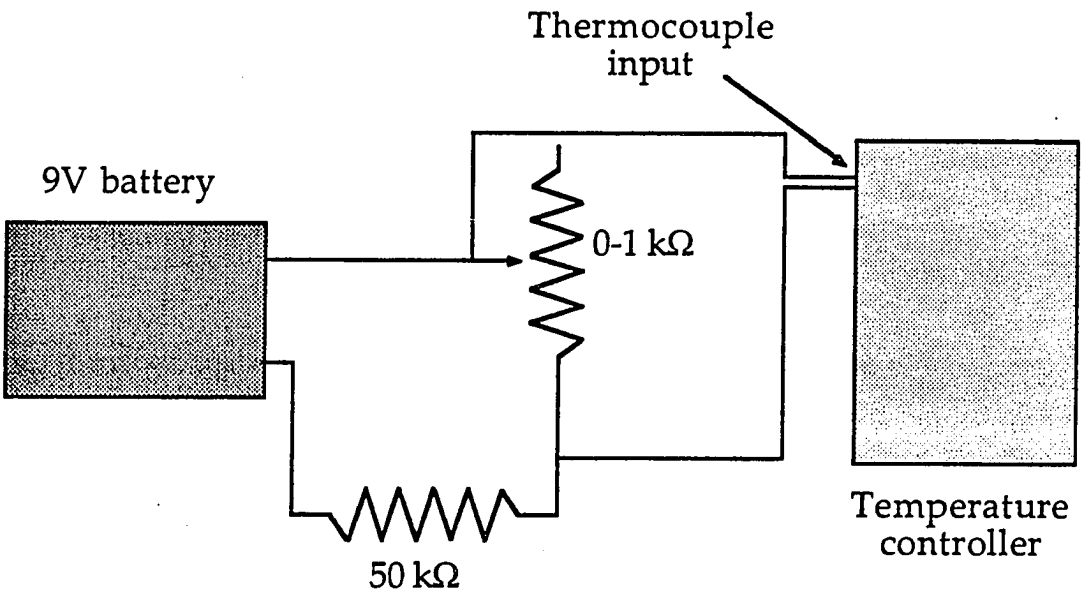

Figure 3. Reference voltage source utilizing a 9V transistor battery and a variable resistor network

Record this frequency with the recorded voltage. Repeat this, increasing the input voltage by ~ 0.5 mV up to a final value of ~ 25 mV.

2) Enter CD\CURVEFIT\POLYNOM to change to that directory. Create a file by entering QED (This accesses the QED editor) and choosing the EDIT option; enter the total number of data pairs (voltage, frequency) on the first line; enter the first data pair on the second line with only one space between the data values. (This format must be followed exactly or the POLYPF program might crash when processing the file.) After the last data pair is entered, choose the QUIT option; choose SAVE from the QUIT options. Title the file XXXX.DAT. Choose EXIT from the QUIT options to complete the storage of the file in the CURVEFIT\POLYNOM directory. Create two more files in a similar manner: One for voltage values between -2.5 mV and +11 mV titled XXXX.LO and one for voltage values between 9 mV and 25 mV titled XXXX.HI

3) Use the POLYPF program in the CURVEFIT\POLYNOM directory to obtain a polynomial fit for the data pairs. Begin by deleting the POLYOUT file. (Enter DEL POLYOUT. If this is not done before the POLYPF program is

executed, it will lock up!!) Copy the XXXX.DAT file into the FOR005 file by entering COPY XXXX.DAT FOR005. Run the POLYPF program by entering POLYPF. Several parameters will be requested before it will provide a polynomial fit; the most important to provide are to treat the data pairs as F(X),X combinations, and to determine an 8th order fit. Obtain a printout of the coefficients. Repeat for the XXXX.LO and XXXX.HI files requesting 4th order fits, remembering to delete the POLYOUT file each time before using the POLYPF program.

4) Access the T2TP subroutine: Enter CD\TDS-NOW to change to that directory. Enter WORD T2TP.FOR to access the text. Substitute the new polynomial coefficients into the appropriate equations: Use the coefficients from XXXX.LO for frequencies less than 3800, the coefficients from XXXX.HI for frequencies greater than 3800, and coefficients from XXXX.DAT for determining the final temperature frequency. Compile and link the altered program as described in Step #6 in the SLOTA1P calibration procedure.

ACKNOWLEDGEMENTS

First and foremost, I would like to acknowledge my advisor, Dr. Patricia Thiel. She has contributed, more than any other individual, to my development as a scientist, as well as a human being, over the past seven years; her guidance and friendship are much appreciated.

To the members of my research group who have gone on to "bigger" things: Dr. Sheng-Liang Chang, Dr. Mary Walczak, Dr. Pam Leavitt, Dr. Pete Schmitz, Dr. Wendi Wang, Dr. Diane Sanders and (soon-to-be) Dr. Barb Nielsen, I give thanks for your comradery over the years. Special thanks to Sheng-Liang for listening to my diatribes in the early days, to Barb for sharing the light at the end of the tunnel, and to Pam for making me realize how much a reliable friend can be missed.

To the more recent members of my research group, thank you for making me realize how much I had actually learned as a graduate student (especially Mark Jensen and Tim Ehler) and how much I will never know (especially Oden Warren). I would also like to thank Anna Crabtree for helping me in the collection of some of the data presented in this dissertation.

I would like to thank some of my friends who have helped me get through the "graduate school experience": to the "Stantonians", Tom Jones, Ray Garant, Chuck Rodrigues, and Jon Schoer, and the other "groupies", Dan and Lisa Van Wyk, I will always remember the "Manor" because of all of you; to Ryan Hopkins, Mike Davitt, Mike Blutt, Argha Saha, and Jim and Rochelle Lockridge, you all made Iowa feel like home; and, to Chinkap Chung, your kindness and gentle spirit of acceptance have and always will touch my heart.

Acknowledgement is made to the donors of the Petroleum Research Fund, administered by the American Chemical Society, for the support of this research. Some equipment and all facilities are provided by the Ames Laboratory, which is operated for the U. S. Department of Energy by Iowa State University under Contract No. W-7405-ENG-82. This dissertation has been assigned the IS-T No. 1540 by the U. S. Department of Energy.